# Material study and properties of polymers used in composite high voltage insulators

**by**

**MOHAMED ELBUZEDI**

**Thesis presented in partial fulfilment of the requirements for the degree of Master of Science (Polymer Science)**

**at the**

**University of Stellenbosch**

**Study leader**

**Dr. P. E. Mallon**

**Stellenbosch**

**December 2007**

# Declaration

I, the undersigned, hereby declare that the work contained in this thesis is my original work and that I have not previously in its entirety or in part submitted it at any university for a degree.

Signature……  Date…….

# Abstract

Silicone rubber, particularly poly(dimethylsiloxane) (PDMS), has been increasingly used in the manufacture of outdoor high voltage insulators in the recent years. PDMS offers several advantages that make it suitable for outdoor use, such as low weight, a hydrophobic surface, stability, and excellent performance in heavily polluted environments. PDMS surfaces can, however, become progressively hydrophilic due to surface oxidation caused by corona discharge, UV radiation and acid rain.

In this study, PDMS samples of controlled formulations as well as six commercial insulator materials four PDMS based and two ethylene propylene diene monomer (EPDM) based were exposed to various accelerated weathering conditions for various periods of time in order to track changes in the material over time. The ageing regimes developed and used to simulate the potential surface degradation that may occur during in-service usage included needle corona and French corona ageing, thermal ageing, UV-B irradiation (up to 8000 hours) and acid rain (up to 200 days).

Both the chemical and physical changes in the materials were monitored using a wide range of analytical techniques, including: static contact angle measurements (SCA), optical microscopy (OM), scanning electron microscopy (SEM), energy dispersive spectroscopy (EDS), gas chromatography (GC), gas chromatography/mass spectroscopy (GC/MS), size-exclusion chromatography (SEC), Fourier-transform infrared photo-acoustic spectroscopy (FTIR-PAS) and slow positron beam techniques (PAS).

A low molecular weight (LMW) uncrosslinked PDMS model compound was used to further study the chemical effects of corona exposure on PDMS materials.

PDMS showed far better performance than EPDM, in terms of resistance to the various ageing regimes and “hydrophobicity recovery”.

# Opsomming

Silikoonrubber, spesifiek polidimetielsiloksaan (PDMS), is gedurende die afgelope paar jaar toenemend gebruik in die vervaardiging van buitelughoogspanningisolators. PDMS het baie voordele vir gebruik in elektriese isolators soos ‘n laer massa, ’n hidrofobiese oppervlak, stabiliteit en uitstekende werking in hoogsbesoedelde omgewings. Die hidrofobiese oppervlakte kan egter gelydelik hidrofilies word weens oppervlakoksidasie as gevolg van korona-ontlading, UV-bestraling en suurreën.

In hierdie studie is PDMS monsters van verskillende samestellings sowel as ses kommersiële isolators (vier PDMS en twee etileenpropileenrubber (EPDM)) blootgestel aan verskillende versnelde weersomstandighede vir verskillende periodes om die veranderinge in die materiale te monitor. Die verskillende materiale is gerangskik volgens hulle werking oor ‘n periode van tyd. Dit het ook ‘n geleentheid gebied om die eienskappe van die verskillende samestellings te bestudeer. Die tegnieke wat ontwikkel is om die moontlike oppervlakdegradasie te simuleer, het naald-korona, “French” korona, UVB-bestraling (tot 8000 uur) en suurreën (tot 200 dae) ingesluit.

Beide die chemiese en die fisiese veranderinge in die materiale is gemonitor met behulp van verskeie tegnieke soos statiese kontakhoekbepaling, optiese mikroskopie, skandeerelektronmikroskopie, energieverspreidingsspektroskopie, gaschromatografie, grootte-uitsluitingschromatografie, foto-akoestiese Fouriertransforminfrarooi (PAS-FTIR) en stadige-positronspektroskopie (PAS). ’n Lae molekulêre massa PDMS modelverbinding is gebruik om die chemiese effek van korona te bestudeer.

Die PDMS materiale het baie beter vertoon teenoor die EPDM materiale in terme van hulle herstel van hidrofobisiteit.

## Acknowledgments

I would like to express my deep and sincere appreciation to the following people and institutions for their valuable support during my study:

Dr. Mallon for his time, guidance, support, valuable comments and shared knowledge throughout the course of my project.

Dr. Margie Hundall for very patiently trying to correct my grammar and for her good suggestions and advice.

The Libyan Centre of Macromolecular Chemistry and Technology, Tripoli, Libya, for giving me the opportunity to study in South Africa, and for the financial support.

The University of Stellenbosch, particularly the Department of Chemistry and Polymer Science.

My family for their limitless love and inspiration.

My thanks also go to all my friends, at Polymer Science and further away, for encouragement and support.

## List of abbreviations

| | |
|---|---|
| AC | Alternating current |
| AFM | Atomic force microscopy |
| A-R | Acid rain |
| ATH | Aluminum tri-hydrate |
| BSE | Backscattered electron |
| CE | Cycloaliphatic epoxies |
| CFM | Chemical force microscopy |
| DNA | Deoxyribonucleic acid |
| DSET | Desert Sunshine Exposure Test |
| EDS | Energy dispersive X-ray spectroscopy |
| EPDM | Ethylene propylene diene monomer |
| EPM | Ethylene propylene monomer |
| ESCA | Electron spectroscopy for chemical analysis |
| F-C | French corona |
| FO | Flashover |
| FTIR-PAS | Fourier-transform infrared photo-acoustic spectroscopy |
| GC | Gas chromatography |
| GC/MS | Gas chromatography/mass spectroscopy |
| HTV-SiR | High-temperature vulcanized silicone rubber |
| HV | High voltage |
| ID | Sample code (identification) |
| KeV | Kilo electron volt |
| KIPTS | Koeberg Insulator Pollution Test Station |
| KV | Kilo volt |
| LMW | Low molecular weight |
| Ma | mili-Ampere |
| Mag | Magnification |
| N-C | needle corona |
| NCIs | Non-ceramic insulators |
| NS | Neutron scattering |

| | |
|---|---|
| OM | Optical microscopy |
| o-Ps | Ortho-positronium |
| p-Ps | Para-positronium |
| PAS | Positron annihilation spectroscopy |
| Ps | Positronium |
| PDMS | Polydimethylsiloxane |
| RTV-SiR | Room-temperature vulcanized silicone rubber |
| SCA | Static contact angle |
| SEC | Size-exclusion chromatography |
| SEM | Scanning electron microscopy |
| $SiO_x$ | Silicone oxide where x is bonded to 3 or 4 oxygen atoms |
| SiR | Silicone rubber |
| STM | Scanning tunneling microscopy |
| T | Temperature |
| TEM | Transmission electron microscopy |
| TGA | Thermal gravimetric analysis |
| V | Virgin |
| XPS | X-ray photoelectron spectroscopy |
| XS | X-ray scattering |

# Table of Contents

# List of Figures

# List of Tables

# CHAPTER 1

# INTRODUCTION AND OBJECTIVES

## 1.1 Insulators

Reliability is one of the most important properties of high voltage insulators. The worst failure of a line insulator is if it breaks mechanically and drops the line. A second type of failure is flashover (FO), which may be caused by overvoltages or pollution [1].

Conventional ceramic materials including porcelain and glass have been used worldwide in outdoor high voltage (HV) insulation for many years. They show some special properties, which means they are still widely used today; they withstand heat and dry-band arcing and they do not age or degrade under normal environmental conditions [2]. However, these materials have high surface tension, meaning that their surfaces are highly wettable when exposed to wet conditions such as rain, fog, and a marine environment (saturated, salty, sea winds). This leads to the development of high leakage currents that can result in FO. A FO is the abnormal discharge or arcing from a conductor to ground or to another conductor. It occurs as a result of the dielectric breakdown of an insulator, which may then cause an outage on the network [3, 4].

The worldwide growing demand for new and more effective materials for use in electric power utilities has prompted researchers to investigate different insulating materials, in efforts to obtain good alternatives with superior performance and at preferably lower costs. From an economic point of view the new materials should offer better performance, be relatively inexpensive and the processing costs should be economical.

Recently, the focus has been on non-ceramic (NC) polymeric materials. They are being increasingly used to replace their conventional counterparts, such as glass and porcelain, especially in heavily polluted environments [4, 5], because of their exceptional properties and desirable reliability.

## 1.2 Silicone rubbers and polydimethylsiloxane

Silicone rubber (SiR) is classified as an organic-silicone compound. It is a hydrophobic material (it repels water). This is due to the organic groups attached to the silicone atom. Because of the silicone-oxygen backbone, silicon rubber is resistant to sunlight and heat, and is flexible over a wide range of temperatures. The silicon-oxygen bond is however susceptible to heterolytic cleavage, i.e. attack by acids and bases [5, 6]. Many different silicone polymers are commercially available but relatively few are suitable for high voltage applications. Extensive analysis and testing is required to ensure a suitable match of material characteristics with application needs.

Silicon rubbers based on polydimethylsiloxane (PDMS) composite materials are very interesting because of their unique and superior properties, particularly in heavily polluted regions [7]. They provide several additional advantages, such as low weight, less breakage, good insulating properties, and good performance under severe wet and polluted environments. Compared to porcelain or glass insulators they show a better water repellence, limited leakage current flows, as well as a good ability to withstand high voltages. PDMS is thermally stable and performs well over a wide range of temperatures.

During their service life, however, PDMS housings are exposed to various environmental conditions, which may lead to the hydrophobic surface gradually becoming hydrophilic due to degradation. Hydrophobicity loss may also be the result of electrical discharge activity on the surface. These materials do however have the unique ability to regain their hydrophobicity after it is lost. This is very often referred to as “hydrophobicity recovery”, which is considered as an advantageous property of PDMS materials.

## 1.3 The Koeberg Insulator Pollution Test Station (KIPTS)

One of the pioneering facilities to use polymeric insulators in heavy polluted areas was Eskom, South Africa. They started testing polymeric/non-ceramic insulators (NCIs) that were made from a number of different materials, including room-temperature vulcanized silicone rubber (RTV-SiR), ethylene propylene diene monomer (EPDM), and epoxies.

The Koeberg site is a natural-ageing insulator test station, located along the Western Cape coast (South Africa), 50 m from the sea. This station was established in 1994 to evaluate the performance of a variety of insulators. Here various types of energized insulators are exposed to actual severe environmental conditions in order to determine the pollution and ageing performance of the insulators. The site is equipped with pollution monitoring units as well as a leakage current logger system [8].

Recently an environmental survey was carried out by Vosloo and Holtzhausen on the area around Koeberg to investigate the origin of pollution sources [8]. It was found that the main pollution source surrounding KIPTS is the Atlantic Ocean, which lies to the west of the test site. Wave actions and breezes cause salt particle deposition and moisture in the station. Northeast of the site there is an industrial area that emits coal and heavy fuel oil particles into the atmosphere. To the southeast, heavy industry, such as an oil refinery, is the main cause of severe particle emissions. The pollution index at KIPTS is 2000 μs/cm, which is very high [9]. The test site has both marine and industrial pollution condensation. Hence KIPTS is an ideal environment in which to evaluate insulators.

## 1.4 Objectives

It is very important to be able to evaluate the life-expectancy of NCIs. Since little knowledge of the degradation mechanisms of polymeric housing insulating materials is available in the literature, their modes of insulator failure, early-stage indications of failure and lifetime expectancy are still largely unknown. Therefore, the overall aim of this project was to investigate the behaviour of various types of polymeric housings upon ageing and degradation, specifically that of the commercially available PDMS and EPDM, in order to contribute to the fundamental understanding of the degradation mechanisms of outdoor insulating materials.

Understanding the fundamental mechanisms of material degradation and the modes of failure of such composite materials should increase the knowledge ultimately required to develop more appropriate accelerated ageing techniques for the tracking of insulator performance. An improved correlation between laboratory-accelerating ageing techniques and in-service natural ageing is very necessary.

The focus of this study will be on determining how different insulators behave under various ageing conditions, to what extent the different materials respond to the different ageing techniques, and what role the compositions of the respective insulators plays. Such data should contribute to an explanation of the modes of material failure under certain circumstances, and subsequently enable better choices of suitable composite material for electrical insulators to be made.

The following specific objectives were included:

1. Obtain PDMS samples of known and controlled formulations (prepared in the laboratory) and samples of PDMS and EPDM (from industry).

2. Evaluate the selected materials in terms of their material performances under selected accelerated ageing conditions, including needle corona and French corona, thermal exposure, UV degradation and acid rain. This was to be done using a systematic approach, in which controlled-formulation samples were to be aged in parallel with commercial compounds. Results should contribute to a better understanding of the roles of the various components that are included in the commercial samples.

3. Evaluate various ageing techniques in terms of the difference between various techniques and do time dependent studies to determine optimum testing times.

4. Determine what effects the various existing accelerated ageing techniques have on the material ageing of the above samples.

## 1.5 Methodology

Four different controlled-formulation PDMS samples were prepared in the laboratory via room-temperature vulcanization (samples C, E, G and I). In parallel to this, six different high-temperature commercial insulators were used: four of the PDMS type (samples J, K, M and O) and two of the EPDM type (samples L and N). In addition to samples of the virgin materials, samples that had been aged for 1 year were also included in the study.

All samples were subjected to the following laboratory-accelerated ageing techniques:

1. needle corona and French corona, to simulate electrical discharge

2. UV-B ageing, to simulate exposure to sunlight
3. high temperature, to simulate dry-band arcing, and
4. acid rain immersion, to simulate weathering.

Various analytical techniques were used to track changes in the morphology of the surfaces of the insulators, such as cracks, roughness and erosion, and surface properties, caused by the different types of ageing tests. These included: optical microscopy (OM), scanning electron microscopy (SEM), energy dispersive spectroscopy (EDS), thermal gravimetric analysis (TGA), positron annihilation spectroscopy (PAS), gas chromatography (GC), gas chromatography/mass spectroscopy (GC/MS), size-exclusion chromatography (SEC) and Fourier-transform infrared photo-acoustic spectroscopy (FTIR-PAS). Chemical analysis of surface structures was also carried out in order to determine the chemical changes taking place after ageing.

## 1.6 References

1. T. G. Gustavsson, Silicone Rubber Insulators, PhD dissertation, Chalmers University of Technology, Sweden, 2002.
2. R. Hackam, IEEE Trans. Diel. Elect. Insul., Vol. 6, 556-575, 1999.
3. S. H. Kim, E. A. Cherney and R. Hackam, IEEE Trans. Diel. Elect. Insul., Vol. 27, 1065-1070, 1992.
4. J. K. Kim and I. H. Kim, J. Appl. Polym. Sci., Vol. 79, 2251-2257, 2001.
5. R. Hackam, IEEE Trans. Diel. Elect. Insul., Vol. 7, 1257-1280, 2001.
6. J. Kim, M. K. Chaudhury and M. J. Owen, IEEE Trans. Diel. Elect. Insul., Vol. 6, 695-704, 1999.
7. H. Hillborg and U. W. Gedde, IEEE Trans. Diel. Elect. Insul., Vol. 6, 703-717, 1999.
8. W. L. Vosloo and J. P. Holtzhausen, 13th International Symposium on High Voltage Engineering, The Netherlands, 2003.
9. W. L. Vosloo, A Comparison of the Performance of High Voltage Insulator Materials in A Severely Polluted Costal Environment, PhD dissertation, University of Stellenbosch, 2002.

# CHAPTER 2

# HISTORICAL AND THEORETICAL BACKGROUND

## 2.1 History of non-ceramic insulators

The first polymeric insulators used for electrical applications in the mid 1940s were made of bisphenol and cycloaliphatic epoxy resins. They were commercially introduced and are still used today for indoor and outdoor electrical applications [1]. Cycloaliphatic epoxies (CE) were first introduced in 1957 [2]. Although they have better resistance to carbon formation than bisphenols, the first commercial CE insulators failed after only a short period of time in an outdoor environment because of bad design [3]. In the early 1960s the first commercially distributed class of CE insulators was sold in the USA, under the name GEPOL, but these units failed as a result of puncture and surface damage [3, 4]. At that time, for various reasons, including poor cold-temperature performance, CE did not gain acceptance in the USA for use in outdoor high voltage suspension insulators. Today, however, CE insulators are widely used in indoor applications. Later in the 1960s, an insulator that had sheds of porcelain and an epoxy resin fibreglass rod was developed but it was not commercially used due to even newer developments of lighter weight polymeric insulators [5, 6].

In 1964 polymeric insulators for outdoor applications were developed in Germany, England, Italy, France and the USA. In the early 1970s the first generation of commercial polymeric transmission line insulators was introduced and soon many utilities started testing these insulators [7]. As the initial results were generally not encouraging (failures were reported) several manufacturers stopped using these insulators, while others carried out further extensive investigations, which has resulted in the second generation of composite insulators used today.

## 2.2 Comparison of ceramic and non-ceramic insulators

A brief summary of a comparison between ceramic and non-ceramic insulators is given below.

| **Ceramic insulators** | **Non-ceramic insulators** |
|---|---|
| Made of inorganic materials | Made of organic materials |
| Do not age | Age |
| More wettable (hydrophilic) | Non-wettable (hydrophobic) |
| Resistant to heat and dry-band arcing | Generally better pollution performance |

One of the characteristics of ceramic insulators such as porcelain and glass is that they are made from non-homogeneous materials produced from natural minerals such as calcium carbonate, silica, etc., and their performances are therefore largely dependent on the actual properties of the raw materials used. Materials manufactured at different plants thus differ, and such differences need to be taken into consideration in the insulator design [8].

The main positive feature of porcelain is that it is inert, and of an inorganic nature, making it non-susceptible to degradation by environmental factors such as UV and aggressive contaminants. Porcelain exhibits good resistance to damage by corona discharge and leakage current and it has a high compressive strength. However, it has some limitations, such as being brittle, so it breaks and cracks easily [2].

On the other hand, non-ceramic polymeric insulators show unique properties in electrical high voltage applications, including a high tensile strength to weight ratio and improved performance in highly polluted areas. However, there are some limitations associated with them; they are subject to leakage current erosion, and deflection under load occurs in certain applications [9]. The main advantages of non-ceramic materials are their non-wettability and low weight relative to glass and porcelain. The former contributes to better electrical insulation performance and the latter leads to cost reduction. Polymeric insulators are easy to handle, require limited maintenance, and have limited leakage current. As a consequence, polymeric insulators are now being increasingly used to

replace conventional insulators such as glass and porcelain, and are gaining a high market share.

Due to differences in physical properties between porcelain and polymers, a comparison is normally made of short-term electrical characteristics of complete insulators, e.g. wet and dry 50 Hz flashover, and critical impulse flashover. However, there are several physical properties of a candidate polymer material that must first be understood, and then adequately controlled, to provide the thermal characteristics necessary to provide long life as high voltage insulators [1].

### 2.3 Polymers and fillers used in high voltage applications

There are several types of polymers that can be used for manufacturing non-ceramic insulators, such as polydimethylsiloxane, ethylene propylene diene monomer, ethylene propylene monomer (EPM), and cycloaliphatic and aromatic epoxies. In order to obtain the desired electrical and mechanical properties these basic materials are combined with various fillers, including silica and aluminium trihydrate (ATH) [8]. EPM relies largely on the ATH to avoid degradation. When an EPM rubber surface is exposed to ultraviolet light and electrical arcing the ATH filler is gradually reduced to a white aluminium powder on the insulator surface. The alumina may affect the level of wet flashover of an insulator. Although silicone rubbers do contain ATH, they rely largely on hydrophobicity to prevent leakage current and arcing [9].

The electrical performance of a polymeric insulator depends mainly on the material characteristics and the shape of the housing material [10]. It is important to note that it is not sufficient for a housing material to only have excellent performance when exposed to service stresses, it is also very important to incorporate specific additives in the formulation so that it has optimum processing properties during fabrication. Therefore, the final formulation is always a compromise between these requirements, which are not necessarily compatible [11].

EPDM rubber contains a higher carbon content than silicone rubber does. Consequently, it is critical to include agents such as ATH in the formulation, which will counteract the possibility of having carbon residues on the insulator surface when it is subjected to

electrical arcs. EPDM is usually peroxide cured. All EPDM formulations contain fairly high quantities of mineral filler, usually ATH. Several additives are also introduced, such as plasticizers, UV stabilizers, antioxidants and colouring agents.

Silicon rubbers, primarily PDMS materials, have now gained wide acceptance in the field of polymeric insulation materials, especially in high voltage applications [12].

### 2.4 Polydimethylsiloxane (PDMS)

Polydimethylsiloxane is a silicone rubber polymer consisting of inorganic silicone and oxygen atoms, alternating with methyl groups attached to the silicone atom, to form the repeating unit of the polymer [13]. PDMS has several characteristics associated with its chemical structure that make it the better choice for high voltage outdoor applications in comparison to other polymeric materials. PDMS is currently the most widely used polymeric material in high voltage insulators due to its unique properties, which include:

1. low glass transition temperature (-127 °C), so it is a soft material
2. low surface tension and good water repellence
3. good hydrophobicity recovery and the ability to transfer hydrophobicity to pollutants
4. UV resistance
5. thermal and oxidative stability
6. reliability for desirable construction designs, and
7. PDMS performs much better than glass and porcelain, especially in highly polluted environments [14].

The low surface tension of PDMS is due to the close packing of the methyl groups on the surface. The interfacial tension between PDMS and pure water is low compared to between PDMS and hydrocarbons. The polar nature of the siloxane bonds makes PDMS susceptible to hydrolysis under acidic or basic conditions. Methyl groups in PDMS behave differently to those in hydrocarbon polymers; they have high thermal and oxidative stability. PDMS used in high voltage applications is normally crosslinked, as well as highly filled, typically with silica and alumina, usually about 40% by mass. The

incorporation of filler particles imparts mechanical strength to the resultant composite. Other types of fillers such as calcium carbonate can be added for economic reasons [14].

### 2.5 The role of fillers in PDMS

NCIs usually contain mainly inorganic silica ($SiO_2$) and aluminium trihydrate ($Al_2O_3(H_2O)_3$) as fillers. Fillers are used to reinforce the base elastomer to improve the physical properties or impart certain processing characteristics. The reinforcing effect largely depends on the surface area of the filler. Some commercial samples may contain inert fillers added for cost reduction. Silica in PDMS serves as a reinforcing filler and provides the required tensile strength [13].

In addition to $SiO_2$ and ATH the most common fillers are chalk ($CaCO_3$), talc and quartz powder. There are two types of fillers: reinforcing and extending fillers. The reinforcing type can improve tensile strength, modulus, tear strength and abrasion resistance of a compound. The extending filler is a loading or non-reinforcing material. Alumina trihydrate is used in almost all insulator compounds to impart a high resistance to electrical tracking, inflammability and thermal stability [14].

There is a difference between PDMS with a small content of ATH and PDMS with high content of ATH. Samples with lower levels of ATH exhibit a delayed onset of degradation, but once damaged they degrade more rapidly than samples with higher ATH content. The ATH is completely decomposed, to form a white layer of aluminium powder ($Al_2O_3$) at the eroded surface regions [14].

Fillers also play an important role in the surface hardness. Higher ratios of filler in insulator formulations result in rougher surfaces, which in turn affect the pollution performance [15].

Filler levels in polymeric insulators play a role in the manufacturing requirements, as they affect the viscosity and final thermal properties. The addition of too much filler to the insulator formulation has a negative effect on the insulator performance. There is an increase in insulator surface wettability and therefore a decrease in static contact angle

values will be observed. If the deposited pollution layer contains conductive species then insulator FO may occur [16].

### 2.6 Vulcanization (crosslinked network) of PDMS rubber

Vulcanization is the reaction by which chemical links are incorporated into PDMS rubber to form a crosslinked polymer network. Hence rubber changes from being a soft material to a hard material. Sometimes it is also referred to the "crosslinking reaction". Based on the vulcanization temperature, two different types of crosslinked PDMS materials can be obtained [17].

#### 2.6.1 Room-temperature vulcanization

Room-temperature vulcanization (RTV) takes place either by a polycondensation reaction between the silanol groups of PDMS, to form siloxane bonds, or via an addition reaction between siloxane-containing vinyl groups and a siloxane crosslinking agent with a Si-H functional group [18]. A problem with RTV is that the catalyst used for the condensation curing remains in the vulcanized rubber, and therefore makes the rubber more sensitive to hydrolysis and less thermally stable, compared to high-temperature vulcanized (HTV) PDMS.



#### 2.6.2 High-temperature vulcanization

Crosslinking of PDMS occurs in the presence of organic peroxides, such as benzoyl peroxide, m-chlorobenzoyl peroxide and di-butyl peroxide. The curing temperature is normally high (100 °C) and high pressure is used, since the free radicals are formed by the decomposition of peroxide. The free radicals abstract a hydrogen atom from the dimethylsiloxane chain, which leads to the formation of chain-free radicals. The free radicals generated along the polymer chain recombine and form crosslinks between the siloxane chains [18]. HTV PDMS has higher thermal stability than RTV PDMS samples, as the curing agent is inactivated or evaporated after post curing [16-19].

## 2.7 Hydrophobicity of PDMS

PDMS's exceptional hydrophobicity makes it appropriate for use in high voltage insulators. This property is due to the presence of methyl groups attached to the highly flexible siloxane backbone, which allows for the rearrangements of methyl groups on the insulator surface with very low intermolecular interactions, therefore the surface tension of the PDMS surface is quite low [20]. Free mobility of the silicone oils from the bulk of the PDMS material to the surface is facile, providing a hydrophobic layer on the surface. In conventional insulating materials such as glass and porcelain, water readily forms a continuous film where leakage currents can develop, and in most cases this leads to flashovers. Water drops readily bead off PDMS insulator sheds, however, which means that a continuous water film does not form on the insulator, and therefore the leakage current is minimized [21].

### 2.7.1 Loss and recovery of hydrophobicity of PDMS

Prolonged electrical discharge exposure of a PDMS surface is accepted to be the cause of the loss of hydrophobicity of an insulator surface. Under wet conditions, oxidation of the surface occurs; hydroxyl groups form and the wettability increases as a continuous water film forms. This is associated with leakage current [22]. Surface pollution and long-term immersion in water can also cause loss of hydrophobicity. Sea salts, dew and fog, and industrial pollution contain conductive particles. Their presence on an insulator further leads to loss of hydrophobicity and alteration of the electrical performance of the material.

After a relatively short period of time with no discharge activity, typically from hours to a few days, a PDMS surface can regain its initial hydrophobicity. This change from a hydrophilic to a hydrophobic surface is often referred to as "hydrophobicity recovery". It is believed that migration of low molecular weight (LMW) oligomers of PDMS from the bulk to the surface is the most dominant mechanism responsible for this unique hydrophobicity recovery [22].

Toth et al. [22] suggest that the diffusion-controlled migration of LMW species plays the greatest role in the recovery process, greater than the reorientation of newly formed

hydrophilic groups in the bulk. Recovery rates depend on the applied voltage and duration of exposure. A "thick" silica-like layer forms, which inhibits the migration of the LMW oligomers to the surface, hence slowing the recovery rate. Mechanical stresses and temperature also affect the recovery rate. Mechanical forces might originate from external stresses, such as bending, or be a result of the shrinkage associated with densification when PDMS is transformed to a highly oxidized layer. A consequence of this is that the lowest recovery takes place if the surface is weakly oxidized. Gubanski and Vlastos [23] found that the recovery of untouched samples was slower than the recovery of mechanically deformed ones. This can be explained in terms of the cracks that develop along the silica-like layer surface, induced by mechanical stresses, which facilitates migration of LMW oligomers from the bulk to the surface, hence enhancing the hydrophobicity recovery rates.

According to Hillborg and Gedde [24], corona treatment results in the formation of an inorganic silica-like layer on the sample surface, as proved by X-ray photoelectron spectroscopy (XPS) measurements. Mallon et al. [25] have also shown evidence for the formation of a silica-like layer, using slow positron beam techniques. They show that there is a marked change in the "S-parameter" at the surface after corona exposure. It is assumed that the free volume and mobility of the silica-like surface layer is relatively smaller than in the PDMS due to the short bond lengths of Si-O and crosslinking. This, together with a possible chemical effect, appears to be the reason behind the decrease in the S parameter near the surface after corona treatment. The plateau observed in the S parameter curve is consistent with a silica-like layer with a 40-nm thickness forming on the polymer surface. The main effects of corona treatment take place in the near surface region. On increasing relaxation times after corona treatment there is a progressive shift in the curves to lower $-\Delta S$ values, indicating some recovery of the S parameter. This recovery may be due to the diffusion of LMW PDMS, formed upon corona, through the cracked silica-like layer to the surface.

Bar et al. [26] reported a pronounced change in surface stiffness in a corona-treated PDMS surface due to oxidation. They showed that there is an increase in the modulus of the surface with increasing oxidation time; cracks essentially form, which are normally

associated with a large change in surface roughness. Hillborg et al. [27] tracked the hydrophobicity of UV/ozone treated PDMS using chemical force microscopy (CFM) and found a direct relationship between treatment time and surface roughness.

Meincken et al. [28] investigated the surface hydrophobicity of corona treated PDMS samples using atomic force microscopy (AFM) force-distance measurements and found that the adhesive force increased significantly and instantaneously after corona treatment as the sample becomes more hydrophilic. With increasing recovery time the adhesive force declines, until the PDMS recovers its original value, indicating complete recovery of hydrophobicity.

One of the advantages associated with the hydrophobicity recovery of PDMS insulators is the ability to transfer the hydrophobicity to pollutants, meaning that the hydrophobic character of the surface is maintained at all times, especially in regions of high pollution. The significance of the oligomer diffusion for restoring the hydrophobicity of SiR rubbers raises the question of how long the recovery will take. In other words, are oligomers forming during service-life due to depolymerization or not? If not, then the ability to recover will cease when the initial reserve of oligomers is consumed. Performance results of insulators over many years have shown no decrease in the content of extracted oligomers, indicating that depolymerization of crosslinked PDMS might have taken place [23]. Depolymerization occurs thermally at high temperatures, but at temperatures below 350 °C the depolymerization must be catalyzed by ionic catalysts. However, the ionic nature of the siloxane backbone makes PDMS sensitive to hydrolysis.

Deposition of pollutant particles on an insulator surface may lead to the development of leakage currents, as such particles may exist in the form of conductive ionic salts and other moieties. Although the deposition of pollutants happens on PDMS insulators, the LMW silicones still migrate to the surface and coat the pollutants with a thin layer of LMW silicones, and therefore the surface hydrophobicity is retained [24].

### 2.7.2 Possible mechanisms of hydrophobicity recovery

Several mechanisms are suggested for the hydrophobicity recovery [18, 29-31]:

1. loss of highly volatile oxygen species and other polar compounds to the atmosphere
2. diffusion of treated polymeric segments from the surface to the bulk, and migration of untreated polymer chains to the surface
3. reaction of active species such as polar groups, resulting in products that hinder chain reorganization
4. reorientation of hydrophilic groups away from the surface
5. presence of contaminants on the polymer surface
6. change in the surface roughness
7. diffusion of existing low molecular weight oligomers from the bulk to the surface
8. condensation of the surface hydroxyl groups
9. reorientation of polar groups from the bulk phase to the surface, and
10. migration of in-situ created LMW species during corona discharge.

For a clean surface, polymer backbone reorientation can result in hydrophobicity being recovered after mild oxidation since the recovery process is fast. Two silanol groups can condense to form siloxane crosslinks, which improves hydrophobicity [32].

Surface reorientation and diffusion of LMW oligomers are the most likely mechanisms of hydrophobicity recovery. These have been investigated, especially in the case of PDMS. The extreme flexibility of the siloxane chains and low intermolecular forces between methyl groups, which impart the low glass transition temperature and high free volume of PDMS, permit ease of reorientation of molecules on the surface and also allow for the diffusion of LMW components often present in commercial PDMS materials [21].

However, insulators in outdoor applications are polluted and chain reorientation alone cannot explain the transfer of hydrophobicity to the pollution layers. Instead, the diffusion of oligomers can transfer hydrophobic properties to both damaged surfaces and to pollution layers. This process is slower than reorientation [21].

### 2.8 Degradation stability of PDMS

Silicone rubbers, specifically PDMS, exhibit good stability against oxidative and thermal degradation. The observed stability of PDMS is presumed to be due to the ionic character

of the siloxane bond. The oxygen atom plays the role of an electron drain, which increases the stability, even in the methyl-silicone bonds, making the methyl group slightly polarized [15].

Local heating may occur when electrical discharges on the insulator surface result in dry conductive paths, where leakage current develops. As a result, the surface temperature increases significantly, so much so that the temperature in some spots might exceed the required temperature for quick depolymerization of LMW PDMS. Methyl-terminated PDMS is thermally more stable than hydroxyl-terminated PDMS. When thermal ageing occurs in an oxygen-containing atmosphere, the removal of methyl groups followed by formation of siloxane crosslinks will dominate over the depolymerization process, and eventually a silica like-layer structure forms [16].

Photo-oxidative attack on the PDMS side groups may take place by bond cleavage upon radiation, or by bond cleavage by atmospheric oxygen [20]. UV light with a wavelength shorter than 290 nm can initiate photo-oxidation. Both reaction paths lead to the formation of hydroxyl groups, inducing depolymerization by backbiting reactions, resulting in siloxane crosslinks. Photodegradation is normally dominated by crosslinking.

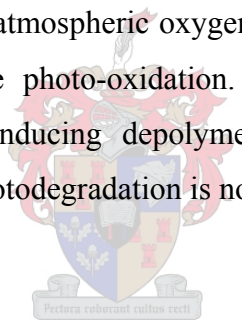


## 2.9 References

1. S. H. Kim, E. A. Cherney and R. Hackam, IEEE Trans. Pow. Deliv., Vol. 5, 1491-1495, 1990.
2. R. Hackam, IEEE Trans. Diel. Elect. Insul., Vol. 6, 556-585, 1999.
3. H. Yasuda and A. K. Sharma, J. Polym. Sci., Polym. Phys. Ed., Vol. 9, 1285-1292, 1991.
4. J. K. Kim and I. H. Kim, J. Appl. Polym. Sci., Vol. 79, 2251-2257, 2001.
5. J. F. Hall, IEEE Trans. Pow. Deliv., Vol. 8, 376-384, 1993.
6. S. Kumagai, X. Wang and N. Yoshimura, IEEE Trans. Diel. Elect. Insul., Vol. 5, 281-289, 1998.
7. J. Kindersberger and M. Kuhl, 6th International Symposium on High Voltage Engineering, New Orleans, USA, 1989.

8. H. Hillborg, J. F Anker, U. W. Gedde, D. D. Smith, H. K. Yasuda and K. Wikstrom, Polymer, Vol. 41, 6851-6863, 2000.
9. J. Kim, M. K. Chaudhury and M. J. Owen, IEEE Trans. Diel. Elect. Insul., Vol. 6, 695-702, 1999.
10. A. J. Miller, Amer. Chem. Soc., Vol. 82, 3519-3524, 1960.
11. Y. Suzuki, M. Kusakabe, M. Iwaki, and M. Suzuki, Nucl. Instrum. Methods Phys. Res., B 32, 120-129, 1988.
12. P. C. Painter and M. M. Coleman, Fund. Polym. Sci., Vol. 8, 24-26, 1994.
13. J. L. Speier and M. J. Hunter, Silicone Chemistry, International Science and Technology, New York, 1963.
14. R. S. Gorur and T. Orbeck, IEEE Trans. Diel. Elect. Insul., Vol. 26, 1064-1072, 1991.
15. J. L. Goudie, M. J. Owen and T. Orbeck, Annual Report CEIDP, Vol. 1, 120-127, 1997.
16. A. Vlastos and S. Gubanski, IEEE Trans. Pow. Deliv., Vol. 6, 88-95, 1991.
17. H. F. Mark, N. M. Bikales, C. G. Overberger and G. Menges, Encyclopedia of Polymer Science and Engineering, John Wiley & Sons, New York, Vol. 4, 388-390, 1986.
18. H. Hillborg and U. W. Gedde, Polymer, Vol. 39, 1991-1998, 1998.
19. R. Anderson, B. Arkles and G. L. Larson, Silicon compounds (Register and Review), Petrach Systems, Bristol, PA, 1987.
20. T. G. Gustavsson, Silicone Rubber Insulators, PhD dissertation, Chalmers University of Technology, Sweden, 2002.
21. S. H. Kim, E. A. Cherney, R. Hackam and K. G. Rutherford, IEEE Trans. Diel Elect. Insul., Vol. 1, 106-123, 1994.
22. A. Toth, I. Bertoti, M. Blazso, G. Banhegyi, A. Bognar and P. Szaplonczay, J. Appl. Polym. Sci., Vol. 52, 1293-1307, 1994.
23. M. Gubanski and A. E. Vlastos, IEEE Trans. Diel. Elect. Insul., Vol. 5, 1527-1535, 1990.
24. H. Hillborg and U. W. Gedde, IEEE Trans. Diel. Elect. Insul., Vol. 6, 703-717, 1999.

25. P. E. Mallon, T. A. Berhane, C. J. Greyling, W. L. Vosloo, H. Chen and Y. C. Jean, Mat. Sci. Foru., Vol. 27, 445-446, 2004.
26. G. Bar, L. Delineau, A. Hafel and M. Whangbo, Polymer, Vol. 42, 3627-3632, 2001.
27. H. Hillborg, N. Tomczak, A. Olah, H. Schoenherr and G. J. Vansco, Langmuir, Vol. 20, 785-794, 2004.
28. M. Meincken, T. A. Berhane and P. E. Mallon, Polymer, Vol. 46, 203-208, 2005.
29. J. Kim, M. K. Chaudhury and M. J. Owen, J. Coll. Interf. Sci., Vol. 226, 231-236, 2000.
30. J. Kim, M. K. Chaudhury, M. J. Owen and T. Orbeck, J. Coll. Interf. Sci., Vol. 244, 200-207, 2001.
31. S. Kumagai and N. Yoshimura, IEEE Trans. Pow. Deliv., Vol. 18, 506-516, 2003.
32. Y. Zhu, M. Otsubo, C. Honda and T. Tanaka, J. Polym. Degr. Stab., Vol. 91, 1448-1454, 2006.

# CHAPTER 3

# ACCELERATED AGEING TECHNIQUES

## 3.1 Environmental ageing factors

One of the main concerns regarding NCIs is their long-term performance since they are more susceptible to degradation, due to environmental factors, than glass and porcelain are. Environmental conditions play an important role in the degradation and failure of polymeric insulators since insulators along a HV tower are directly exposed to various environmental ageing factors such as UV, pollutants, salts and dust. All these factors can interact with the active groups on the insulator surface and lead to both chemical changes and physical changes in the insulator materials. There may be a change in colour, shape, tensile strength or conductivity. These changes reduce the durability of the actual materials, hence the material no longer functions in the way in which it was intended to do. In extreme cases these changes can lead to insulator failure, leading to flashover [1].

There are several forms of stress that the materials are exposed to that can lead to degradation: thermal degradation, chemical degradation, stress cracking, photodegradation, biodegradation and degradation due to the high voltage environment. During an insulator's service life most of the environmental factors are present to a certain extent but one may become predominant and be the main cause of the material failure. Environmental stresses, high voltages, partial discharge, leakage current, dry-band arcing, acid rain, heat cycling and UV light can affect the material performance and consequently change the chemical composition or physical properties of the polymeric composites. Furthermore, cracks develop through internal surface layers of the material and moisture diffuses inside. This in turn causes the hydrophobic recovery rate to decrease, leading to flashover and outage of an electric station facility [2].

Failure of outdoor insulators can also be due to mechanical stresses. Wind currents may reach high strength and cause insulators along towers to fall down, resulting in electricity outage problems. The interface between the housing material and end-fitting creates

internal mechanical stress and, in the presence of thermal cycling during service, cracks develop near the end-fitting, creating preferential sites for electrical discharges. If end-fittings are badly designed, or are not correctly fitted with arc protection devices, they can melt, which results in their being no longer able to hold the insulator core. In extreme cases, segregation may take place shortly after an arcing occurrence. Damage can also occur if the heat generated by electricity is enough to soften the core. Various environmental factors are discussed in this section [3].

### 3.1.1 Stresses due to high voltage environments

The important considerations for an insulator in a high voltage environment are the influences of tracking, corona, flashover and dry-band arcing. Tracking is a form of irreversible degradation of an insulator surface due to the formation of conductive moieties. Such degradation arises from the breakdown of dielectric paths caused by strong electric fields. Moisture, dust, salt particles and pollutants can generate areas with different sensitivities on the surface, which in turn magnify the electric fields, initiating tracking points. Once this occurs, degradation goes further along the material surface and erodes the surface away [4].

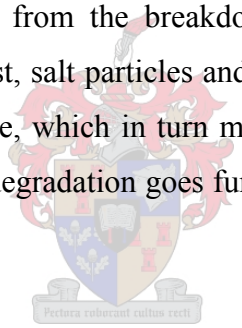

#### 3.1.1.1 Corona discharge

Corona is discharge caused by electrical overstress. Corona can appear in solid, liquid or gaseous insulating materials. In solids, the occurrence of corona generally results in deterioration of the material, while in liquids and gases removal of the electrical overstresses eliminates the discharge and the material regains its original insulating properties [5, 6].

The corona discharges observed at a conductor surface are due to the formation of electron avalanches, which occur when the intensity of the electric field at the conductor surface exceeds a certain critical value. In air there are usually a few free electrons as a result of radioactive material traces. As the conductor becomes energized on each half cycle of the AC voltage wave, the electrons in the air near its surface are accelerated by an electrostatic field. These negatively charged electrons are accelerated toward the

positive half cycle of the conductor [7]. The velocity attained by a free electron is dependent upon the intensity of the electric field. If the electric field intensity is not too great then the collision between an electron and an air molecule, such as oxygen or nitrogen, is elastic; the electron bounces off the air molecule, with no transfer of energy to it. On the other hand, if the intensity of the electrical field exceeds a certain critical value, any free electron will acquire sufficient velocity so that collision with an air molecule is inelastic. That electron then has sufficient energy to knock one of the outer-orbit electrons out of one of the two atoms of the air molecule. This is known as ionization, and the molecule with the missing electron becomes a positive ion. The initial electron, which has lost most of its velocity in the collision, and the electron knocked out of the air molecule with low velocity, are both accelerated by the electric field. At the next collision each electron is capable of ionizing another air molecule. All the time, electrons are advancing toward the positive electrode, and after many collisions the number of such electrons has grown enormously. This is the process by which the so-called electron avalanches are built up [7].

The generation of corona is primarily dependent on atmospheric conditions such as air density, humidity, and geometry of the insulator. The effects of corona are radio interference, TV interference, noise generation, ozone production and energy loss [7].

The discharges produced by electron avalanches may be seen in the laboratory in two different ways. Perhaps the best known is visual corona, which appears as a violet-coloured light coming from the overstressed electrical regions when the test is performed in the dark. This light is produced by the recombination of positive nitrogen ions with free electrons [8]. The second type is audible corona, which appears as a hissing or frying sound when the sample is energized above the corona threshold voltage. The sound waves are produced by the disturbances set up in air in the vicinity of the discharge, possibly by the movement of the positive ions as they are suddenly created in an intense electric field [8].

Corona speeds up the polymer ageing by forming ozone and UV light. The UV short wavelengths may cause polymer damage and failure. The electric discharge subjects the

insulator to severe electrical strain and chemical degradation. A good polymer insulator must be able to withstand this chemical degradation during its service lifetime [2].

#### 3.1.1.2 Dry-band arcing

When moisture and pollution are coated on surfaces that have lost their hydrophobicity leakage current may result . Dry areas in the wet and polluted layer develop from the heat generated by the leakage current [9]. When this takes place the voltage across the insulator appears across the dry areas in the wet and polluted layers and localized arcing begins. The heat generated by the arcing may thermally degrade the surface, so a method is needed to slow down the thermal degradation of the coating or polymer during dry-band arcing. Hence fillers are included in the compositions (see Section 2.5) [10].

High temperatures caused by dry-band arcing lead to tracking and erosion of polymeric insulators (since hydrolysis, scission and interchange of the siloxane bonds occur) [4]. If the resultant temperature is above the boiling point of the silicone oligomers (which contribute to the recovery of hydrophobicity) they escape via evaporation of the volatile linear and cyclic silicone oils. It is here that the fillers play an important role (see also Section 2.5). Fillers, such as ATH, absorb the heat that results from dry-band arcing, then release molecular water, thereby cooling the surface and helping to prevent heat decomposition of the coating. However, in doing so, the molecular water is released in the form of steam and its passage to the surface may actually destroy the surface smoothness [11]. As a result, the surface begins to roughen, and eventually the surface begins to accumulate more pollution in these roughened regions. As the pollution layer accumulates, and under wet conditions, the coating loses its characteristic property of hydrophobicity at an earlier stage and dry-band arcing begins sooner than usual. This process begins progressively earlier with each dry-band activity, accelerating the degradation process. Eventually the insulator becomes ineffective and flashover of the insulator occurs.

### 3.1.2 Ultraviolet radiation

Sunlight contains a range of rays, but it is particularly the UV short waves that are primarily responsible for material ageing and failure. Forms of failure can be seen as discolouration, which is a change in the base colour of the composite material. Chalking is the appearance of some filler particles of the housing material, which forms a rough or powdery surface [4].

Photodegradation takes place on PDMS side groups by bond cleavage, by radiation and as a result of the presence of oxygen in the atmosphere. UV light with a wavelength shorter than 290 nm can initiate the oxidation process [4]. Such a degradation path plays an important role in the ageing of HV silicone rubber insulators. Photodegradation induces depolymerization reactions and chain scission. UV radiation with a wavelength shorter than 281 nm causes organic crosslinks to form, as photons break bonds between hydrogen and carbon atoms in methyl groups [11].

### 3.1.3 Other factors

Weather parameters can have detrimental effects (cracking and chalking) on the ageing of non-ceramic materials. The direction and speed of wind, precipitation, relative humidity and the position of pollution sources all determine the final pollution deposit on an insulator surface [9]. Sunlight can heat up the insulator surface during the day and help prevent wetting. Thus environmental factors can play an important role in insulator pollution flashover [4].

### 3.1.4 Pollutants

Salt storms or industrial fog can also cause the deposition of a highly conductive electrolytic layer on an insulator surface [4].

Pollutants come into contact with the polymeric active groups of insulating materials and result in new chemical compositions of the original polymer, substantially altering the insulator performance. In industrial areas factories emit hydrocarbons, which can form a thin layer on the surface of the composite insulator. One advantage is that this layer

prevents the UV rays from getting through to the material, hence the material may age more slowly. On the other hand, some researchers suggest that the presence of pollutants alters the recovery process of hydrophobicity of the surface by prevention of the diffusion of LMW oligomers from the bulk to the surface, leading to faster ageing of the material [9]. Researchers have proved that even though there is deposition of pollutants on the PDMS surface, these pollutants can adhere to the surface by means of hydrophobicity transfer from polymer surface to contaminants [10]. This is a specific property of PDMS (not found in other non-silicone rubbers). This property enhances the durability of the insulators in-service life, especially in highly polluted environments.

Rain contains various types of chemical species such as nitric acid, calcium carbonate, magnesium sulphate, sodium chloride and potassium chloride. Hydrolysis of the insulator surfaces takes place when hydroxyl groups and other polar conductive precursors form on the insulator surface. This leads to an increase in conductivity of an insulator, hence the insulator becomes hydrophilic. Nitric acid present in rain can have a detrimental effect on the end-fittings of insulators. When acid rain diffuses into the interface between the housing material and the metal end-fitting, and it reaches the core, corrosion is introduced, which causes the metal end-fitting to wear off and then fall to the ground [4].



### 3.2 Laboratory accelerated ageing techniques

In nature, insulators age over long periods of time and hence it takes a very long time before noticeable failure can be observed. This makes it very difficult to investigate insulator failure under natural in-service conditions. It is also not economically viable due to the high costs of testing and the long times before any measurable observations can be made. It is a great challenge to develop accelerated ageing techniques to determine intrinsic material surface changes within a relatively short time that can mimic natural field-ageing, therefore saving money and time. Currently, various laboratory-ageing procedures are used to accelerate the degradation process, in efforts to draw meaningful correlations between naturally-aged insulators and artificially-aged samples. The results from these accelerated ageing techniques can be used to obtain a better understanding of the modes of degradation of polymeric insulators [4, 9, 10].

In this study various accelerated ageing methods were used in order to simulate the potential stresses in selected NCI materials due to their use in outdoor high voltage environments.

### 3.2.1 Corona treatments

Two different types of corona discharge treatments are currently available in our laboratories: the needle corona and French cell corona. The former is sometimes also called "desktop corona" while the latter is called "coco corona". There are also various other types of corona dischargers used by other researchers to simulate the potential electrical stress on materials [5, 12].

It is an important requirement to investigate the effects of different types of corona treatments on polymeric insulators. Since each technique has its own parameters, variations in terms of the effects and extent of degradation might be expected. Consequently, insulator housing materials may behave differently and show different extents of response, under different test conditions. An investigation to compare the effects of the abovementioned two treatments was therefore carried out.

#### 3.2.1.1 Needle corona ageing

Needle corona generates high electrical voltage associated with ozone gas generation. A schematic diagram of the model BD-20 AC high frequency laboratory corona discharger (a product of Electro-Technic, USA) is illustrated in Figure 3.1. In this type of corona treatment the sample surface is exposed to ion bombardment, which causes a high degree of surface damage [12].

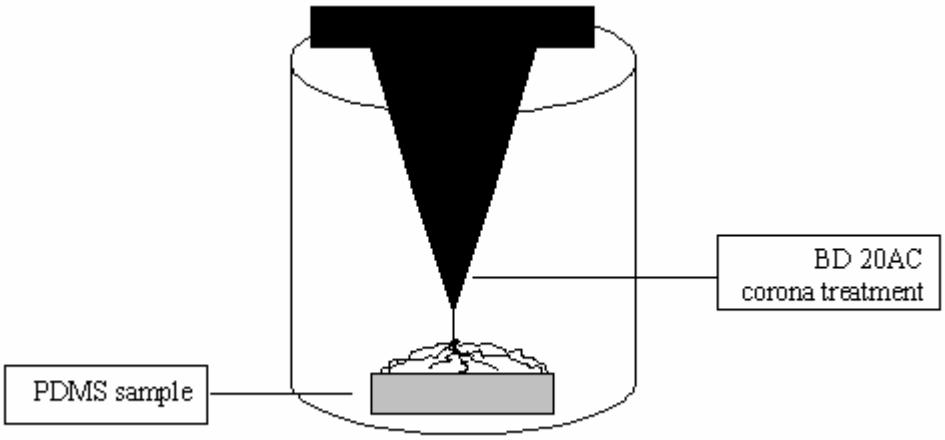


**Figure 3.1: Schematic diagram of needle corona discharger (Electro-Technic, USA).**

### 3.2.1.2 French cell corona ageing

This design is based on a system developed in France [5], and has a high standard of safety. It has a safety-glass window and ventilation for the release of hazardous excess amounts of ozone generated during operation. An important factor here with regard to sample treatment is the sample permittivity; samples with the same permittivity must be treated for the same period of time. Samples of the same thickness require an exact air gap to provide the same surface stresses and ensure similar doses of corona exposure. A diagram of a French cell corona discharger type is shown in Figure 3.2.

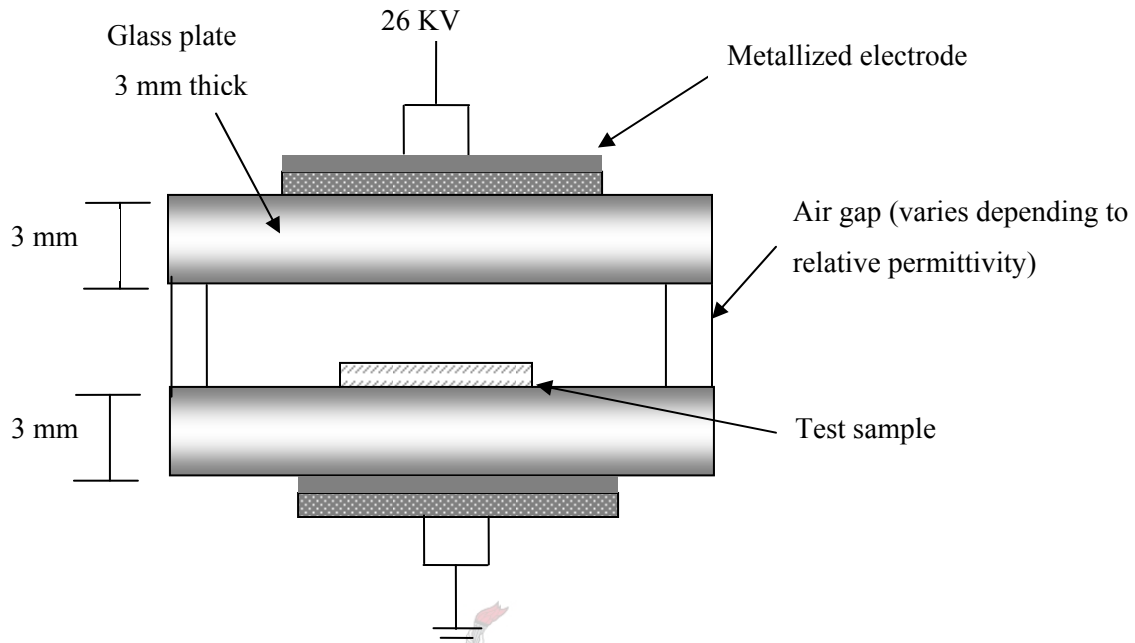


**Figure 3.2: Schematic diagram of French cell corona discharger.**

The French cell corona has a milder effect on surface degradation compared to the needle corona. The manner in which the sample surface is exposed to corona discharge is different. French cell corona has a dispersive effect on a surface. The high voltage electrode is covered by a glass plate, resulting in less electrical discharge activity along the material surface, therefore less electrical discharge density is exposed on the sample surface, which leads to a lesser degree of surface damage. The duration of electrical discharge has a significant effect on the extent of surface degradation; the longer the sample is exposed the higher is the degree of damage.

High amounts of ozone are normally generated and this requires some kind of extraction by a vacuum fan. During operation, warning signs should be observed, to avoid high levels of ozone exposure and any possible accidents.

### 3.2.2 UV-B exposure

The sun radiates energy in a wide range of wavelengths, most of which are invisible to the human eye. The shorter the wavelength the more energetic is the radiation and the greater the potential of it causing damage. UV radiation that reaches the earth's surface is in the wavelength range of 290 to 400 nm [13]. UV radiation plays an important role in our environment and often damages materials used outdoors. Although UV comprises only about 5% sunlight, it is responsible for most of the photochemical damage to materials [14].

UV radiations with different wavelengths have different effects. Radiation of longer wavelengths (320-400 nm) is referred to as UV-A, which causes sunburn of the skin. UV-B radiation (290-320 nm) causes damage at the molecular level to the fundamental building blocks of human DNA and also degrades polymeric materials [15]. To simulate the degradation caused by sunlight it is not necessary to reproduce the entire spectrum of sunlight; it is only the short wavelength of UV-B that must be reproduced. A secondary effect on outdoor insulators arises from corona discharge activity, when UV radiation is generated during light wetting and subsequent corona discharge.

To obtain a good correlation between the results of UV-B exposure obtained from the laboratory conditions and actual field conditions, a logical link must be introduced. UV duration and intensity to which samples were exposed in the laboratory were based on the effects observed by natural exposure of insulators to sunlight over a period of 10 years in outdoor high voltage applications. (See experimental section 4.4.3).

The focus of this study is therefore on determining the effect of UV-B on the ageing of NCIs in order to gain a better understanding of UV ageing mechanisms. An accelerated evaluation can be performed in a weatherometer or QUV tester. When results of tests performed at the Desert Sunshine Exposure Test (DSET) site in Arizona (considered to constitute the most severe natural ageing conditions in the USA) and QUV accelerated test were compared, a ratio of about 8:1 emerged, i.e. one hour of accelerated testing (in the laboratory) is equivalent to eight hours of exposure in the Arizona Desert [16].

### 3.2.3 Hydrolysis ageing (immersion in a synthetic acid rain solution)

Acid rain is a term used to describe fog and wet depositions of sulphates and nitrates. When oxides of sulphur ($SO_2$) and nitrogen ($NO_2$) are emitted through the burning of fossil fuels into the atmosphere they come into contact with water and are converted to sulphur and nitrogen based acids [14]. Acid rain alters an insulator by means of the introduction of conductive polar moieties to the insulator surface, changing it to a hydrophilic surface and increasing leakage current activity. Acid rain causes tracking and erosion of the insulator surface of housing materials, which in most cases leads to a rapid failure of the insulator [17]. It is therefore important to investigate the effect of acid rain on the performance of high voltage insulators.

To simulate the hydrolysis caused by acid rain, an artificial acid rain formulation was used. It contained the basic conductive electrolytic salts such as sodium chloride, ammonium chloride, nitric acid, potassium chloride and calcium sulphate. The ion content and composition was similar to the real acid rain.

A study by Wang et al. [18] was carried out to investigate the tracking and erosion caused by acid rain on polystyrene insulators. They used an artificial acid rain solution, which included the ingredients as tabulated in Table 3.1. They found that the higher the acid rain concentration to which insulator surfaces were exposed, the more severe the tracking and erosion were.

**Table 3.1: Composition of synthetic acid rain used for ageing of insulator samples [18]**

| Components | Concentration (g/l) |
|---|---|
| $NH_4Cl$ | 0.50 |
| NaCl | 1.27 |
| KCl | 0.09 |
| $HNO_3$ | 0.45 |
| $MgSO_4$ | 0.52 |
| $CaSO_4.2H_2O$ | 0.45 |

### 3.3 References


1. R. Anderson, B. Arkles and G. L. Larson, Silicone compounds (Register and Review), Petrach Systems, Bristol, PA, 1987.
2. T. G. Gustavsson, Silicone rubber insulators, PhD dissertation, Chalmers University of Technology, Sweden, 2002.
3. T. Kikuchi, S. Nishimura, M. Nagao, K. Izumi, Y. Kubota and M. Sakata, IEEE Trans. Diel. Elect. Insul., Vol. 6, 548-556, 1999.
4. J. W. Chang and R. S. Gorur, IEEE Trans. Diel. Elect. Insul., Vol. 1, 1039-1046, 1994.
5. H. F. Mark, N. M. Bikales, C. G. Overberger and G. Menges, Encyclopedia of Polymer Science and Engineering, John Wiley & Sons, New York, Vol. 5, 512-542, 1986.
6. A. Toth, I. Bertoti, M. Blazso, G. Banhegyi, A. Bognar and P. Szaplonczay, J. Appl. Polym. Sci., Vol. 52, 1293-1307, 1994.
7. http://www.hubbellpowersystems.ca/powertest/literature_library/pdfs4lib/OB/EU1234-H.pdf (10-06-2006).
8. http://www.answers.com/topic/corona-discharge?cat=technology (22-06-2006).
9. H. Hillborg and U. W. Geede, IEEE Trans. Diel. Elect. Insul., Vol 6, 703-717, 1999.
10. J. P. Reynders, I. R. Jandrell and S. M. Reynders, IEEE Trans. Diel. Elect. Insul., Vol. 6, 620-631, 1999.
11. Y. Koshino, I. Umeda and M. Ishiwari, IEEE Trans. Diel. Elect. Insul., Vol. 118, 638-688, 1998.
12. H. Hillborg and U. W. Gedde, Polymer, Vol. 39, 1991-1998, 1998.
13. V. M. Moreno, R. S. Gorur and A. Kroese, IEEE Trans. Diel. Elect. Insul., Vol. 10, 80-90, 2003.
14. N. Yoshimura, S. Kumagai and S. Nishimura, IEEE Trans. Diel. Elect. Insul., Vol. 6, 632-649, 1999.
15. J. Kim, M. K. Chaudhury and M. J. Owen, J. Coll. Interf. Sci., Vol. 226, 231-236, 2000.

16. R. A. Bernstorf, R. K. Niedermier and D. S. Winkler, Hubbell Power System, United States, Canada, 2000.
17. R. Hackam, IEEE Trans. Diel. Elect. Insul,. Vol. 6, 557-585, 1999.
18. X. Wang, L. Chen and N. Yoshimura, J. Phys. D: Appl. Phys., Vol. 33, 1117-1127, 2000.

# CHAPTER 4

# EXPERIMENTAL

## 4.1 PDMS samples

In this study use was made, first, of PDMS compounds of controlled formulations, prepared in our laboratory (see Section 4.2) that have relatively simple, known structures and compositions. This was required in efforts to interpret the results obtained upon degradation of the samples caused by different forms of accelerated ageing. Second, in parallel to these controlled formulation samples, six different commercial insulators (four PDMS based and two EPDM based) supplied by Eskom, were used. These included one virgin sample and a one-year field-aged sample. The samples were selected based on their relative electrical performance (performance of 75 insulators tested at the KIPTS site) as well as the preliminary results of material analysis. Analysis of the virgin materials was carried out in order to later compare these results with results obtained after laboratory-accelerating ageing and those obtained after natural-field ageing. The samples that were investigated in this study are tabulated in Table 4.1. The controlled formulations prepared in our laboratory were samples C, E, G, I and the commercial samples were samples J, K, L, M, N, and O.

A LMW form of uncrosslinked PDMS was obtained from Wacker Chemie (Germany) and used as a model compound to investigate the chemical effects of corona treatment on PDMS samples (Section 5.2.2.8).

**Table 4.1: Identification of samples used in this study**

| ID | Rubber type |
|---|---|
| C | PDMS / controlled formulation |
| E | PDMS / controlled formulation |
| G | PDMS /controlled formulation |
| I | PDMS / controlled formulation |
| J | PDMS / commercial sample |
| K | PDMS / commercial sample |
| L | EPDM / commercial sample |
| M | PDMS / commercial sample |
| N | EPDM / commercial sample |
| O | PDMS / commercial sample |

## 4.2 Synthesis of crosslinked polydimethylsiloxane

Controlled formulations of room-temperature vulcanized samples of PDMS were prepared in accordance with the instructions supplied by Wacker Chemie, (Germany).

The weight percentages of the following materials used to prepare the various PDMS formulations (in 100 g quantities) are tabulated in Table 4.2: virgin PDMS polymer (Mw 7000 g/mol), inhibitor, crosslinking agent, filler (silica or aluminium trihydrate), and platinum catalyst.

**Table 4.2: Formulations of PDMS (100 g samples) used in this study**

| ID | PDMS (g) | Crosslinking agent (g) | Fillers (g) | | Inhibitor (g) | Catalyst (g) |
|---|---|---|---|---|---|---|
| | | | Silica | ATH | | |
| C | 96.6 | 3.2 | - | - | 0.07 | 0.10 |
| E | 81.1 | 3.2 | 15.5 | - | 0.08 | 0.10 |
| G | 73.7 | 3.2 | - | 26.0 | 0.07 | 0.17 |
| I | 54.2 | 4.0 | 15.5 | 26.0 | 0.07 | 0.19 |

First, inhibitor was added to the virgin polymer to avoid premature crosslinking, followed by the addition of proportional amounts of the other components. The catalyst was added

while stirring, to prevent cluster formation prior to polymerization. All components were mixed well in order to achieve good dispersion of filler particles within the polymer matrix. The resultant mixture was placed in a steel mould on Teflon sheets in the presence of a mould-releasing agent. Samples were cured in a mould press for 15 min at 100 °C. Cured samples, with sizes of 6 mm thickness and 5.5 cm width and length, were placed in a vacuum oven at 100 °C for an hour to complete the curing.

Upon mixing the components prior to curing it was noticed that the crosslinking reaction occurred quite readily, especially during the summer when the ambient temperature was as high as 30-35 ˚C. This is because temperature accelerates the crosslinking reaction. The reaction mixture was therefore placed in a water bath at 15 ˚C to reduce the reaction rate, allowing sufficient time for better mixing. This was especially important in the case of filled formulations such as G and I, which require longer times for good mixing (filler particles must be dispersed within the polymer matrix to achieve smooth uniform films). Good mixing is also very necessary in the curing reaction in order to obtain a uniform film and prevent cluster formation.

### 4.3 Extraction of low molecular weight oligomers

Low molecular weight oligomers are believed to be the species responsible for hydrophobicity recovery of PDMS insulating materials [1] and hence it is important to characterize these species. They must however first be separated from the PDMS insulating materials, by means of appropriate separation techniques, and then their concentrations after accelerated ageing determined.

Chloroform was initially used to extract the LMW oligomers from the sample surfaces. However, chloroform is highly volatile and good extraction was not achieved; therefore hexane was subsequently used for sample extractions.

The PDMS samples to be extracted were cut into suitable dimensions (1 cm x 1 cm), immersed in 1 ml of hexane in labelled poly tops vials, and then left for 24 h at ambient temperature for the extraction to take place. Care was taken to ensure the same dimensions of the samples prior to LMW oligomers extraction, to limit variables.

## 4.4 Laboratory weathering methods

Various laboratory weathering ageing procedures were used in this study, including: corona ageing (needle corona and French corona), UV-B ageing, hydrolysis/acid rain ageing, and high-temperature treatment.

### 4.4.1 Needle corona ageing

A sample of an untreated insulator surface was cut to the appropriate dimensions (1 cm x 1 cm) and placed on a Petri dish, in a beaker. The distance between the needle tip of the discharger and sample surface was 5 mm. When the voltage was applied for 30 min, a violet-coloured glow appeared, coming from the needle tip, as ion bombardment striking the sample surface. The corona-aged sample was then stored in a clean Petri dish for static contact angle measurements. Care was taken to transfer the aged sample without mechanical deformation into the Petri dish, and also to eliminate other contaminants such as moisture and dust prior to analysis.

### 4.4.2 French corona ageing

Prior to French corona ageing, samples with the same thickness were cut to the appropriate dimensions (1 cm x 1 cm). This was necessary in order to attain the same electrical stress on the samples surfaces when high electrical voltage is applied. The sample surface to be exposed to corona was marked using a permanent marker to indicate the treated surface, and then the samples were packed on the glass plate covering the electrical electrode. The air gap between the sample surfaces and covering plate was fixed at 5 mm, to allow all samples to recieve the same surface stresses. The safety window was closed and then a high electrical voltage was slowly applied, until it reached 26 KV (maximum voltage). Samples were subjected to French corona for various periods of times. The aged samples were then stored in labelled Petri dishes to prevent contamination, prior to static contact angle measurements and further analysis.

### 4.4.3 UV-B ageing

Shorter UV wavelengths are believed to play a significant role in the degradation of outdoor insulating materials [2]. Therefore the effect of the UV-B light must be established. Insulators were cut to the appropriate dimensions (2 cm x 2 cm), labelled and stacked separately onto UV-B cabinet panels. Care was taken not to handle or cut the samples after ageing as this could interfere with the analyses. The sample surface should be parallel to the UV-B cabinet plate with the top surface 3 mm from the base sample plate.

The samples were aged in a QUV-type cabinet (Chemtra, ) under the following conditions: no moisture cycle, dry atmosphere/no rain cycle. The following full time exposure was performed: 100% duty (24 h per day), chamber temperature 43 ˚C. Commercially available UV-B lamps with a wavelength of 313 nm were used. The intensity of the radiation was measured once a fortnight, followed by replacement of the light bulbs to ensure consistent irradiation. UV-B ageing was carried out over a period of 1000 h to 8000 h. During this time, samples were taken at various intervals for testing, while ageing of the remaining samples continued, in order to determine any changes over an extended period of time.

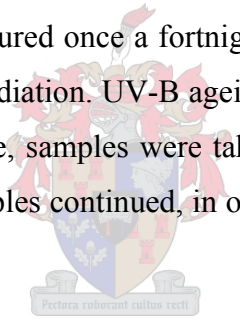

At each sampling time, static contact angles were measured to determine the degree of hydrophobicity, followed by optical microscopy analysis to characterize the surface morphology. An aged sample of each type was kept aside for further surface analysis, such as by SEM and FTIR.

### 4.4.4 Hydrolysis ageing using a synthetic acid rain solution

The synthetic acid rain solution used to age the samples was similar to the one discussed earlier in Section 3.2.3.

Prior to treatment, samples were cut to the correct dimensions (3 cm x 2 cm), with smooth edges. Samples from each formulation were placed in synthetic acid rain solution, in separate containers (to prevent cross-contamination of the possible soluble degradation products). Samples were immersed in an oil bath at 50 °C and left in the acid-rain

solution for 50 days, after which the initial characterization was carried out while the rest of the samples were kept in acid-rain solutions for additional periods to investigate any further possible material surface changes. After 50 days, samples were dried at ambient temperature, then kept in labelled Petri dishes for static contact angle measurements.

### 4.4.5 High temperature simulation of dry-band arcing (in-situ thermal analysis)

Surface morphology changes of insulator samples under conditions of dry-band arcing, caused by high temperature exposure, were investigated. Samples were exposed to elevated temperatures (400 °C) for short time durations (1 min) in a muffle oven, to simulate dry-band arcing conditions. Samples were removed from the oven using tongs, and then allowed to cool to ambient temperature. They were stored in Petri dishes to prevent contamination. The surface of the aged samples was visually characterized using an optical microscope, to investigate any surface changes. Samples were also analysed by TGA to monitor any changes in the samples. The experimental conditions were the following: 20±2 mg samples were heated at 40 °C/min to 400 °C, held isothermal for 1 min followed by rapid cooling, at 40 °C/min, to room temperature. The mass loss curve was determined by heating the sample at 10 °C/min to 550 °C.



## 4.5 Characterization

Characterization of samples was carried out using the following instrumental and analytical techniques.

### 4.5.1 Thermal gravimetric analysis (TGA)

The relative thermal stability was determined by TGA. Accurate TGA determinations require samples of about 20 mg, with uniform shaped surfaces. Analyses were carried out using a TGA-50 SHIMADZU thermogravimetric instrument with a TA-50WSI thermal analyzer connected to a computer, under a nitrogen atmosphere, with heating from room temperature to 700 ˚C, at a heating rate of 10 °C/min.

### 4.5.2 Static contact angle measurements (SCA)

A high-resolution digital camera (Sony CCD-IRIS model) was connected to a light microscope (Carl Zeiss, Axiolab) to capture the images.

The sample to be analyzed was placed horizontally to obtain well-defined dimensions. Deionised water (1 µl) was placed on the sample surface and within 5 sec an image of the water drop was captured. Control over the captured image dimensions was maintained by adjusting the magnification keys. Care should be taken to avoid surface contamination prior to SCA measurements. The SCA (θ) of the sample was determined using the following equation:

$$\tan(\theta/2) = h/r \qquad (4.1)$$

where: h is the height of the water drop and r is the radius.

Normally an average of 10 images (one image per a drop) for each sample is recommended to ensure reproducible measurements.

### 4.5.3 Optical microscopy (OM)

The light microscope that was used was a model of Carl Zeiss, Axiolab, connected to a CCD-IRIS SONY type digital camera to capture the images.

Visual observation was carried out to investigate surface features that appeared after the ageing. Various magnifications were used, ranging from 50 to 500, depending on the best resolutions obtained for the features concerned. Aged samples were kept in Petri dishes to avoid cross-contamination, such as by dust and moisture, which may interfere with the analyses. Images were taken on surface spots where they showed changes, followed by zooming in to detect any further features. Surface features can be in the form of cracks or roughness, depending on the type of treatment and the type of insulator.

### 4.5.4 Energy dispersive spectroscopy-scanning electron microscopy (EDS-SEM)

Imaging of the samples and analysis of phase compositions were accomplished using a Leo® 1430VP Scanning Electron Microscope at the Stellenbosch University.

Samples were identified with backscattered electron (BSE) and/or secondary electron images, and phase compositions were quantified by EDS analysis using an Oxford Instruments® 133KeV detector and Oxford INCA software. A typical EDS spectrum is shown in Figure 4.1.

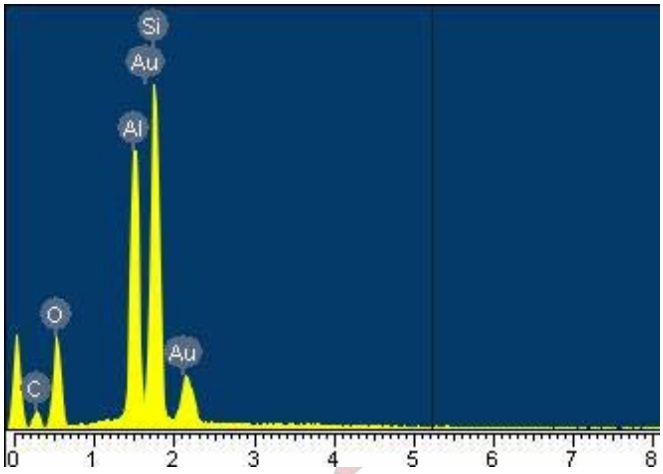


**Figure 4.1: EDS spectrum shows various elements of a PDMS insulator surface.**

This spectrum shows the various elements in a typical PDMS insulator. The C, O and Si peaks are due to the atoms in the basic structure of PDMS and the $SiO_2$ filler. The Al is the aluminum from the ATH filler and the Au (gold) is from the coating of the surface to make it more conductive. (This Au layer is important since the samples are insulators and can therefore not be analyzed by SEM directly.)

### 4.5.5 Gas chromatography (GC)

GC is a separation technique used to separate compounds of different molecular masses or composition in mixtures and also a quantitative tool to determine the concentrations of separated molecules. It is only applicable for volatile organic compounds with low boiling points because it can operate only up to 300 °C. Hence compounds with higher boiling points cannot be detected since samples must be in the gaseous phase. An advantage of this technique is that it is accurate, easy, fast, and does not require special sample preparation.

The gas chromatograph that was used in this study was a Perkin Elmer Autosystem XL instrument, equipped with a Quedrex 007 series 98% methyl-silicone capillary column (30 m x 0.32 mm I.D) and FID detector. Samples (1 µl) were injected manually and run for 30 min at a sampling rate of 12.5 parts per second. Nitrogen was used as the carrier gas, at a pressure of 23 kPa. The oven temperature programme was set as follows: initial temp: 80 °C, initial hold: 0.00 min, total run time: 30 min, maximum temp 350 °C, equilibration time 2 min, ramp 1:2/min to 100 °C, hold for 0.00 min, ramp 2:10/min to 250 °C, hold for 20 min. The injection port of the GC was set at 250 °C, and the detector was set at 300 °C.

### 4.5.6 Size-exclusion chromatography (SEC)

SEC is the most commonly used technique to determine polymer molar masses based on size in solution. A PDMS sample was dissolved in THF (5 mg/ml) and filtered through a 0.45-µm nylon filter. Analysis was performed with a system comprising a Waters 2690 Separations module (Alliance), Plgel column mixed E, 5 µm and 300 X 7.5 mm (X1) (Polymer Laboratories). The column oven was set at 30 ˚C. The THF solvent flow rate was 1.0 ml/min, and the injection volume was 100 µl. The following detection system and conditions were used: PL-ELS 1000 evaporative light scattering detector with nebuliser at 40 $^{o}$C and evaporating chamber at 90 $^{o}$C, and a $N_2$ carrier gas flow rate of 1 SLM (standard liters per minute).

### 4.5.7 Fourier-transform infrared photo-acoustic spectroscopy (FTIR-PAS)

Infrared techniques provide important information concerning the chemical bonds in PDMS surface layers. The principle of FTIR-PAS is based on a modulated infrared beam from the FTIR spectrometer that strikes the sample, the light is absorbed and produces heat that alters the pressure of the surrounding gas. The changing pressure is detected as sound by a microphone and is then converted to an absorption spectrum, which is used to identify and quantify the sample [3].

The chemical composition of the surface structure of the samples after the various accelerated weathering, including needle corona, French corona, UV and acid rain, was

carried out using a Perkin Elmer FTIR Spectrometer PARAGON 1000 PC instrument. Carbon black was used as a background scan. Both virgin and aged samples were characterized to investigate the relative changes in surface composition in the form of various absorption bands present in the surface, including OH, CH in methyl groups, Si-$CH_3$ and Si-O-Si were detected in the FTIR spectrums.

### 4.5.8 Positron annihilation spectroscopy (PAS)

Positron annihilation spectroscopy (PAS) is a unique technique and well recognized as a powerful nano-probe for microstructural analysis of polymeric materials [3-6]. PAS is able to directly determine the free-volume properties in polymeric materials. Positrons ($e^+$) are the anti-particles of electrons ($e^-$). Typically they are produced in a radioactive source such as Sodium-22 and Germanium-68. When they come in contact with electrons they can form positronium (Ps), which is the bond state of an electron, and positron. Positronium can be formed in two states: para-positronium (spins anti-aligned) (p-Ps) and ortho-positronium (o-Ps). The positron and electron have parallel spin (spins aligned). The formation probability for these two states is 1:3. However, o-Ps has a longer lifetime in molecular substrates [7]. Positron analytical techniques are based on the measurement of the annihilation radiation produced when positrons are implanted into a polymer matrix and the electron in the polymer matrix meet and annihilate. The annihilation occurs since a positron is essentially the anti-matter of an electron. During annihilation both the positron and electron are destroyed and the masses of each converted to energy (photons).

As mentioned above, the basic principle of PAS lies in the fact that the electromagnetic interaction between electrons and positrons leads to the annihilation of the $e^+$- $e^-$ pair, in which the total energy of the pair is transferred to photons. These annihilation gamma photons carry information on the electronic environment in which the positron annihilates. In polymers, the positronium atoms formed are localized in the free volume holes of the polymer. The annihilation characteristics of the positronium atoms contain information about the nature of the free volume holes. Due to the localization of the positronium in the open spaces, the positron annihilation technique has proven to be the

most sensitive technique for tracking changes that occur in a polymer structure. Positron annihilation lifetime spectroscopy can provide important information on defect size and concentration, and on open volume defects in most solid materials [8].

There are other methods available for the general detection of open volume defects. Some of the best known are the microscopic techniques such as transmission electron microscopy (TEM), AFM, SEM and OM. Others are neutron scattering (NS), scanning tunneling microscopy (STM) and X-ray scattering (XS). As is shown in Figure 4.2, all have specific regions of sensitivity and resolution.

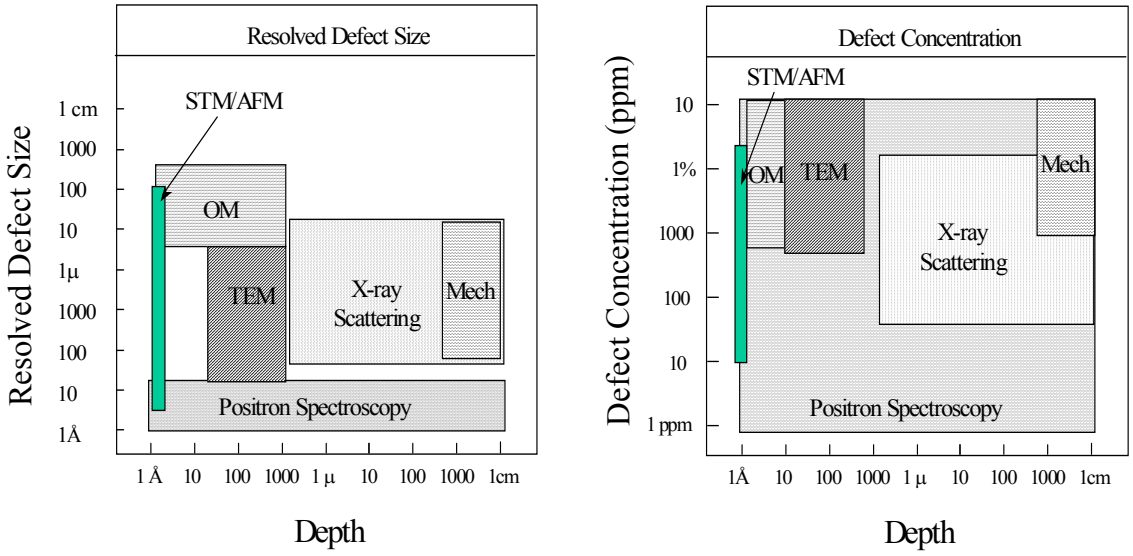


**Figure 4.2**: **Schematic representation showing that PAS analysis has a special position in vacancy defect analysis over OM, NS, TEM, STM, AFM and XS [6].**

Positron annihilation lifetime spectroscopy is however very sensitive and hence useful; it provides information on defect sizes at any sample depth, below the effective resolution of the other techniques mentioned above.

In this study the positron beam results will be reported as the S parameter or defect parameter, as calculated from Doppler broadening energy spectra. The S parameter is defined as the ratio of the central area to the total area of the 511 keV annihilation peak after the background is subtracted. Figure 4.3 shows an example of a Doppler broadening

energy spectrum and the definition of the S parameter. The energy parameters ($E_1$ and $E_2$) are chosen so that the value of the S parameter = 0.50 for pure silicon.

In polymeric materials the S parameter represents the contribution of the low momentum part of the positron-electron annihilation radiation in sub-nanometer defects, such as free volume and holes [6].

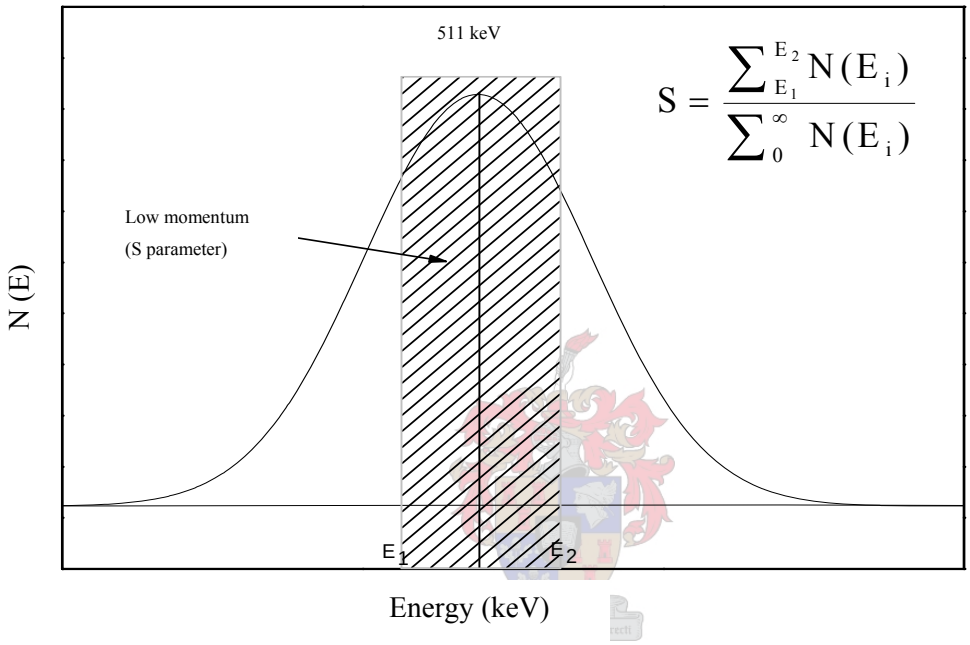


**Figure 4.3: Doppler broadening energy distribution of annihilation radiation showing the definition of the S parameter.**

When a positron with well-defined energy is accelerated from a vacuum into a polymer, it either reflects back to the surface or penetrates into the polymer. The fraction of positrons penetrating the polymer substrates increases rapidly as a function of positron energy. This means that implementation depth as a result of inelastic interactions with polymer molecules is expressed as [7]:

$$Z(E_+) = \left(\frac{40 \times 10^{3}}{\rho}\right) E_+^{1.6} \qquad (4.2)$$

where Z is the thickness of the material in nanometers, $\rho$ is the density of the PDMS material in kilograms per cubic meter, and $E_+$ is the incident energy in kilo electron volts (keV).

The depth profiling information on the free volume properties of a polymer can therefore be obtained by controlling the implantation energy, varying it from 0.1 keV to 30.0 keV, and can provide information on the free volume from the very near surface region (<1 μm from the surface) to the bulk (±9 μm from the surface).

As mentioned earlier, in this study the positron beam results are reported as the S parameter or defect parameter, as calculated from Doppler broadening energy spectra. The positron beam measurements were performed on the variable mono-energetic positron-beam at the University of Missouri, Kansas City, USA. A detailed description of the procedure is described by Zhang et al. [8].

**4.6 References**

1. V. M. Moreno, R. S. Gorur and A. Kroese, IEEE Trans. Diel. Elect. Insul., Vol. 10, 80-95, 2003.
2. H. F. Mark, N. M. Bikales, C. G. Overberger and G. Menges, Encyclopedia of Polymer Science and Engineering, John Wiley & Sons, New York, Vol. 5, 539, 1986.
3. N. Yoshimura, S. Kumagai and S. Nishimura, IEEE Trans. Diel. Elect. Insul., Vol. 6, 632-650, 1999.
4. Y. C. Wu, C. Huang, Y. Ll, R. Zhang, H. Chen, P. E. Mallon, J. Zhang, T. C. Sanderczki, D.M. Zhu, Y. C. Jean, R. Suzuki and T. Ohdaira, J. Polym. Sci. Part B, Polym. Phys., Vol. 39, 2290-2301, 2001.
5. Cao, Y. He, R. Zhang, J. P. Yuan, T. C. Sanderczki, Y. C. Jean and B. Nielsen, J. Polym. Sci. Part B, Polym. Phys., Vol. 37, 1289-1305, 1999.
6. Y. C. Jean, P. E. Mallon and D. M. Schrader, Principles and applications of Positronium and Positronium Chemistry, World Scientific Publishing, Singapore, 2003.

7. H. Cao, R. Zhang, C. S. Sundar, J. P. Yuan, Y. He, T. C. Sandreczki and Y. C. Jean, Macromolecules, Vol. 31, 6627-6635, 1998.
8. R. Zhang, H. Cao, C. M. Huang, P. E. Mallon, T. C. Sandreczki, J. R. Richardson, Y. C. Jean, B. Nielsen, R. Suzuki and T. Ohdaira, J. Radiat. Phys. Chem., Vol. 58, 639-644, 2000.

# CHAPTER 5

# RESULTS AND DISCUSSION

## 5.1 Characterization of virgin materials

It was necessary to characterize the virgin samples in terms of their surface properties such as surface wettability (hydrophobicity), surface morphology and thermal stability before any accelerated ageing was done in order to gain a clear idea about the surface conditions of the insulators under study. This information was to be used as a baseline, from which to track the material changes as a result of accelerated ageing, and would facilitate drawing a meaningful comparison between untreated and aged samples. In the case of the commercial samples, TGA analysis was also used to determine the composition of the different NCI materials.

### 5.1.1 Compositional analysis by TGA

TGA analysis was performed on virgin samples of both controlled formulations and commercial insulators to evaluate the relative thermal stability of the different compositions as well as to determine the composition of the commercial insulators. TGA analysis for compositional determinations already forms part of the recommended procedures for the fingerprinting of commercial NCI materials. The TGA thermograms of controlled samples C, E, G and I are shown in Figure 5.1.

The weight remaining after the TGA experiment is due to the fillers and non-volatile degradation compounds. Basically, NCIs contain mainly inorganic silica ($SiO_2$) and ATH ($Al_2O_3.(H_2O)_3$) as fillers. Silica in PDMS is a reinforcing filler used to provide the tensile strength needed. The ATH also adds mechanical strength and provides protection against the high temperature that may develop during electrical discharge. See also Sections 2.3 and 2.5.

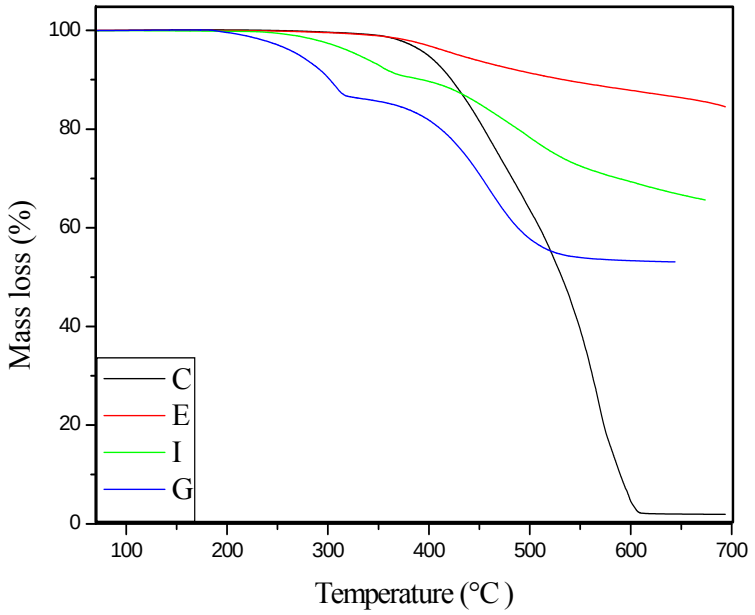


**Figure 5.1: TGA thermograms of controlled formulation samples C, E, G and I.**

A summary of the TGA results of the controlled formulation samples is displayed in Table 5.1.

**Table 5.1: TGA analysis of the controlled formulations samples C, E, G and I**

| ID | Sample mass (mg) | T (ºC) per mass loss | | | Mass loss (%) as a function of temperature | | | T Onset1 (ºC) | T Onset2 (ºC) | Residue (%) | ATH filler (%) |
|---|---|---|---|---|---|---|---|---|---|---|---|
| | | 2% | 5% | 10% | 350 ºC | 450 ºC | 550 ºC | | | | |
| C | 14.8 | 375 | 400 | 425 | 100 | 83 | 38 | - | 399 | 3.0 | - |
| E | 17.3 | 385 | 430 | 535 | 100 | 94 | 90 | - | 415 | 87.3 | - |
| G | 11.0 | 245 | 265 | 310 | 85 | 72 | 54 | 285 | 410 | 45.0 | 25.0 |
| I | 16.3 | 300 | 335 | 410 | 93 | 85 | 73 | 320 | 420 | 65.0 | 25.3 |

The TGA thermograms in Figure 5.1 show a significant effect of the sample compositions. The TGA curves of samples G and I show two separate mass losses. The first occurs at a low temperature ($T_1$) and is associated with the dehydration of ATH filler present in the formulations. The ATH loss curve is shown later in Figure 5.6. The second mass loss occurs at a higher temperature ($T_2$), which corresponds to the onset of polymer degradation.

Samples C and E show only a single mass loss at high temperature, which indicates the degradation of PDMS polymer.

Sample I has the highest polymer degradation temperature ($T_2$), followed by samples E, and G, and sample C which has the lowest, as shown in Table 5.1. The presence of ATH filler in samples G and I has the potential advantage in that it decomposes to aluminium oxide and water molecules when heated above 200 ˚C. The liberation of water is endothermic and the surface is cooled, which may provide protection to the polymer surface during arcing on the surface.

In order to investigate the role of filler particles on the thermal stability of the resulting filled PDMS samples it is necessary to obtain the net corrected mass losses of the actual polymer degradation of the filled samples by excluding the amount of filler in the formulations and then the corrected temperatures for a specific polymer mass can be extrapolated. The results are shown in Table 5.2. The percentage mass losses in Table 5.2 refer to the second mass loss, which corresponds to the degradation of the polymer. This gives a clear indication of where the actual polymer degradation occurs as well as an indication of the rate of the polymer degradation.

**Table 5.2: The temperature onsets for the corrected mass loss of the controlled formulation samples C, E, G and I**

| ID | Sample mass (mg) | Polymer mass percent (%) | Polymer mass (mg) | Corrected T (ºC) at 2% mass loss | Corrected T (ºC) at 5% mass loss | Corrected T (ºC) at 10% mass loss |
|---|---|---|---|---|---|---|
| C | 14.8 | 100.0 | 14.8 | 375 | 400 | 425 |
| E | 17.3 | 84.5 | 14.7 | 390 | 425 | 540 |
| G | 11.0 | 58.5 | 8.3 | 340 | 395 | 415 |
| I | 16.3 | 74.0 | 12.3 | 395 | 435 | 475 |

The data in Table 5.2 for the corrected percentage polymer mass loss shows that the formulation also has an effect on the rate of the polymer mass loss during the degradation. In general, in the case of the presence of a filler, the polymer degrades at a

higher temperature and the rate of mass loss is lower than the unfilled sample, as is indicated by the smaller temperature intervals between the 2, 5 and 10% corrected mass loss for sample C compared to the filled samples.

TGA thermogram of the commercial samples are shown in Figure 5.2 and data are summarised in Table 5.3.

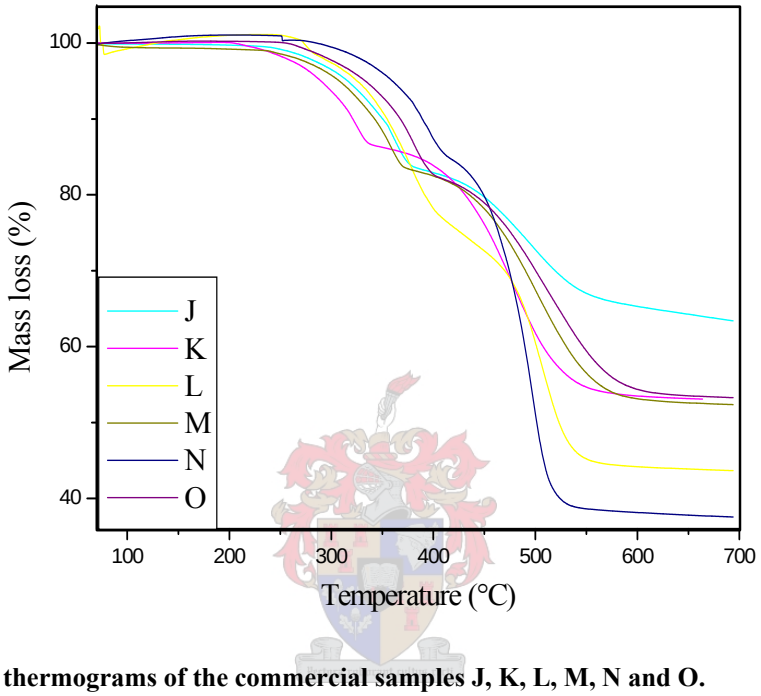


**Figure 5.2: TGA thermograms of the commercial samples J, K, L, M, N and O.**

**Table 5.3: TGA analysis of commercial samples J, K, L, M, N and O**

| ID | Sample mass (mg) | T (ºC) per mass loss | | | Mass loss (%) as a function of temperature | | | T Onset1 (ºC) | T Onset2 (ºC) | Residue (%) | ATH filler (%) |
|---|---|---|---|---|---|---|---|---|---|---|---|
| | | 2% | 5% | 10% | 350ºC | 450ºC | 550ºC | | | | |
| J | 11.0 | 280 | 320 | 350 | 90 | 80 | 67 | 295 | 375 | 66.0 | 25.0 |
| K | 9.0 | 250 | 290 | 320 | 87 | 77 | 54 | 310 | 350 | 52.1 | 32.1 |
| L | 17.3 | 290 | 330 | 360 | 91 | 73 | 55 | 305 | 373 | 47.0 | 20.0 |
| M | 8.3 | 275 | 315 | 340 | 89 | 78 | 57 | 290 | 365 | 52.4 | 28.2 |
| N | 16.3 | 330 | 360 | 385 | 94 | 80 | 40 | 330 | 420 | 38.4 | 13.0 |
| O | 18.0 | 290 | 335 | 370 | 92 | 79 | 60 | 320 | 400 | 53.0 | 28.7 |

In the TGA curve the first mass loss in the graph corresponds to the degradation of the ATH filler at lower temperature and the second mass loss is correlated to the onset of polymer degradation. The TGA curves show that all the samples contain ATH filler. In the case of the PDMS based compounds, sample K has the lowest onset temperature for the polymer degradation and sample O has the highest.

The two EPDM commercial samples, L and N show rapid mass loss during the polymer degradation step.

The difference in the thermal behaviour between the PDMS and EPDM samples is attributed to the variation in the relative thermal stability between the two types of materials. The PDMS samples have a better thermal stability towards high temperatures than EPDM samples due to the high dissociation energy of the siloxane bonds, namely 445 kJ/mol [1]. The dissociation energy of the Si-C bond is lower, namely 306 kJ/mol. However, the methyl groups on silicone have a higher thermal and oxidative stability than a methyl group on a hydrocarbon chain, such as polypropylene in the EPDM. The partial polar ionic nature of the siloxane bond has a dipolar arrangement, where the silicone atom carries the partial positive charge and the oxygen atom the partial negative charge. This results in a greater stability of this bond. The silicone atom can act as an electron drain, polarizing the methyl group and rendering it less susceptible to attack than its bond energy suggests [2]. Another possible reason for the high thermal stability may be explained by the findings of Hillborg and Gedde [3] who reported that thermal ageing of silicone rubber in air led to the formation of an inorganic silica-like layer caused by oxidative crosslinking. This protects the bulk from further oxidation, therefore increasing the thermal decomposition temperature. In the case of EPDM rubber, prolonged exposure to thermal ageing leads to the formation of carbon on the surface. This is conductive and results in the insulator surface conductivity increasing, which may lead to an increased leakage current. In the latter stages of degradation the EPDM surface degrades, cracks and filler particles are exposed on the surface as a white layer.

### 5.1.2 Static contact angle measurements and surface roughness

Static contact angle measurements were performed on the virgin samples. Table 5.4 tabulates the average static contact angle values obtained for the virgin samples.

**Table 5.4: Average static contact angles of the virgin samples**

| ID | Average static contact angle (degrees) |
|---|---|
| C | 107 |
| E | 111 |
| G | 115 |
| I | 108 |
| J | 109 |
| K | 106 |
| L | 90 |
| M | 107 |
| N | 84 |
| O | 101 |

Most virgin samples have SCA values > 90°, which clearly demonstrates that they have a hydrophobic character. The two commercial EPDM samples L and N show the least hydrophobic character, with SCA values of 90° and 84° respectively.

During the moulding of some insulators, fabrication lines were introduced on the surface to improve the hydrophobicity of the materials. It is believed that these lines increase the hydrophobicity of the surface by introducing a "roughness" to the surface. The extent of hydrophobicity of the surface can be controlled to some extent by controlling the distances between fabrication lines. Three commercial insulators in this study show such lines, as is illustrated in the SEM images of the surfaces shown in Figure 5.3.

The distance between the fabrication lines on the sample surface, obtained from SEM images, was calculated by measuring the distance from a fixed central point of a line to a central point on a neighboring line on the insulator's surface. An average of four readings

from different sampled areas was determined and recorded. The data are displayed in Table 5.5.

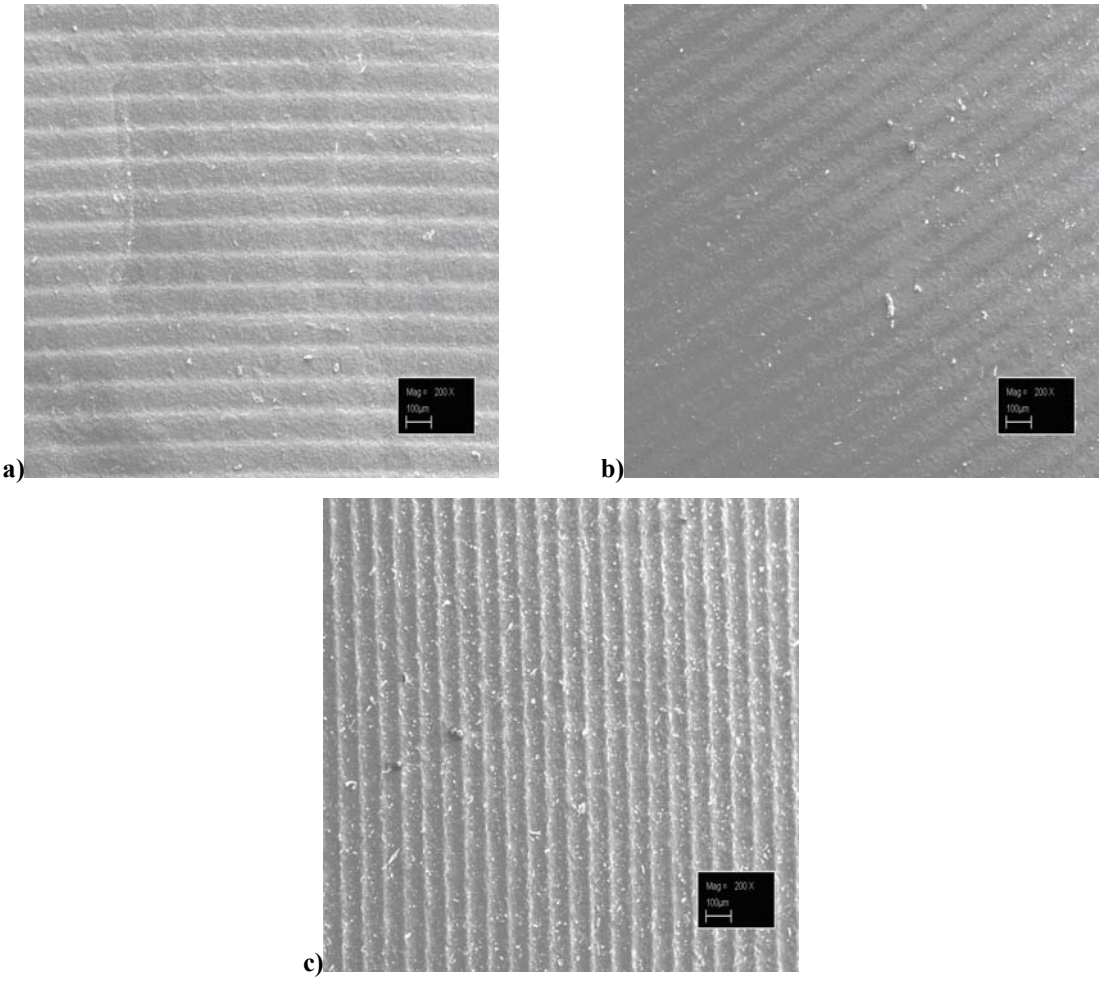


**Figure 5.3: SEM images of typical insulators showing lines on the surface: (a) sample J, (b) sample K, and (c) sample O.**

A direct relationship between the average line distances and an increase in static contact angle values was found in this study. These results illustrate the importance of not only the nature of the material used in insulator sheds, but also the nature of the surface in terms of the roughness.

**Table 5.5: The distance between surface fabrication lines on the surface of the commercial insulators**

| ID | Distance between lines* (µm) | Average distance between lines (µm) | Average SCA of virgin samples (degrees) |
|---|---|---|---|
| J | 95.7 | 92.2 | 109 |
| | 91.6 | | |
| | 88.4 | | |
| | 93.0 | | |
| K | 95.1 | 90.4 | 106 |
| | 90.0 | | |
| | 86.5 | | |
| | 89.8 | | |
| O | 73.9 | 66.3 | 101 |
| | 59.6 | | |
| | 63.1 | | |
| | 68.8 | | |

*Distance recorded at 500 Mag

### 5.1.3 FTIR analysis

The chemical nature of the virgin samples was investigated by means of FTIR-PAS. The technique provides qualitative information regarding the relative changes in the PDMS surface chemical structure after accelerated ageing, which can be very helpful in determining any changes in the surface properties. Figures 5.4 (a) and (b) show the FTIR spectra of the virgin controlled formulation samples C, E, G and I and the commercial samples J, K, L, M, N and O, respectively.

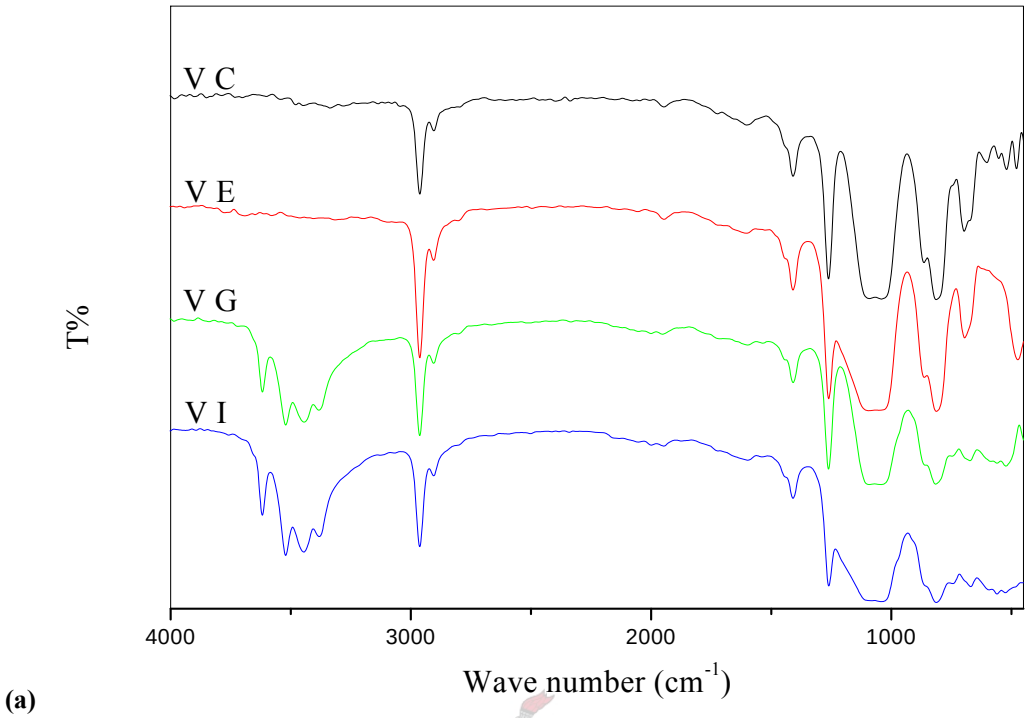


**(a)**

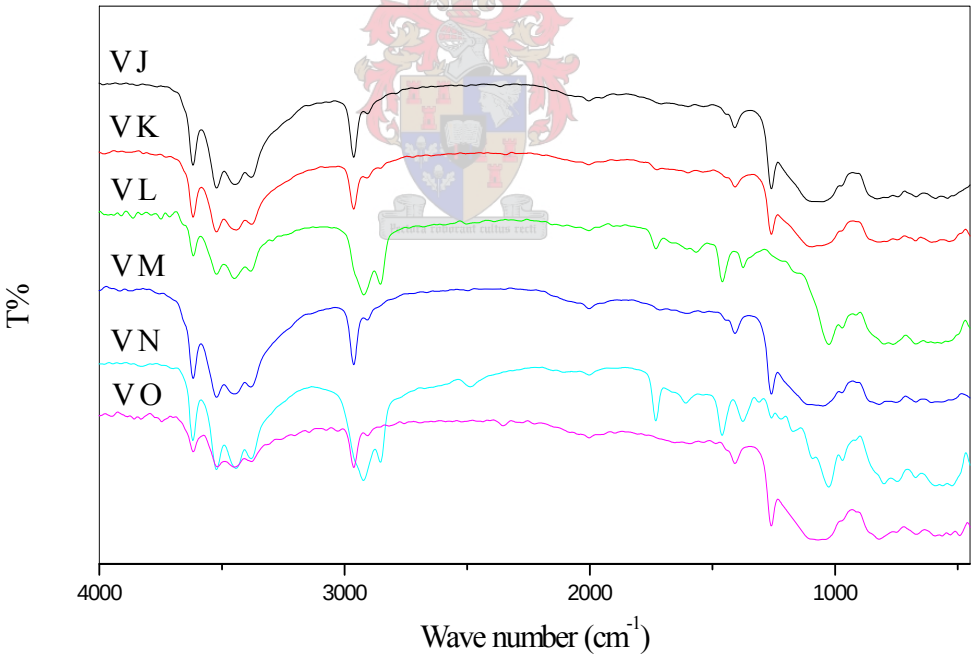


**(b)**

**Figure 5.4: FTIR spectra of (a) virgin (V) controlled formulation samples C, E, G, I and (b) virgin commercial samples J, K, L, M, N and O.**

**Table 5.6: IR spectroscopic data of PDMS and EPDM virgin samples**

| Wave number ($cm^{-1}$) | Bond |
|---|---|
| 3600-3300 | OH |
| 2962-2955 | CH in $CH_3$ |
| 2955-2854 | $CH_2$ |
| 1730-1680 | CO |
| 1480-1300 | OH in $H_2O$ |
| 1262-1250 | Si-$CH_3$ |
| 1090-1000 | Si-O-Si |
| 870-750 | Si-$(CH_3)_2$ |

The FTIR spectra show the various characteristic absorption bands of the PDMS sample, which include CH bonds from methyl groups at 2962-2955 $cm^{-1}$, Si-$CH_3$ from side chains at 1262-1250 $cm^{-1}$, Si-O-Si bonds in the main chain at 1090-1000 $cm^{-1}$ and Si$(CH_3)_2$ at 870-750 $cm^{-1}$ appear in the spectrum of unaged samples C and E. In the case of samples G, I and commercial samples J, K, L, M, N and O however, additional absorption bands such as OH groups appear at 3600-3300 $cm^{-1}$, and $H_2O$ at 1480-1300 $cm^{-1}$ since the former and the latter correspond to the ATH filler present in their formulation. EPDM samples L and N exhibit sharp absorption bands at 1730-1680 $cm^{-1}$ corresponding to C=O and dual absorption bands at 2955-2854 $cm^{-1}$, which correspond to the $CH_3$ and $CH_2$ groups respectively. The absorption bands at 1090-1000 $cm^{-1}$ of PDMS samples are broad.

## 5.2 Accelerated ageing

### 5.2.1 Thermal ageing

It is known that during dry-band arcing the polymer surfaces of NCI can be exposed to instantaneous high temperature (as high as 400 ºC) [4]. Commercial analyses done on the KIPTS insulators have shown that there are significant differences in the various material performances. In a thermal stability study, this section discusses the development of an in-situ TGA thermal stability method and show the effects of the ATH filler on the

material performance. This may offer an alternative to the currently recommended thermal ageing procedure. The study was conducted on the various controlled formulation RTV PDMS compounds to investigate the effect that high temperature exposure has on these compounds.

This was done by rapidly heating samples in the TGA to a temperature of 400 ºC, holding the temperature for 1 min and then rapidly cooling the sample to about 80 ºC, followed by reheating at a rate of 10 ºC/min. The results of this study on the controlled formulation samples are shown in Figure 5.5. The percentage mass losses during the isothermal treatment of the various samples are shown in Table 5.7. From the results it is clear that samples G and I show the largest percentage mass loss during the isothermal treatment relative to samples C and E. Sample E shows only a 1.5% mass loss while samples G and I show a 10% mass loss. Samples G and I contain ATH filler while C and E do not. The higher percentage mass loss of G and I must be attributed to the effect of the ATH filler.

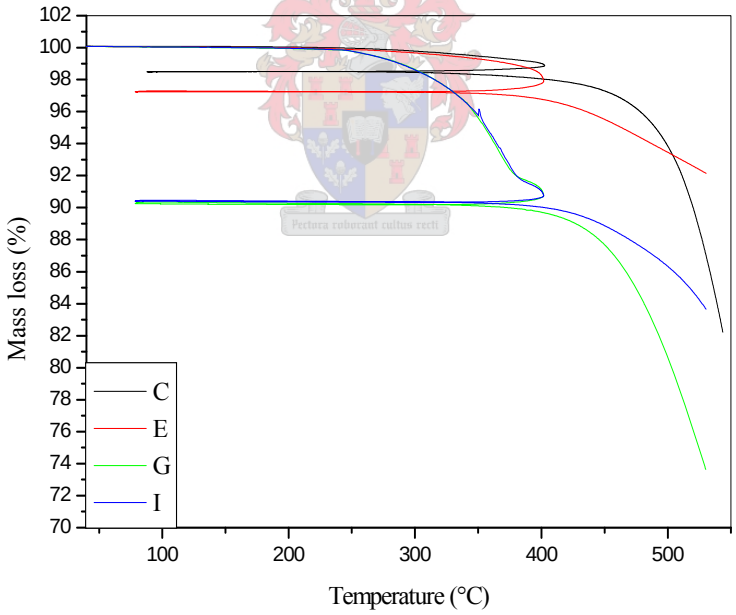


**Figure 5.5: TGA isothermograms of samples C, E, G and I at 400 ˚C.**

On reheating after isothermal treatment, samples C and E show a similar trend to the conventional TGA curve in Figure 5.1. Samples G and I, on the other hand, show that on reheating there is a deviation, which is due to the dehydration of the ATH filler in the initial heating experiment.

**Table 5.7: Mass losses and temperature onsets of samples C, E, G and I after 400 °C isothermal TGA**

| ID | Sample mass (mg) | Sample mass loss (%) | T onset on second heating (˚C) |
|---|---|---|---|
| C | 23.7 | 3.0 | 465 |
| E | 22.9 | 1.5 | 468 |
| G | 23.7 | 10.0 | 445 |
| I | 20.9 | 10.0 | 460 |

Figure 5.6 shows the TGA mass loss curves for the pure ATH and $SiO_2$ fillers. As expected, the $SiO_2$ filler shows a very high thermal stability even at extremely high temperatures. The ATH filler on the other hand shows a rapid mass loss at about 250 °C. This is associated with a dehydration of the filler. The percentage mass loss indicates that all three of the $H_2O$ hydrates are lost at a temperature of 600 ºC and only the residual $Al_2O_3$ remains. It is believed that this dehydration of the ATH filler when exposed to elevated temperature, has a "cooling" effect when ATH is included in NCI materials. This helps to prevent the degradation of the polymer material during dry-band arcing.

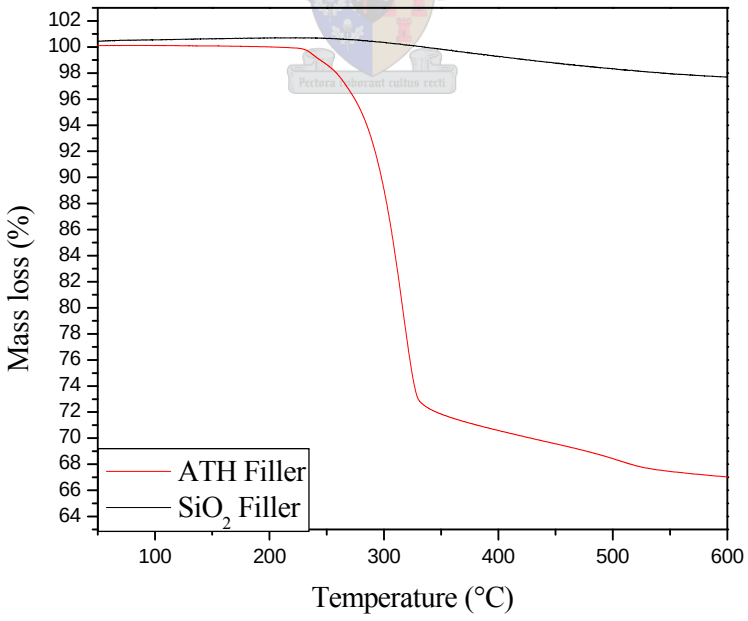


**Figure 5.6: The TGA mass loss curves of pure ATH and $SiO_2$ fillers.**

Figure 5.7 (a) shows the TGA curve for sample I obtained for the virgin materials and the same curve for the sample that had been isothermally treated at 400 ºC for 1 min. Similar plots are shown for samples G, C and E in Figures 5.7 (b), (c) and (d) respectively. In both samples G and I the heating after the thermal treatment shows the absence of the first mass loss observed for the virgin samples. This is a clear indication that the first mass loss in the ATH samples is associated with the dehydration of the ATH filler. After 1 min isothermal treatment the dehydration reaction is more or less complete. This is most obvious in sample G, where the second heating mass percentage corresponds exactly to the mass loss in the first heating of the virgin material. The results of this study suggest that there is a limited capacity of the ATH filler to provide protection against high temperature degradation by the dehydration cooling effect. The practical implication is that if localized dry-band arcing has occurred on a specific spot on the insulator surface, the ability to prevent further degradation due to dry-band arcing at the same spot is significantly reduced.

In the case of samples C and E the reheated samples show a less dramatic difference on the second heating. In all cases it is noticed that the onset of the degradation mass loss of the polymer occurs at a higher temperature than that of the virgin materials. This is most noticeable in the case of sample C, where there is a large increase in the degradation temperature after the thermal treatment.

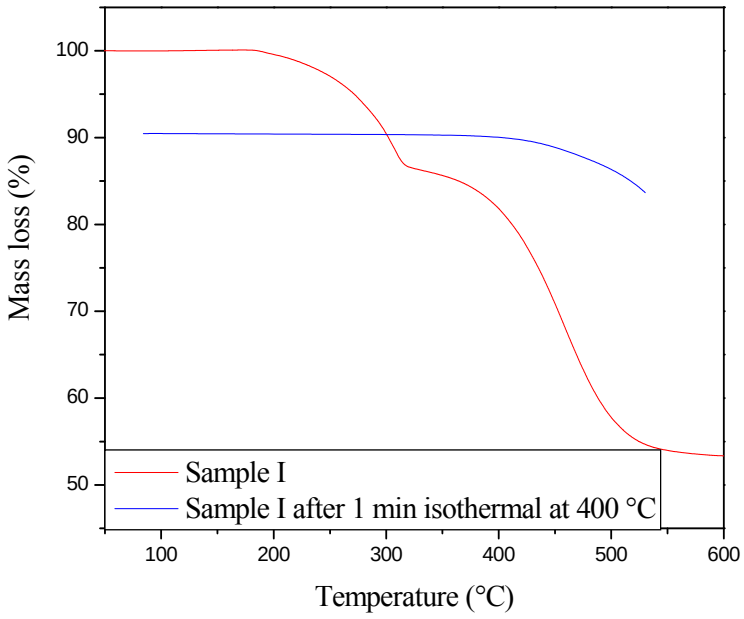
Mass loss (%)
100
90
80
70
60
50
100
200
300
400
500
600
Temperature (°C)
Sample I
Sample I after 1 min isothermal at 400 °C

**(a)**

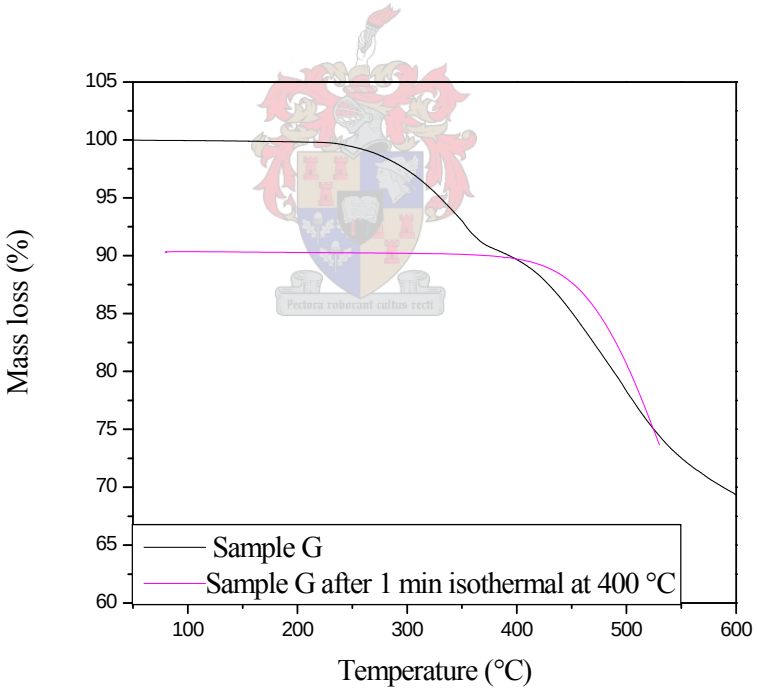
Mass loss (%)
105
100
95
90
85
80
75
70
65
60
100
200
300
400
500
600
Temperature (°C)
Sample G
Sample G after 1 min isothermal at 400 °C

**(b)**

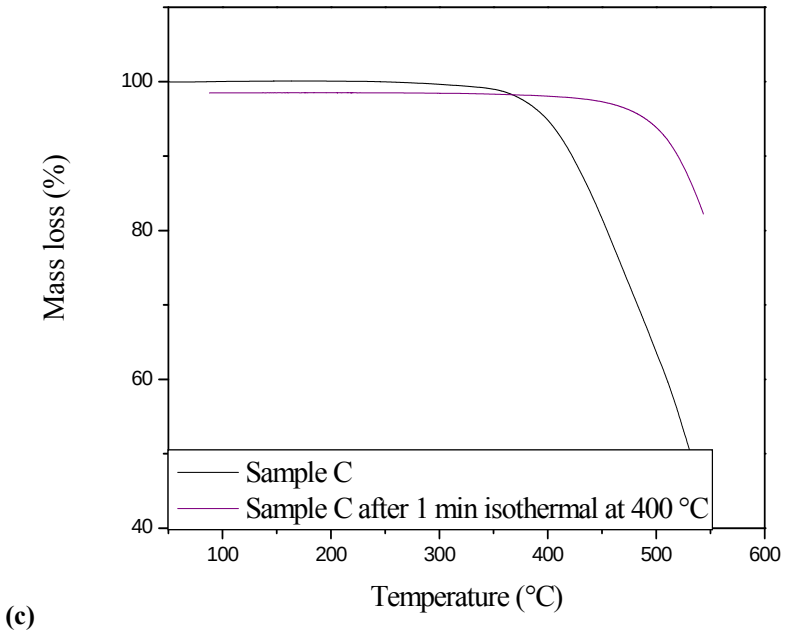


**(c)**

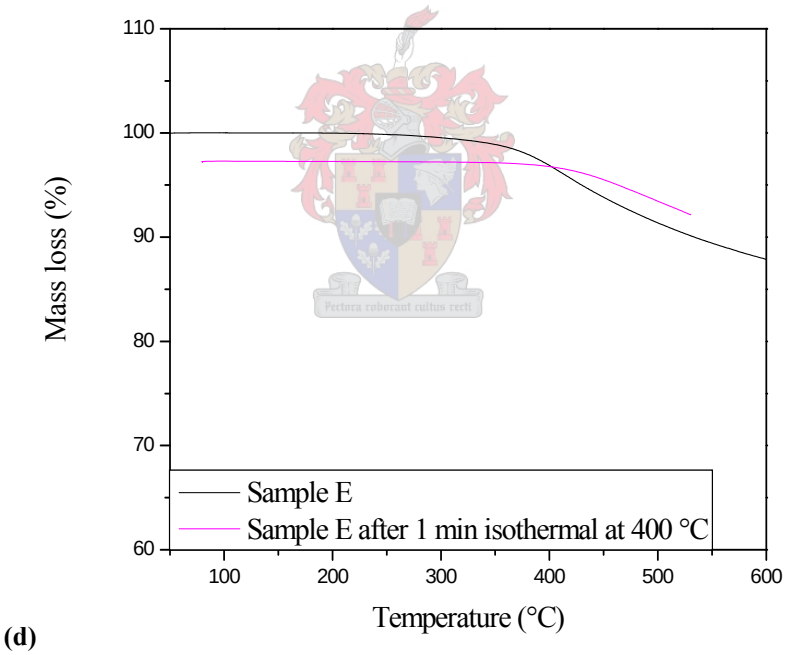


**(d)**

**Figure 5.7: TGA curves of virgin samples and samples isothermally treated at 400 °C for 1 min, (a) sample I, (b) sample G, (c) sample C and (d) sample E.**

The thermally aged sample surfaces were investigated using an optical microscope. The images of the virgin (left) samples and the corresponding aged ones (right) are shown in Figure 5.8 (a)-(f) for samples C, G and I respectively.

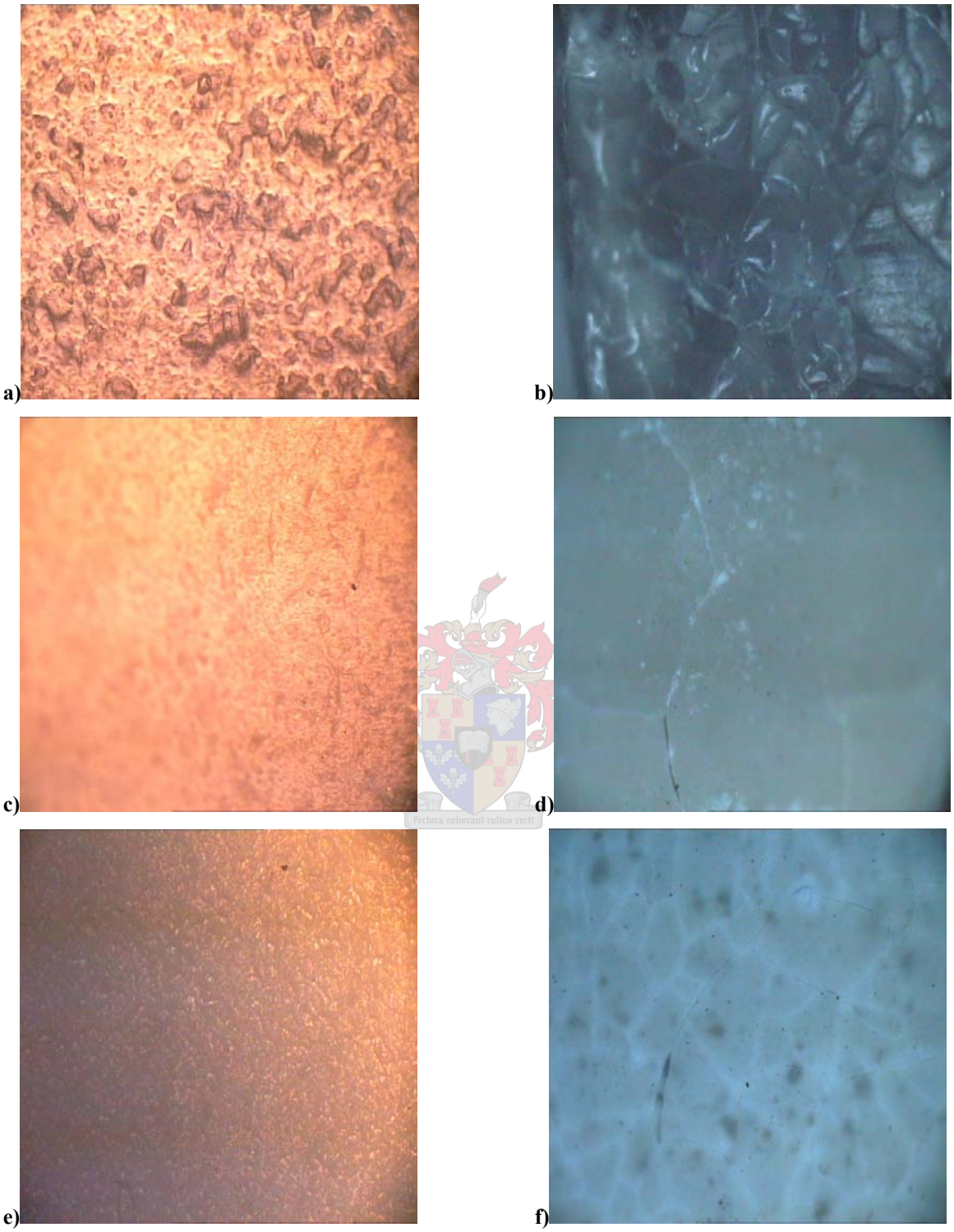


**Figure 5.8: Optical microscope images of (a) virgin sample C, (b) aged sample C, (c) virgin sample G, (d) aged sample G, (e) virgin sample I and (f) aged sample I isothermally treated at 400 ºC for 1 min.**

The visual observation of sample C shows that the surface features changed after thermal treatment relative to the virgin sample. Samples G and I show cracks on their surfaces when compared with the virgin samples. The changes in the surface features can be associated with the "steam" that is released in the ATH filled samples during the isothermal treatment.

### 5.2.2 Corona ageing

One of the most important factors that can lead to deterioration in the polymer materials in NCIs is the effects of corona treatment. There are many different types of laboratory ageing regimes for corona exposure. It is well known that not all of these accelerated corona ageing techniques have the same effect on the polymer materials. Two different types of corona ageing were investigated to determine the relative effects of these ageing regimes. Various techniques were used to track the relative changes in the materials after treatment. Slow positron beam techniques were used to estimate the degree of $SiO_x$ formation for each of the treatment regimes.

#### 5.2.2.1 Hydrophobicity recovery

A water drop, when in contact with a 30 min needle corona aged pure PDMS sample surface, immediately after treatment, forms a completely continuous wetting film on the surface. This is associated with a very small static contact angle (nearly 0º). After a period of time, the water drop becomes discrete, as a result of progressive regain in hydrophobicity, until it recovers fully after a day. The hydrophobicity recovery rate is more rapid in the first few hours after corona treatment. Figure 5.9 shows the typical drop images obtained 15 min after treatment and again 24 h after treatment. The loss and recovery of the hydrophobicity is clearly seen in these images. All of the samples measured in this study showed a similar phenomena to a greater or lesser extent.

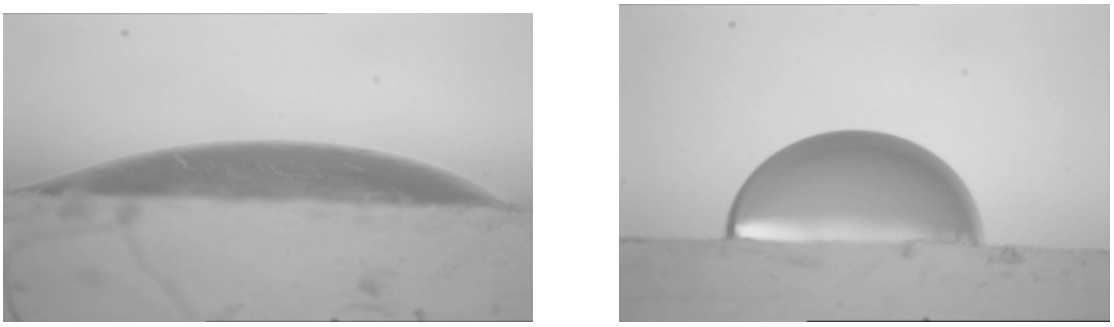

15 min after corona exposure (SCA = 32°) 24 h after corona exposure (SCA = 92°)

**Figure 5.9: Digital images of sample C after 30 min needle corona ageing, indicating hydrophobicity recovery over time.**

The SCA value of sample C approached 32º, 15 min after needle corona treatment, and recovered to 92º, 24 h after treatment. During corona treatment there is generation of active ozone gas and atomic oxygen. These species are considered as strong oxidizing agent, by which surface oxidation is initiated, resulting in a loss of hydrophobicity of the materials [5]. When surface oxidation takes place the surface tension increases and there is a corresponding increase in the surface wettability. As a consequence, water becomes able to form a continuous film on the corona aged sample surface. In this study PDMS samples regardless of their formulations showed complete loss of hydrophobicity after 30 min of needle corona treatment. This is associated with the flatness of the water drop on the surface at the onset of SCA measurements. The speed of hydrophobicity recovery was found to be high within the first hours of static contact angle measurements whereafter the rate started to level off after 6 h to a few days.

### 5.2.2.2 The effect of sample formulation on the hydrophobicity recovery after needle corona treatment

The recovery speed of the controlled formulation samples varied depending on their formulations. Figure 5.10 shows the hydrophobicity recovery graphs of the controlled formulation samples C, E, G and I after 30 min needle corona ageing. Each of the data points in the graph represents the average of at least 10 drop measurements on the surface. In order to quantify the rate of the hydrophobicity recovery, each of the recovery curves was fitted with the following equation:

$$\alpha = A_1 - A_2 e^{(-k\tau)} \qquad (5.1)$$

where $\alpha$ is the SCA measured at log t (min), $\tau$ is the log of t, $A_1$ and $A_2$ are fit constants, and k is the recovery rate constant. The fit of this equation to the data is relatively good, with several $R^2$ values of between 0.93 and 0.99. Meincken et al. [6] used a similar equation to track hydrophobicity recovery using AFM.

The variations in the fitting of equation 5.1 can be attributed to experimental errors and other variables, which may affect the recovery rate. The "half-life" of the recovery process is determined assuming a first-order type kinetics of the recovery process and is determined from the following equation:

$$t_{1/2} = \ln 2/k \qquad (5.2)$$

where k is the rate constant determined for equation 5.1.

The hydrophobicity recovery rate and the half-life of the hydrophobicity recovery ($t_{1/2}$) were determined for the controlled formulation samples C, E, G and I in order to investigate the variation in the recovery speed between the samples. The results are shown in Figure 5.10 and Table 5.8.

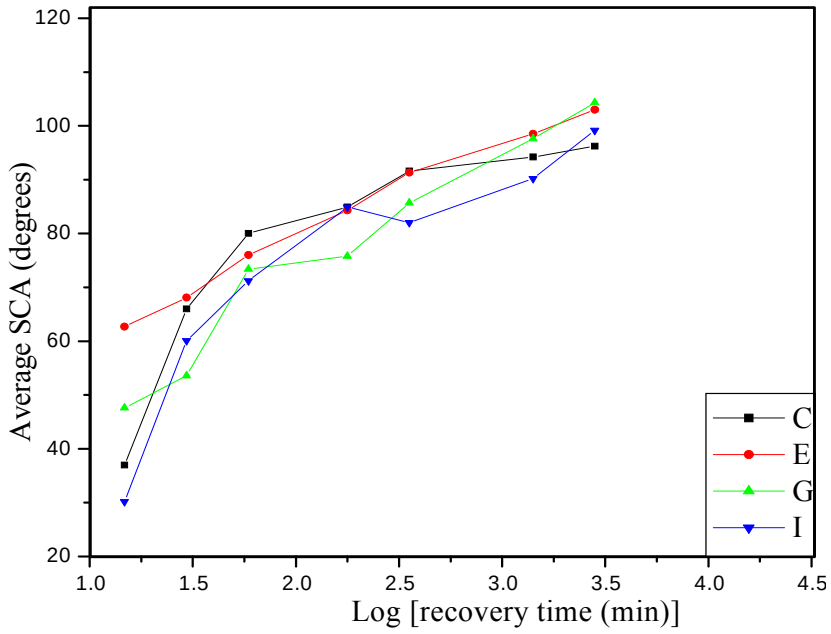


**Figure 5.10: Hydrophobicity recovery of the controlled formulation samples C, E, G and I after 30 min needle corona ageing.**

**Table 5.8: The recovery rate constant (k) and half-life of recovery ($t_{½}$) values of the controlled formulation samples after 30 min needle corona ageing**

| ID | Recovery rate constant (k) | Half-life of recovery ($t_{½}$) (min) |
|---|---|---|
| C | 0.00759 ± (0.00270) | 91 |
| I | 0.00585 ± (0.00236) | 118 |
| G | 0.00405 ± (0.00116) | 171 |
| E | 0.00393 ± (0.00097) | 176 |

The smaller the value of the half-life of recovery, the greatest the recovery rate constant. Sample C had the smallest value of half-life recovery, associated with the fastest recovery rate constant (91 min, 0.00759), followed by sample I (118 min, 0.00585), sample G (171 min, 0.00405) and sample E (176 min, 0.00393). The hydrophobicity recovery of the samples after needle corona ageing exhibited a distinctive variation in the recovery speed between samples.

Sample I showed the most pronounced loss of hydrophobicity, with the accompanying lowest SCA value at the onset of SCA measurements, followed by the pure PDMS sample. The water drop appeared completely flat on the surfaces of both of these samples. Samples C and I recovered the fastest, as is indicated by their shorter $t_{1/2}$ values shown in Table 5.8. Samples G and E had very similar recovery rates, as indicated by the $t_{1/2}$ values of 171 and 176, which means that sample G recovers its hydrophobicity slightly faster than sample E. In the first minute after corona treatment the slower recovery rate of sample I can be attributed to the mechanical strength imparted by filler particles in the polymer network structure. This is in turn retards the depolymerization (in-situ) responsible for the generation of LMW oligomers from the bulk. In addition, the presence of filler particles hampers the speed of diffusion of LMW silicones to the surface resulting in slower recovery rates. Therefore, it can be seen that the filler can have a negative effect on the hydrophobicity recovery, since a smaller amount of LMW oligomers are generated during electrical discharge activities such as corona and dry-band arcing.

Many researchers report that after corona exposure an inorganic silica-like layer is formed [2, 5, 7-11]. This layer retards the recovery of the hydrophobicity. The hydrophobicity recovery speed in needle corona aged samples was determined by the formation of cracks through which LMW oligomers diffuse to the surface and the thickness of the silica-like layer formed upon corona treatment. Therefore a variation in the hydrophobicity recovery was observed in the samples.

#### 5.2.2.3 Comparison between needle corona and French corona

There are currently two different types of corona treatments for accelerated ageing of samples available in our laboratories. These different types of corona treaters are discussed in detail in Chapter 4. In order to draw a meaningful comparison between the two types, samples under study were artificially aged with the two treatments and the subsequent effects were investigated. Needle corona ageing was performed on the samples for 30 min. Static contact angles were measured to determine the hydrophobicity recovery of the samples. In parallel to this, French corona treatments were performed on

the samples for 12 h and hydrophobicity recovery was similarly investigated. Figure 5.11 and Table 5.9 show the hydrophobicity recovery of the controlled formulation samples after needle corona and French corona treatments as well as the rate of the hydrophobicity recovery.

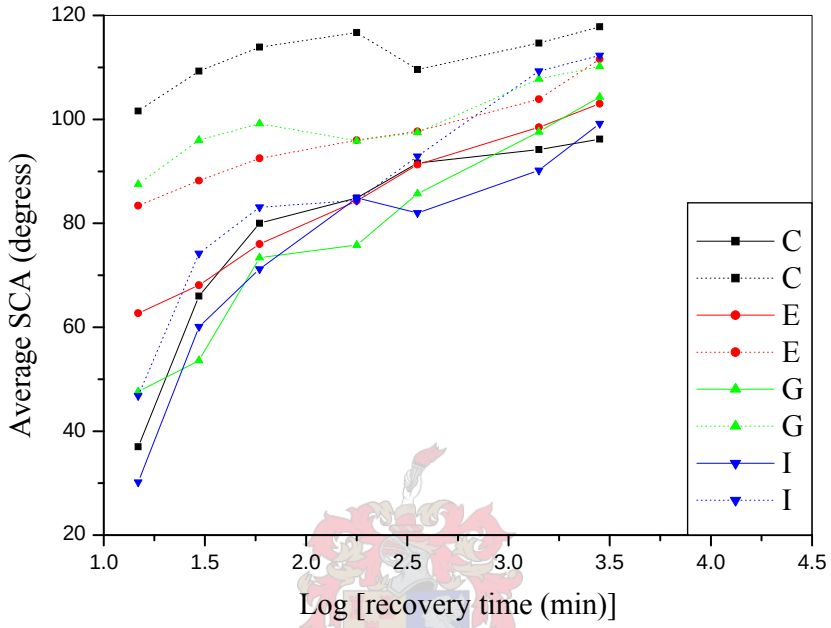


**Figure 5.11: Hydrophobicity recovery of controlled formulation samples C, E, G and I after 30 min needle corona ageing (straight line) and 12 h French corona ageing (dotted line).**

**Table 5.9: Comparison of the recovery rate constant (k) and half-life of recovery ($t_{½}$) between needle corona and French corona aged controlled formulation samples**

| ID | Needle corona | | French corona | |
|---|---|---|---|---|
| | k | $t_{1/2}$ (min) | k | $t_{1/2}$ (min) |
| C | 0.00759 ± (0.00270) | 91 | 0.04518 ± (0.00117) | 15.3 |
| E | 0.00393 ± (0.00097) | 176 | 0.00231± (0.00122) | 300.0 |
| G | 0.00405 ± (0.00116) | 171 | 0.00186± (0.00052) | 372.0 |
| I | 0.00585 ± (0.00236) | 118 | 0.00408± (0.00263) | 169.0 |

The needle corona ageing of the controlled formulation samples C, E, G and I showed higher loss in hydrophobicity, as indicated by the lower SCA values, compared to the

French corona ageing. The recovery rate constant values of the needle corona aged samples were also found to be higher than in the French corona aged samples as displayed in Table 5.9. The commercial samples also showed a similar trend as shown in Figures 5.12 and 5.13, and Table 5.10, for the needle and French corona aged samples.

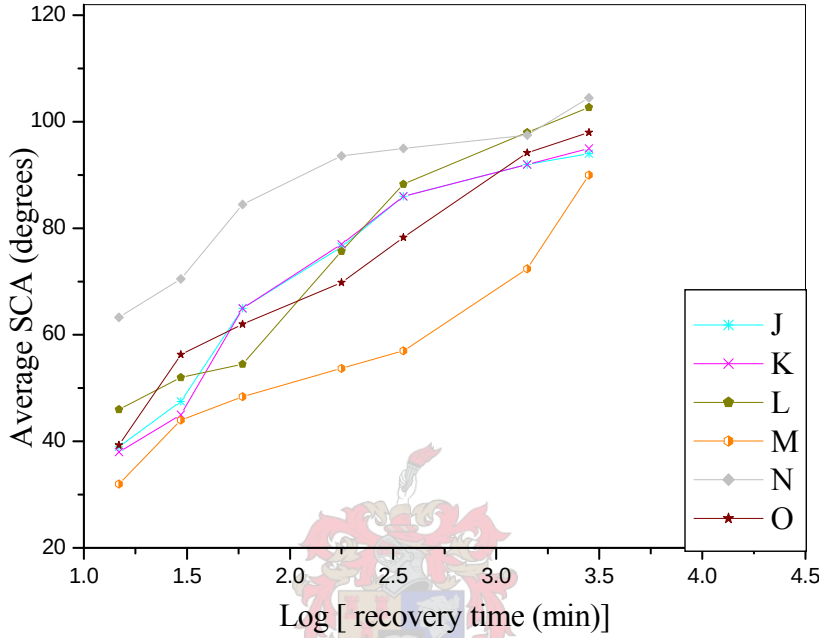


**Figure 5.12: Hydrophobicity recovery of commercial samples after 30 min needle corona ageing.**

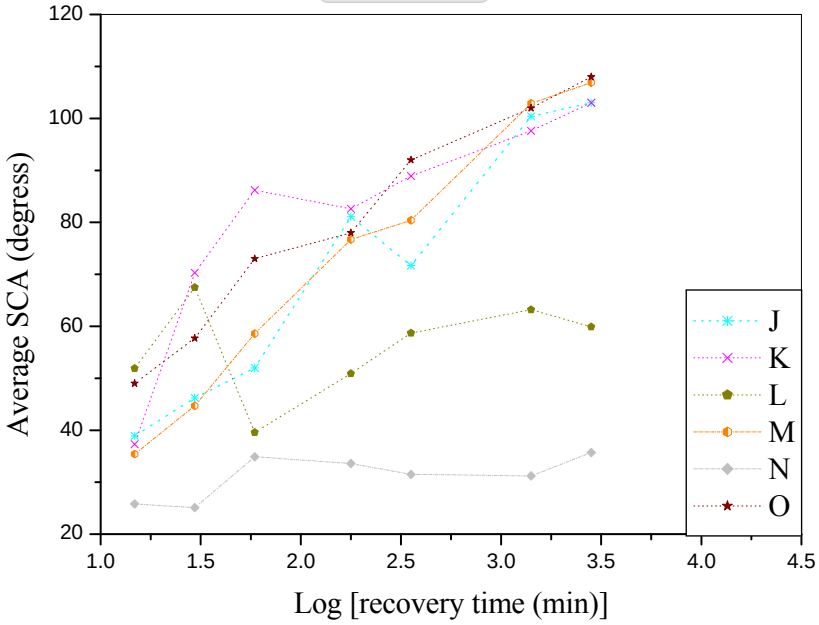


**Figure 5.13: Hydrophobicity recovery of commercial samples after 12 h French corona ageing.**

**Table 5.10: Comparison of the recovery rate constant (k) and half-life of recovery ($t_{½}$) between needle corona and French corona aged commercial samples**

| ID | Needle corona | | French corona | |
|---|---|---|---|---|
| | k | $t_{1/2}$ (min) | k | $t_{1/2}$ (min) |
| J | 0.00930 ± (0.00257) | 74.5 | **0.00060 ± (0.00024)** | **11552.4** |
| K | 0.00854 ± (0.00269) | 81.2 | 0.00719 ± (0.00556) | 96.4 |
| L | 0.00349 ± (0.00132) | 199.0 | **0.00602 ± (0.00213)** | **115.0** |
| M | 0.00445 ± (0.00049) | 156.0 | 0.00402 ± (0.00114) | 172.0 |
| N | 0.00083 ± (0.00059) | 835.0 | **0.00394 ± (0.00360)** | **176.0** |
| O | 0.01770 ± (0.00596) | 39.2 | 0.00464 ± (0.00158) | 149.0 |

Once again, higher recovery rates were observed for the needle corona aged samples over French corona aged samples. However, some results showed an opposite trend, and these are indicated in bold. This may be due to experimental error or, as in the case of the L and N samples, because these samples did not show any significant recovery after the French corona treatment.

The results demonstrate a high degree of surface changes for the needle corona aged samples since low contact angle values were obtained at the onset of measurements (zero time). French corona aged samples on the other hand show a lesser degrees of cracks and higher SCA values immediately after treatment, associated with no flattening of a water drop on the surface.

Commercial samples K, M and O, which are PDMS based, show a faster recovery after needle corona ageing than the French corona aged counterparts, and sample O exhibits the fastest recovery rate. Commercial samples L and N, which are EPDM based, show a very hydrophilic character at zero time, indicating a high degree of surface damage. Samples N and L show very little recovery after the removal of corona treatment and did not reach full hydrophobicity recovery even after a few days. This is expected as these samples do not have the same hydrophobicity recovery mechanism as found in the PDMS based materials.

A lesser degree of surface damage occurs with the French corona in comparison with the needle corona ageing. This is associated with a lower decrease in hydrophobicity and no flattening of water drops observed at the onset of the measurements. The results correspond well with the findings of Berhane [8] who showed, using positron beam techniques, that the surface damage and modification caused by French cell type corona is far less severe than that of the needle corona type. The needle corona aged PDMS samples recover relatively faster than the French corona aged samples, as indicated by the higher recovery rate values. This is due to the greater degree of surface change caused by the more severe treatment. This will lead to the relatively quicker formation in the glassy silica-like layer during the needle corona ageing, leading to a fast recovery. The differences in the two treatment methods were further investigated using slow positron beam techniques.

#### 5.2.2.4 Slow positron beam study of corona treated samples

Positron annihilation spectroscopy is a very useful tool for determining surface degradation of polymeric materials since it provides important information about the free volume in polymer surfaces after being aged by various means. It gives a direct measure of the free volume and holes as a function of the S parameter on the polymer surface. Berhane [8] showed that the effects measured by the slow positron technique on the French corona treated samples were mild in comparison to those of the needle corona treated counterparts. Figure 5.14 shows the S parameter profiles measured for untreated sample C, 30 min needle corona aged and 120 min French corona aged samples.

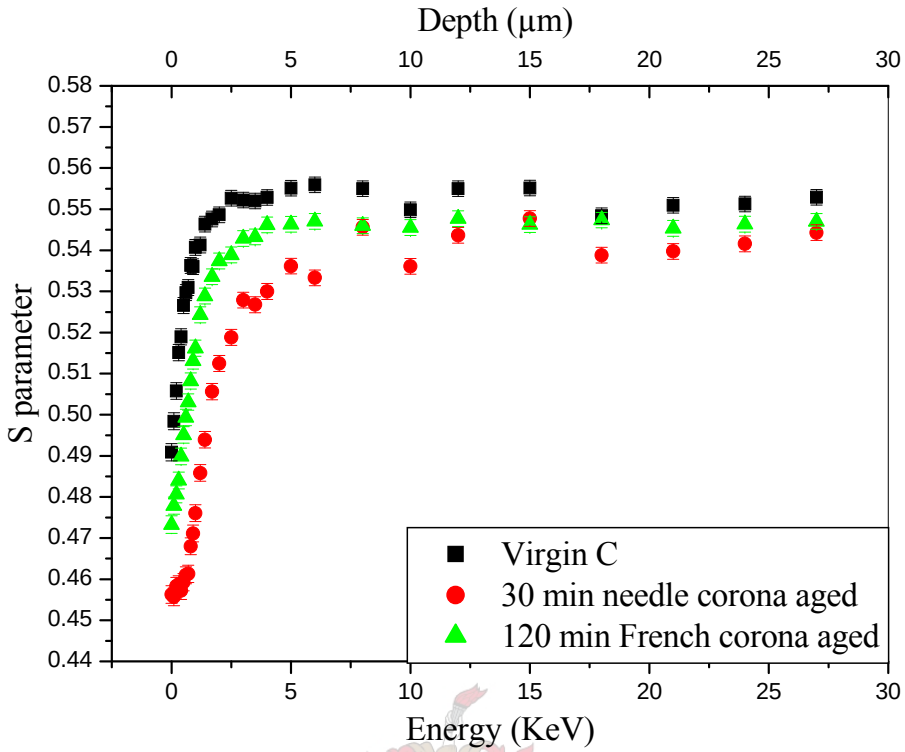


**Figure 5.14: S parameter profiles of virgin, 30 min needle corona and 120 min French corona aged sample C [8].**

Virgin sample C has a large S parameter value at the surface, which corresponds to a high free volume at the near surface, and at low positron energy then the S parameter profile increases reaching a constant value. For both the needle and the French corona treatment there is a marked decrease in the S parameter after treatment but there is a noticeably more pronounced decrease in the S parameter value for the needle corona aged sample C in comparison with the French corona aged counterpart. This indicates that the 30 min needle corona treated sample C has a smaller free volume than the French corona treated sample. The reasons for the decreasing S parameter after treatment are discussed in more detail later in this section.

Several samples were selected to study the difference between the two methods of corona treatments. Two PDMS samples of controlled formulation (samples C and I) as well as the commercial PDMS based sample K were studied. The commercial EPDM based sample L was also included in this study. All the samples were aged for 100 h using the French corona ageing in order to examine the potential polymer degradation. Positron

analysis was carried out on the sample surfaces to investigate the effect of the French corona ageing on the free volume of the samples as a result of surface degradation. S parameter profiles as a function of the positron incident energy of the virgin and 100 h French corona aged samples are shown in Figures 5.15-5.18.

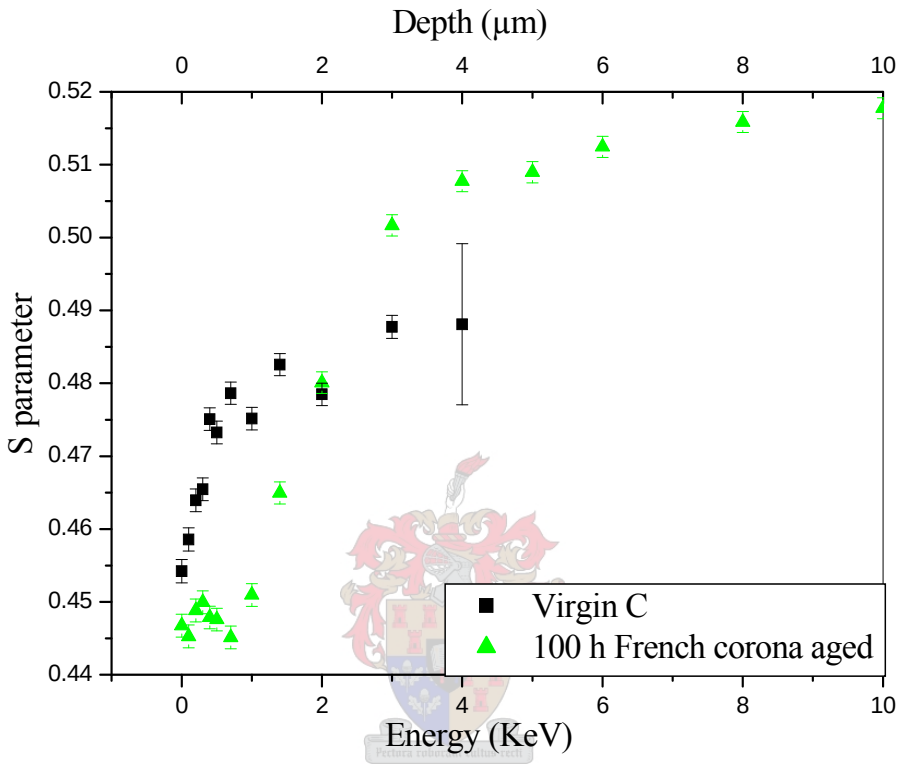


**Figure 5.15: S parameter profiles of virgin and 100 h French corona aged sample C.**

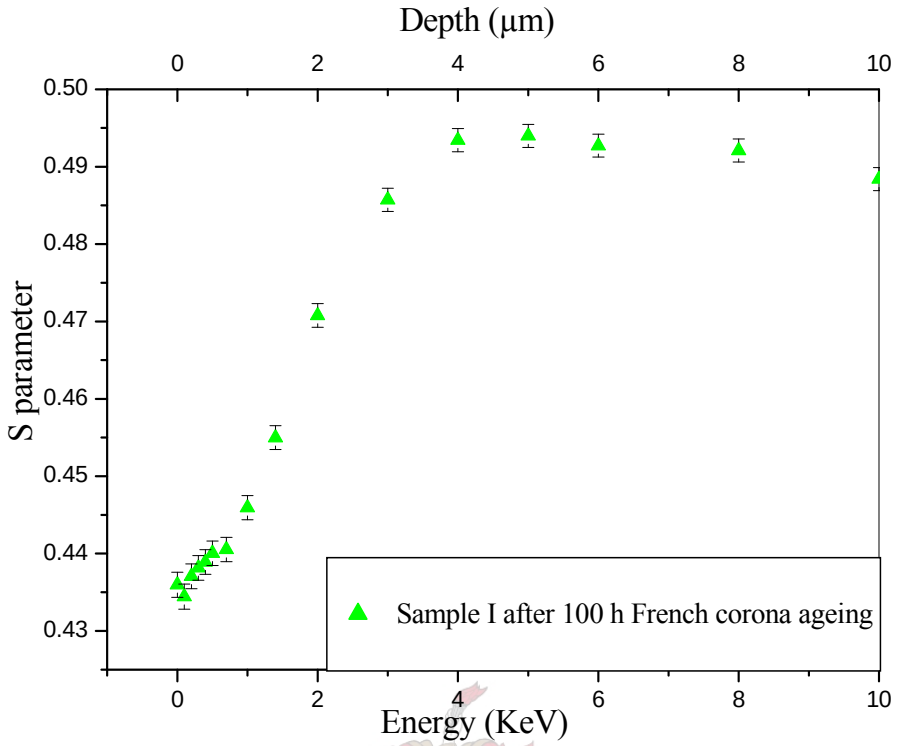


**Figure 5.16: S parameter profiles of 100 h French corona aged sample I.**

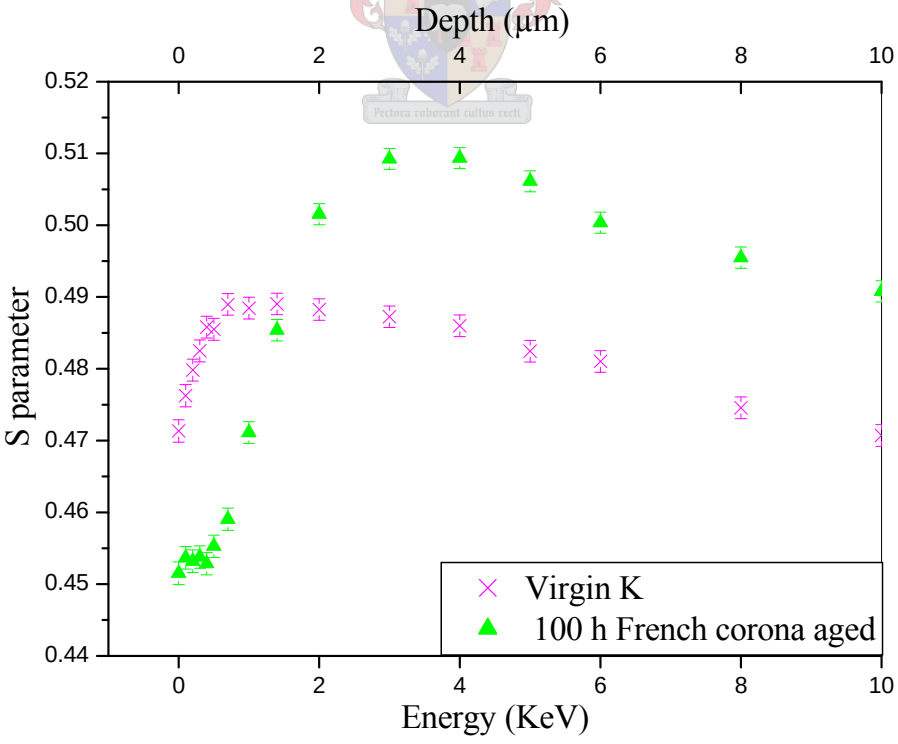


**Figure 5.17: S parameter profiles of virgin and 100 h French corona aged sample K.**

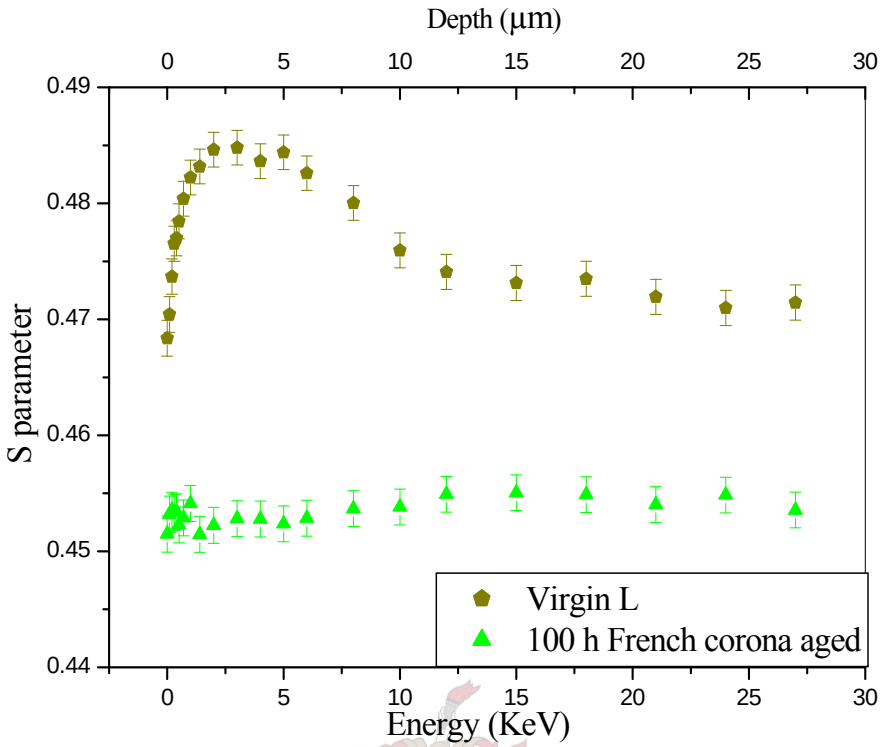


**Figure 5.18: S parameter profiles of virgin and 100 h French corona aged sample L.**

The positron results in the present study indicate that for the virgin controlled formulation PDMS sample C there is a small S parameter values at the very near sample surface. This increase at higher positron implantation depth and reaches a maximum value. The increase at the surface is due to the back scattering and back diffusion of the positrons and the positronum near the PDMS virgin surface. The energy at the point where the S parameter reaches a maximum indicates the diffusion length of the positrons and Ps in the PDMS material. In the virgin commercial PDMS sample K, which contains silica and ATH filler (typical commercial composition), the S parameter shows an increase at low positron energy then reaches a maximum value followed by a large drop in the S parameter at higher positron incident energies as illustrated in Figure 5.17. A similar behaviour is observed in virgin commercial EPDM sample L in Figure 5.18. This is the first example of the measurement of an EPDM based insulator material measured by the slow positron technique. The decrease in the S parameter at higher implantation energies is attributed to the effect of the ATH filler present in the compounds. This creates three distinctive regions in the S parameter profile. Firstly there is a polymer rich skin at the

very near surface where the large S parameter value is observed. Secondly the S parameter approaches a constant value where the ATH filler particles come into play and start to affect the S parameter. Thirdly at higher positron energies and higher mean depth the S profile levels off in the bulk of the material [9]. The results in Figure 5.18 confirms that the EPDM samples have a similar "polymer-rich" surface layer that is observed in PDMS based materials.

After 100 h of French corona treatment all the samples show a significant drop in the S parameter at the very near surface compared to the virgin sample. This corresponds to a lower free volume due to surface degradation taking place after French corona treatment.

Mallon et al. [10] studied corona treated PDMS surfaces by slow positron beam techniques and have shown that the flattening of the S parameter at the surface is due to the formation of an inorganic silica-like layer. It was also shown that the extent of the flatting at the surface could be used to estimate the thickness of the $SiO_x$ layer on the surface. In PDMS compounds of similar formulations, it has been shown that a $SiO_x$ layer of between 30 and 50 nm forms on the surface after 30 min of needle corona treatment. The results of this study show that a similar glassy silica-like layer formed only after 100 h of French corona ageing. The positron results suggest that 100 h French corona ageing is roughly equivalent to 30 min of needle corona ageing, where it was shown that the $SiO_x$ layer of similar thickness formed at much shorter treatment times. This indicates that the needle corona treatment has a far more severe effect on the samples than the French corona treatment. This may be due to the direct exposure to ion bombardment that occurs from the needle tip whereas in the case of French corona there is a much milder effect due to the dispersive effect of the corona exposure.

As mentioned above, the results in Figure 5.18 confirm that the EPDM samples have a similar "polymer-rich" surface layer to that observed in PDMS based materials. After corona treatment there is a complete flattening of the S parameter profile. It is also observed that the measured S parameter value is lower than the value obtained for the virgin materials. This indicates that significant changes have occurred on the surface of the EPDM materials. Unlike in the case of the PDMS based compounds these changes are not limited to the very near surface region, but continue into the bulk of the material. This

result confirms the observation in the hydrophobicity recovery study, where it was found that large changes in the SCA occurred in the EPDM compounds and little to no recovery was observed after French corona treatment, indicating permanent surface degradation.

#### 5.2.2.5 Microscopy analysis of surface morphology

Observation of the surface morphology of the samples after corona treatment was done using optical microscopy and scanning electron microscopy. Typical examples of results are shown in Figure 5.19 for the controlled formulation sample E and the commercial sample L. These samples show the most apparent surface features as a result of needle corona and French cell corona ageing.

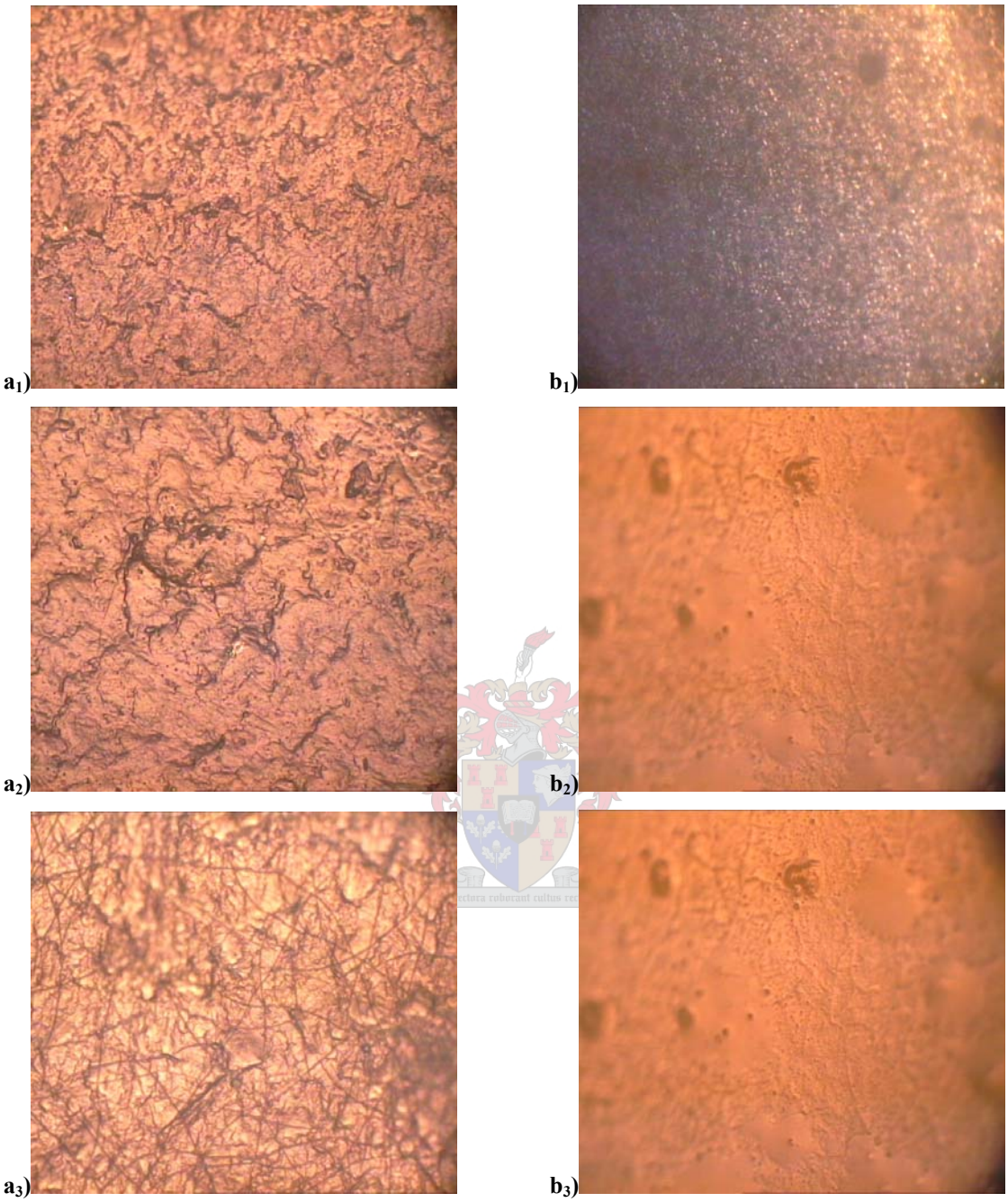


**Figure 5.19: Optical microscope images of controlled formulation samples: ($a_1$) virgin sample E, ($a_2$) 12 h French corona aged sample E, ($a_3$) 30 min needle corona aged sample E, and ($b_1$) virgin sample L, ($b_2$) 12 h French corona aged sample L and ($b_3$) 30 min needle corona aged sample L.**

SEM analysis was carried out on the samples to investigate possible topographical features that may have resulted from the various types of corona treatment. The SEM images are shown in Figure 5.20.

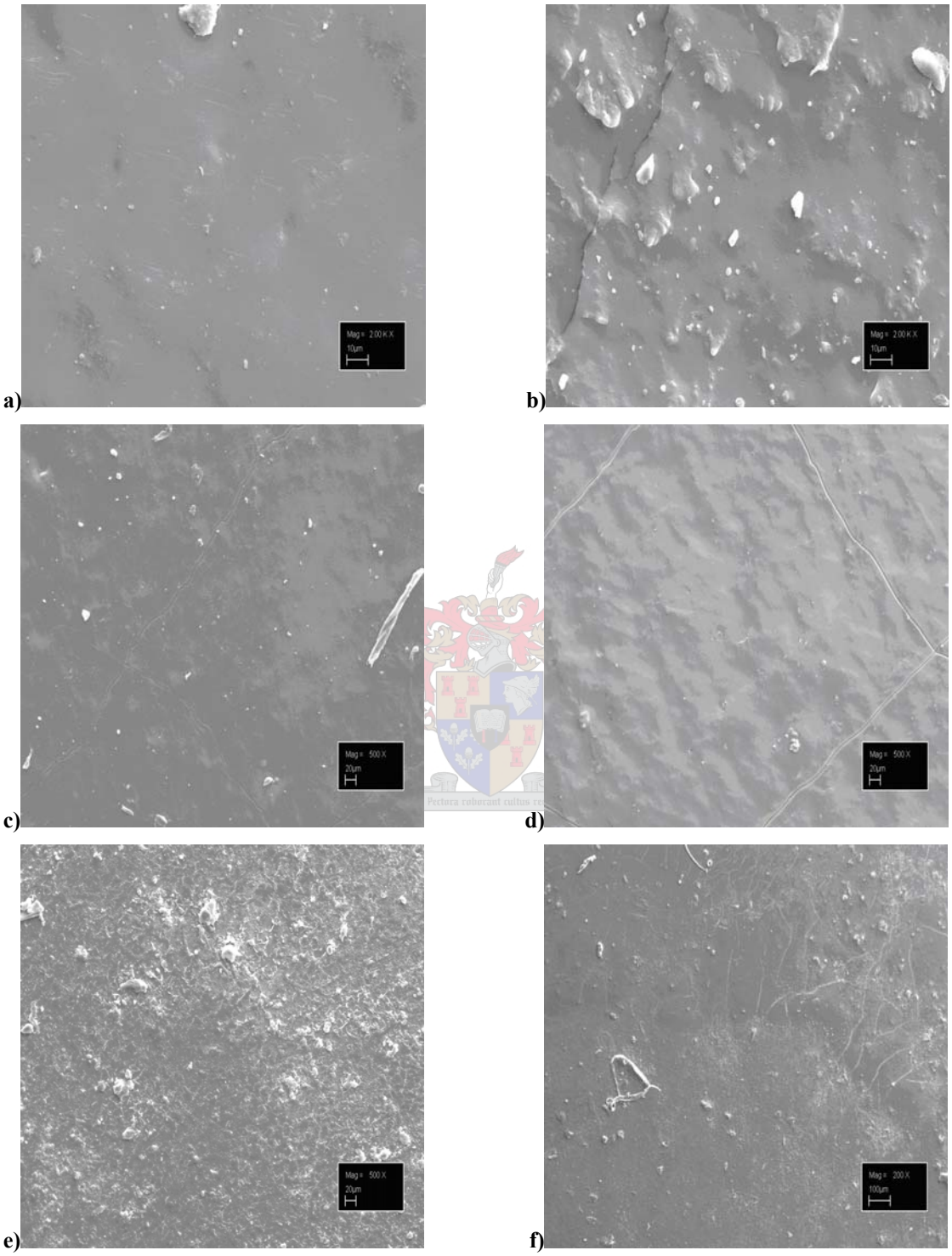


**Figure 5.20: SEM images of samples: (a) virgin sample C, (b) 30 min needle corona aged sample C, (c) virgin sample E, (d) 30 min needle corona aged sample E, (e) virgin sample L and (f) 30 min needle corona aged sample L.**

Visual observation of the virgin samples E and L using optical microscopy shows no cracks and the sample surfaces are smooth, as shown in Figures 5.19 ($a_1$) and ($b_1$) respectively. The surfaces of the corona aged samples E and L do however show that cracks and roughness have developed. This is clearly observed on the surface of both samples, as displayed in the images ($a_2$), ($a_3$), ($b_2$) and ($b_3$) in Figure 5.19, for both the needle corona and French corona aged samples. These cracks may be attributed to the brittle silica-like layer that forms as a result of corona ageing in the case of the PDMS based sample. The needle corona aged samples have a higher degree of cracks on the surface compared with the French corona aged samples. This behaviour is consistent with the lower static contact angle values obtained after needle corona ageing and the positron data, which show that there is a higher degree of surface damage when needle corona is used, relative to the French corona treatment.

SEM analysis shows similar results. Once again, untreated PDMS samples show smooth surfaces, but samples exposed to corona exhibit various degrees of cracks and roughness on their surfaces, as shown in Figure 5.20. The SEM image of virgin sample C in Figure 5.20 (a) exhibits no signs of cracks or roughness and the surface is smooth. Figure 5.20 (b) shows the SEM image of the 30 min needle corona aged sample C. It shows cracks on the surface, due to the formation of a brittle silica-like layer. Figures 5.20 (c) and (d) are the images of virgin sample E and the 30 min needle corona treated sample E.The latter shows a higher degree of cracks and is associated with a rougher surface compared to samples C, G and I.

Figures 5.20 (e) and (f) show the virgin commercial sample L and the 30 min needle corona aged sample. Cracks are clearly seen on the aged sample. Samples G and I also show smooth surfaces for the virgin samples and relatively lesser degrees of roughness for the corona aged samples compared to the other samples as shown in Figure 5.21.

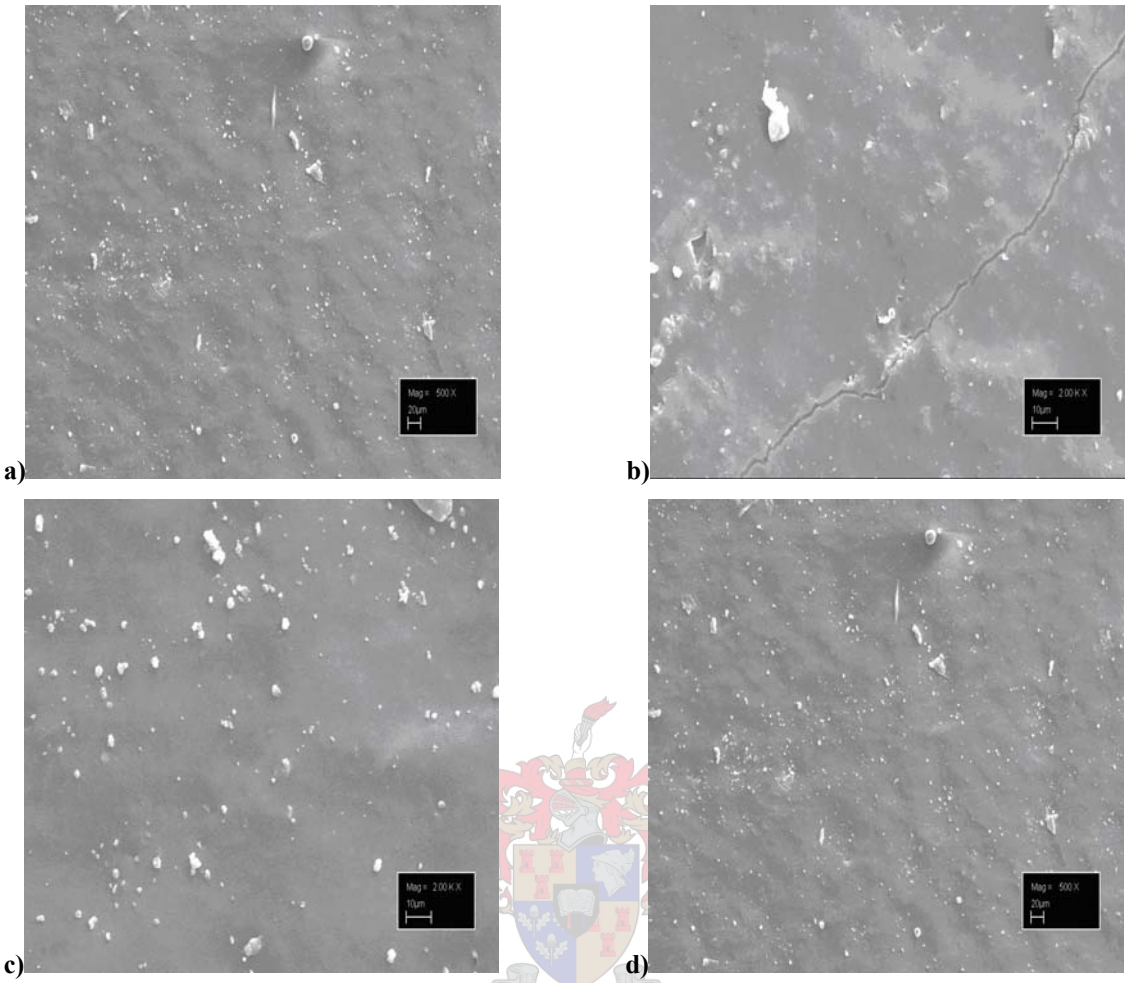


**Figure 5.21: SEM images of samples: (a) virgin sample G, (b) 30 min needle corona aged sample G, (c) virgin sample I and (d) 30 min needle corona aged sample I.**

Figure 5.22 shows that the commercial PDMS samples J and K have smooth surfaces and no signs of cracks after 30 min needle corona treatment. This may be a result of their formulations, which result in a higher mechanical strength imparted by the filler particles, allowing them largely to resist the severe ageing conditions. The higher mechanical strength also prevents the cracking of the brittle $SiO_x$ layer. It has been shown that the commercial samples typically form a $SiO_x$ layer that is thinner than in the controlled formulation samples (from positron studies). This is due to the "thinner" polymer rich layer at the surface. Once again, this makes the degradation on the surface of the commercial samples less apparent than in the controlled formulation samples.

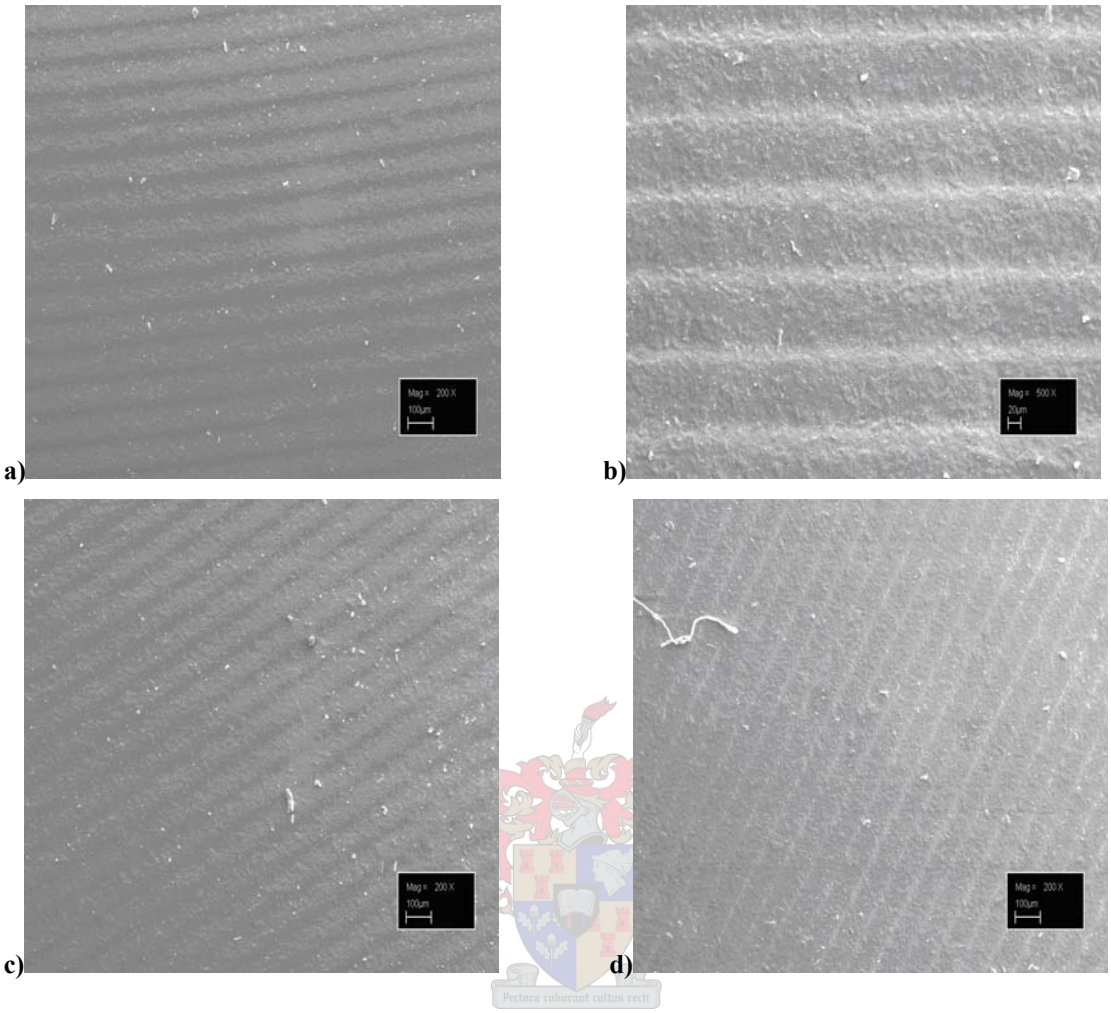


**Figure 5.22: SEM images of samples: (a) virgin sample J, (b) 30 min needle corona aged sample J, (c) virgin sample K and (d) 30 min needle corona aged sample K.**

SEM images of commercial samples M, N and O for both the virgin and corona treated samples also show smooth surfaces and no cracks, but sample N shows a relatively rough surface. These images are shown in Figure 5.23.

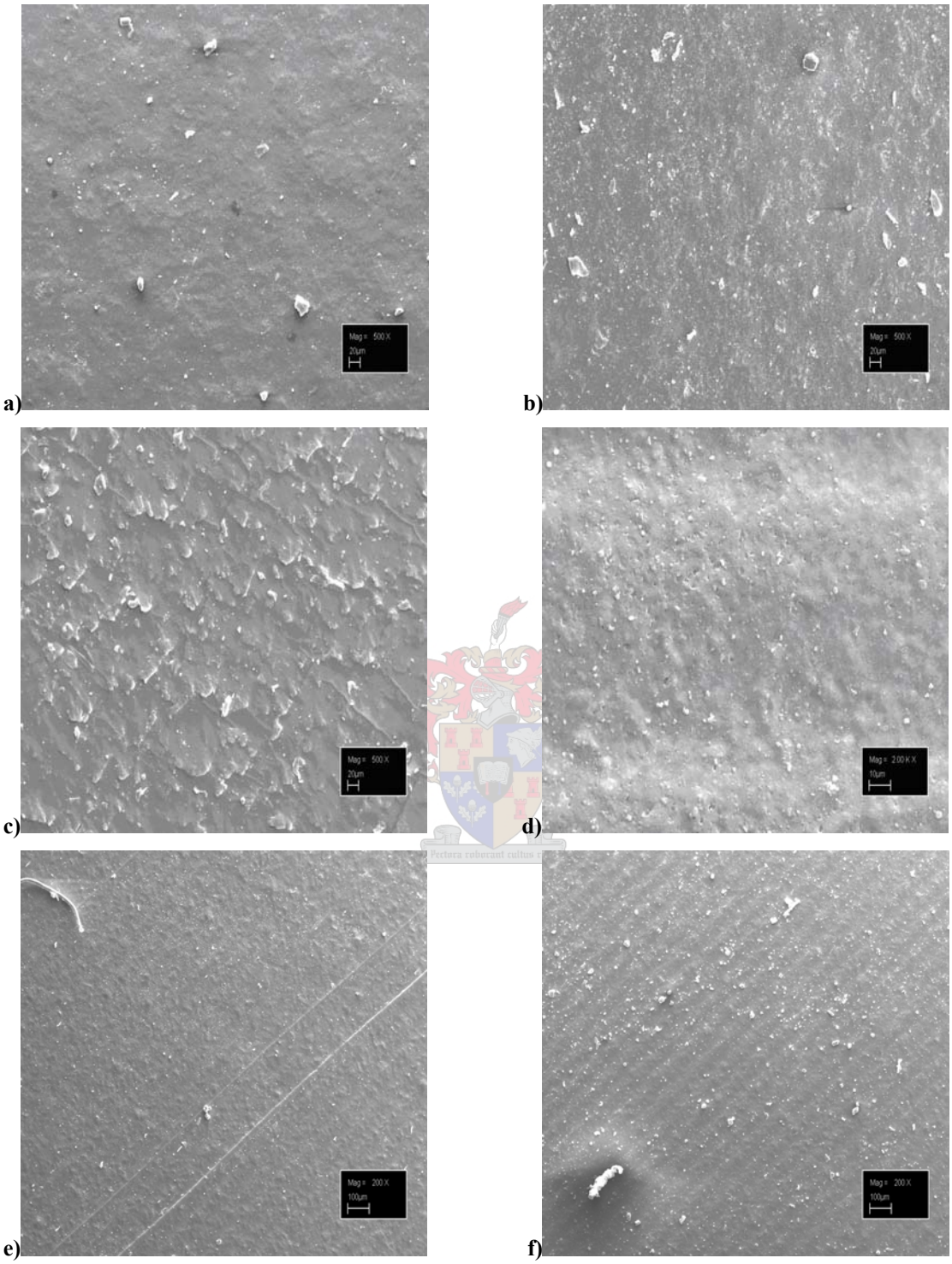


**Figure 5.23: SEM images of samples: (a) virgin sample M, (b) 30 min needle corona aged sample M, (c) virgin sample N, (d) 30 min needle corona aged sample N, (e) virgin sample O and (f) 30 min needle corona aged sample O.**

The results clearly indicate that high-temperature vulcanized rubber commercial housings exhibit a lesser degree of roughness and cracks in comparison with room-temperature vulcanized rubber housings upon corona ageing. The lack of observed cracks in HTV samples J, K, M and O is most probably the result of higher mechanical strength of the formulations of these samples due to the presence of higher amounts of protective fillers, which prevent bending and subsequent cracking of the brittle $SiO_x$ layer. The higher degrees of cracks and roughness observed in commercial samples N and L (compared to the other commercial samples) is explained by the high susceptibility of EPDM rubber towards degradation occurring during corona treatment.

The type of rubber housings have a great effect on the degree of roughness observed. The PDMS samples have relatively smooth surfaces because PDMS is less susceptible to degradation than EPDM. The adherence of LMW oligomers on the surface may also lead to the appearance of a smooth surface. In the PDMS compounds the diffusion of LMW oligomers to the surface essentially "coats" the underlying $SiO_x$ degradation layer. Since the SEM images only show the topography of the surface, this layer may make the surface appear "smooth" in SEM analysis. Attempts to overcome this potential problem are discussed in the next section.

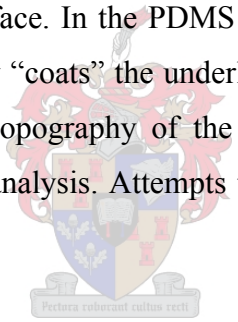

#### 5.2.2.6 The effect of surface cleaning of corona aged samples

The surface of an insulator during corona ageing undergoes both physical and chemical changes caused by the active ozone generated during treatment. As already discussed, physical changes that may occur are the formation of cracks and accompanying surface roughness, which may develop as a result of the "breaking-up" of the $SiO_x$ degradation layer that is formed during the degradation process. To investigate the underlying physical structure in which the subsequent morphology features are visualized, the low molecular weight oligomers that diffuse to the surface were removed from the surface by chloroform extraction. (This was done by dabbing the surface with chloroform then wiping off the surface with Kleenex paper). Cleaned corona treated sample surfaces had deep cracks along the sample surfaces, as shown in Figures 5.24 (a) and (b).

These new features of cracks, which indicate a higher degree of surface oxidation, were formaly hidden by the LMW oligomers that diffused to the surface after corona treatment. During cleaning, these species are removed by chloroform and deep cracks and roughness could be seen on the surface. It should also be noted that the cleaning process may also lead to further changes in the surface as a result of the swelling of the underlying polymer during the cleaning process. This study shows that SEM images after corona treatment of PDMS based samples must be treated with caution since the underlying surface changes may be obscured by the apparent "smooth" LMW oligomers that diffuse to the surface, and are which responsible for the hydrophobicity recovery. These LMW species should be removed from the surface prior to the SEM analysis.

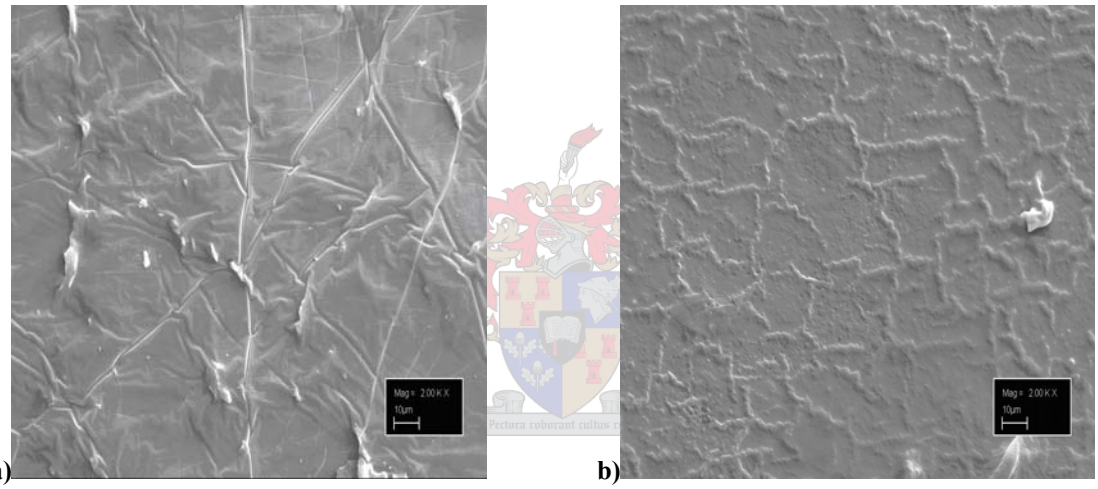


**Figure 5.24: SEM images of (a) 30 min needle corona aged sample E and (b) 30 min needle corona aged sample J after surface cleaning.**

### 5.2.2.7 Characterization of LMW oligomers

Low molecular weight PDMS silicon oligomers are believed to be the species responsible for the hydrophobicity recovery in PDMS insulators. The mechanism of the diffusion of LMW oligomers from the bulk to the surface is the dominant mechanism for the recovery process [12]. LMW oligomers therefore have a significant effect on the insulator electrical performance.

A study was carried out to quantify LMW oligomers that diffuse to the surface after corona exposure and to determine the relative changes in their surface concentrations

after corona ageing. A time dependant study of the sample extractions after 30 min of needle corona ageing was carried out. The LMW oligomers were washed of the sample surface 1 min after treatment and then again after 10 min (see Section 4.3). The same sample volume of hexane and surface area were used for each sample.

The LMW PDMS GC chromatograms of sample C before and after 30 min needle corona ageing are shown in Figures 5.25 (a) and (b) respectively.

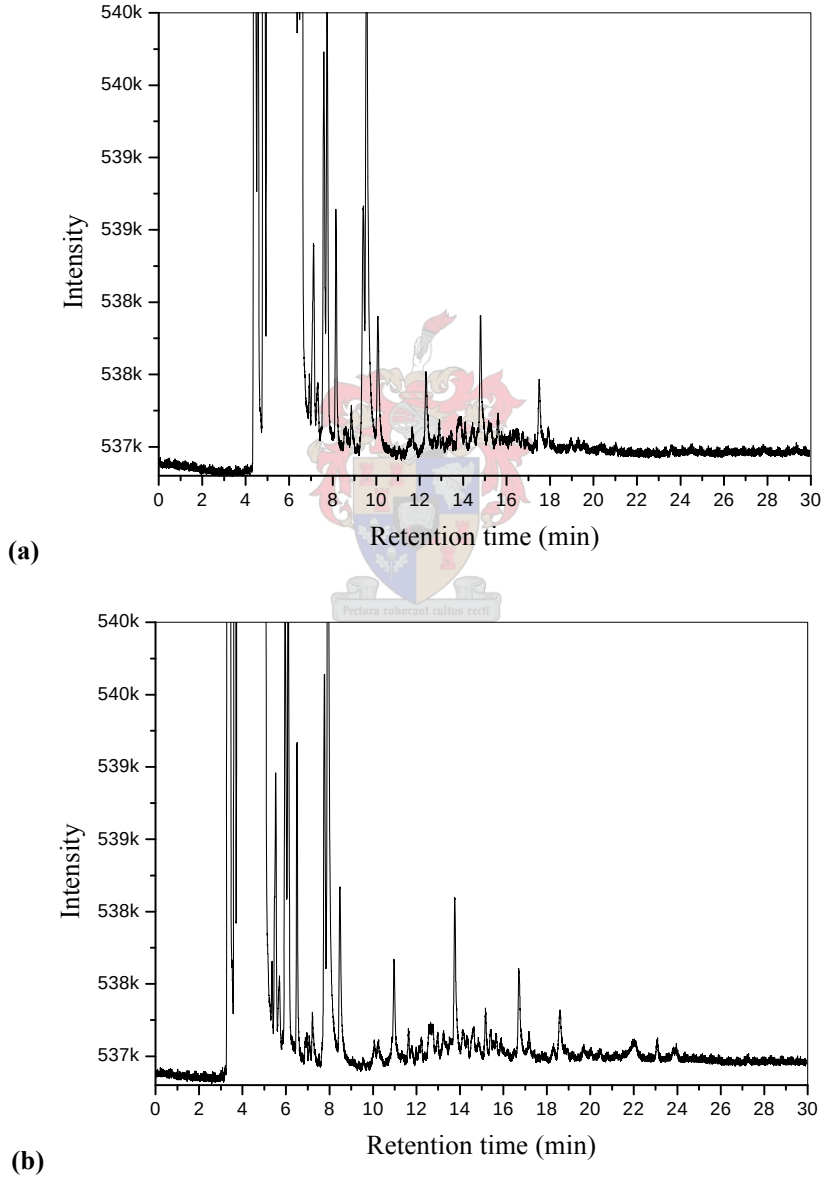


**Figure 5.25: GC chromatograms of LMW PDMS: (a) virgin sample C and (b) 30 min needle corona treated sample C.**

Untreated sample C shows low amounts of LMW silicones at 12, 15 and 17 min retention time in the GC chromatogram. The large peak at 4-10 min retention time corresponds to hexane used to extract the LMW silicones. Sample C after 30 min needle corona ageing yields a high amount of LMW species, associated with an increase in the peak intensities as displayed in Figure 5.25 (b). New peaks appear in the GC chromatogram of needle corona aged sample C at 19 and 22 min. GC/MS results show that after corona ageing the species observed are a range of cyclic LMW silicone species, ranging from $D_3$ up to $D_7$, which results from the breakdown of the crosslinked PDMS structure due to a chain scission reaction taking place during electrical discharge activity.

The extracted low molecular weight oligomers for the virgin samples and the needle corona aged samples C, E, G, I, J, K, M and O are shown in the following tables, 5.11 (a), (b), (c), (d), (e), (f), (g) and (h), respectively.

**Table 5.11: The extracted low molecular weight oligomers of the virgin and the 30 min needle corona aged samples of C, E, G, I, J, K, M and O**

**Table 5.11 (a): Sample C**

| **Retention time (min)** | **Virgin C** | | **C aged extracted after 1 min** | | **C aged extracted after 10 min** | |
|---|---|---|---|---|---|---|
| | Height | Area | Height | Area | Height | Area |
| 12 | 8.0 | 43.3 | 13.3 | 81.8 | 377 | 2888 |
| 15 | 3.9 | 9.4 | 30.0 | 93.0 | 236 | 8050 |
| 17 | 3.9 | 24.9 | 6.9 | 45.9 | 193 | 1250 |
| 19 | - | - | 5.9 | 40.6 | 185 | 1100 |
| 22 | - | - | 1.1 | 30.8 | 13 | 277 |

**Table 5.11 (b): Sample E**

| Retention time (min) | Virgin E | | E aged extracted after 1 min | | E aged extracted after 10 min | |
|---|---|---|---|---|---|---|
| | Height | Area | Height | Area | Height | Area |
| 12 | 13.7 | 53 | 30.9 | 83 | 70.3 | 487 |
| 15 | 125.0 | 180 | 224.0 | 610 | 288.0 | 945 |
| 17 | 49.0 | 125 | 160.0 | 324 | 169.0 | 234 |
| 19 | - | - | 142.0 | 230 | 130.0 | 130 |
| 22 | - | - | 3.8 | 26 | 5.9 | 69 |

**Table 5.11 (c): Sample G**

| Retention time (min) | Virgin G | | G aged extracted after 1 min | | G aged extracted after 10 min | |
|---|---|---|---|---|---|---|
| | Height | Area | Height | Area | Height | Area |
| 12 | 103.0 | 284 | 386.0 | 247.0 | 246.0 | 525 |
| 15 | 643.0 | 23 | 1.7 | 355.0 | 2.0 | 923 |
| 17 | 12.9 | 76 | 0.4 | 12.3 | 1.6 | 317 |
| 19 | - | - | 6.4 | 49.0 | 8.8 | 61 |
| 22 | - | - | 3.4 | 10.8 | 5.2 | 21 |

**Table 5.11 (d): Sample I**

| Retention time (min) | Virgin I | | I aged extracted after 1 min | | I aged extracted after 10 min | |
|---|---|---|---|---|---|---|
| | Height | Area | Height | Area | Height | Area |
| 12 | 5.2 | 30.5 | 20.2 | 27.9 | 47.6 | 70 |
| 15 | 2.3 | 16.0 | 33.1 | 84.3 | 66.0 | 105 |
| 17 | 8.8 | 16.0 | 13.7 | 24.5 | 23.0 | 89 |
| 19 | - | - | 4.7 | 17.9 | 6.0 | 66 |
| 22 | - | - | 2.2 | 9.9 | 3.7 | 20 |

**Table 5.11 (e): Sample J**

| Retention time (min) | Virgin J | | J aged extracted after 1 min | | J aged extracted after 10 min | |
|---|---|---|---|---|---|---|
| | Height | Area | Height | Area | Height | Area |
| 12 | 6.5 | 15.1 | 8.8 | 29.8 | 14.7 | 58 |
| 15 | 4.9 | 10.6 | 6.9 | 11.4 | 12.6 | 80 |
| 17 | 1.8 | 4.2 | 9.1 | 51.0 | 5.3 | 33 |
| 19 | - | - | 2.1 | 9.1 | 2.7 | 17 |
| 22 | - | - | 1.6 | 4.5 | 2.5 | 9 |

**Table 5.11 (f): Sample K**

| Retention time (min) | Virgin K | | K aged extracted after 1 min | | K aged extracted after 10 min | |
|---|---|---|---|---|---|---|
| | Height | Area | Height | Area | Height | Area |
| 12 | 5.3 | 14.3 | 84.8 | 438 | 90.6 | 338 |
| 15 | 7.4 | 8.6 | 1.1 | 4 | 24.5 | 545 |
| 17 | 0.3 | 1.4 | 0.8 | 5 | 0.7 | 160 |
| 19 | - | - | 9.3 | 25 | 14.6 | 100 |
| 22 | - | - | 3.7 | 13 | 5.2 | 26 |

**Table 5.11 (g): Sample M**

| Retention time (min) | Virgin M | | M aged extracted after 1 min | | M aged extracted after 10 min | |
|---|---|---|---|---|---|---|
| | Height | Area | Height | Area | Height | Area |
| 12 | 4.3 | 8.4 | 9.7 | 62.4 | 10.2 | 164 |
| 15 | 8.2 | 5.8 | 32.5 | 32.2 | 34.7 | 331 |
| 17 | 5.4 | 12.6 | 12.9 | 56.5 | 14.0 | 71 |
| 19 | - | - | 4.9 | 12.6 | 10.7 | 35 |
| 22 | - | - | 2.1 | 7.2 | 2.4 | 18 |

**Table 5.11 (h): Sample O**

| Retention time (min) | Virgin O | | O aged extracted after 1 min | | O aged extracted after 10 min | |
|---|---|---|---|---|---|---|
| | Height | Area | Height | Area | Height | Area |
| 12 | 9.9 | 59.7 | 52.2 | 168 | 199.0 | 393 |
| 15 | 5.3 | 18.9 | 1.1 | 5 | 1.50 | 740 |
| 17 | 8.4 | 47.0 | 0.8 | 6 | 0.8 | 188 |
| 19 | - | - | 7.7 | 50 | 15.8 | 68 |
| 22 | - | - | 4.2 | 1 | 6.1 | 39 |

All the samples show an increase in the amount of extractable LMW oligomers 1 min after needle corona treatment and another increase after 10 min of recovery. Some variations can be expected due to the nature of the "washing off" of the LMW oligomers from the surface. Nevertheless, a clear trend of an increasing amount of LMW extractables on the surface as a function of the recovery time is observed. It is these LMW oligomers diffusing back to the surface that are responsible for the hydrophobicity recovery mechanism observed in the PDMS materials.

The corona ageing of the silicone rubber normally causes chain scission reactions to occur, which yielded various LMW silicones short cyclic chains and aliphatics. Intermolecular reactions may also take place, yielding high molar mass cyclics, but these species are probably hindered in terms of migration within the network structure. GC data has revealed that the migrating species contain higher amounts of cyclic LMW silicones than aliphatics, and consist predominantly of the cyclic $D_3$ to $D_7$ oligomers. Most of the silicone oligomers have cyclic structures because in the range of 4 to 6 units these cyclic structures are very stable [13]. Homma et al. [14] characterized the LMW silicone fractions on the surface of naturally-field aged silicone insulators by GC/MS and found that the materials contained predominantly cyclic low molecular oligomers, mainly $D_3$-$D_5$, in the eroded regions while the higher LMW cyclic compounds are more likely to be located in the polymer bulk, and unable to diffuse. The concentration of the LMW silicones was higher in the field- aged samples than in virgin samples. It was found that

the sides of the shed near the live end had a greater amount of LMW oligomers on the surface. The abundant quantities of the cyclic silicones over the linear silicones is most likely due to the more compact shape of the cyclic silicones and their higher diffusivity, as well as their greater stability. The GC results of this study revealed that the amounts of extracted LMW oligomers obtained from the needle corona aged samples are higher than those of the untreated counterparts. This type of behaviour was observed in all the PDMS samples regardless to their formulations. The extractable amounts of LMW silicones of the RTV samples however are generally higher than those of the HTV samples. The results of this study are consistent with the findings of Homma te al.[14].

The proportion of the LMW cyclic silicones in the needle corona aged samples increases with increasing extraction time. Fast hydrophobicity recovery occurs due to the diffusion of larger amounts of LMW cyclic silicones through the cracks in the silica-like layer and leads to regain of the hydrophobicity on the surface [15].

#### 5.2.2.8 LMW PDMS model compound study

A low molecular weight linear PDMS model compound of (Mn 6000 and Mw 10000) was used as a control material. This uncrosslinked LMW PDMS oil was used as a model compound to investigate the chemical effects of the corona ageing on the chemical structure of the PDMS chains. One of the main problems associated with a crosslinked PDMS compound is that the polymer is insoluble, therefore making chemical analysis of the structure extremely difficult. By studying the effects of corona on the LMW model compound, it was envisaged that the chemical analysis of the structural changes due to corona could be more fully understood.

The model compound sample was exposed to 30 min needle corona and 24 h French corona treatments and the aged samples were characterized by OM, GC, GC/MS, SEC and LC-transform to investigate the changes in LMW PDMS silicones. The optical microscope images of the needle and French corona aged sample are shown in Figure 5.26. The figure clearly shows that the corona treatment had a dramatic effect on the surface of the sample.

Wrinkles and cracks are clearly seen on the PDMS surface after needle corona ageing. This is also observed, but to a lesser extent, for the French corona aged sample. The surface appears to shrink during the exposure, resulting in an uneven surface appearance. The surface changes observed in the images show similar features to those observed in the crosslinked PDMS compounds after corona exposure. The surface "shrinkage" and crack formation observed in the model compound study can be attributed to the crosslinking and ultimately $SiO_x$ layer formation in the crosslinked materials.


**Figure 5.26: Optical microscope images of model compound sample: (a) virgin PDMS sample, (b) 30 min needle corona aged PDMS sample and (c) 24 h French corona aged PDMS sample.**

GC/MS analysis was performed on virgin and corona aged PDMS sample in order to characterize the different LMW PDMS silicone species that may be present.The GC/MS

results for the PDMS model compound before and after corona treatments are shown in Figure 5.27 (a)-(d).

The peaks marked 1, 2, 3 and 4 in Figure 5.27 (a) indicate a range of LMW silicon species present in the virgin sample appearing at retention times of 15, 20, 26 and 30 min. The LMW species are only present in very low amounts as indicated by their very low intensities in the GC chromatogram. In Figure 5.27 (c) however an additional peak 0 appears at lower retention time 9 min, which corresponds to a smaller LMW silicon molecule that results after corona treatment. This may be attributed to the degradation via chain scission during the electrical discharge.

Mass spectroscopy was used to identify the material corresponding to each peak in the GC spectra in Figures 5.27 (a) and (c). Figures 5.27 (b) and (d) show the mass spectra corresponding to the peaks present in Figures 5.27 (a) and (c) respectively. The signals in Figures 5.27 (b) and (d) are the ratio of the mean atomic mass (m) and the charge of the detected ion (z). All the mass peaks correspond to the short chain PDMS with a methyl group missing. This occurs because the Si-C bond breaks easily in short chain PDMS ($D_3$-$D_7$).

Before corona treatment there are LMW species with mass numbers m/z = 281, 355, 429 and 475, which correspond to the LMW silicones $D_4$-$D_7$ and are associated with their various small fragments. After corona treatment a LMW compound with mass number m/z = 207 appears in the spectrum in Figure 5.27 (d) and corresponds to $D_3$.

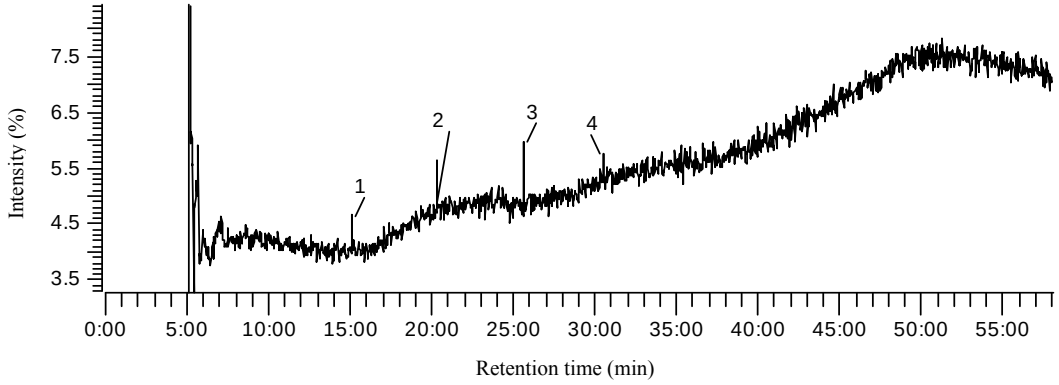


**(a)**

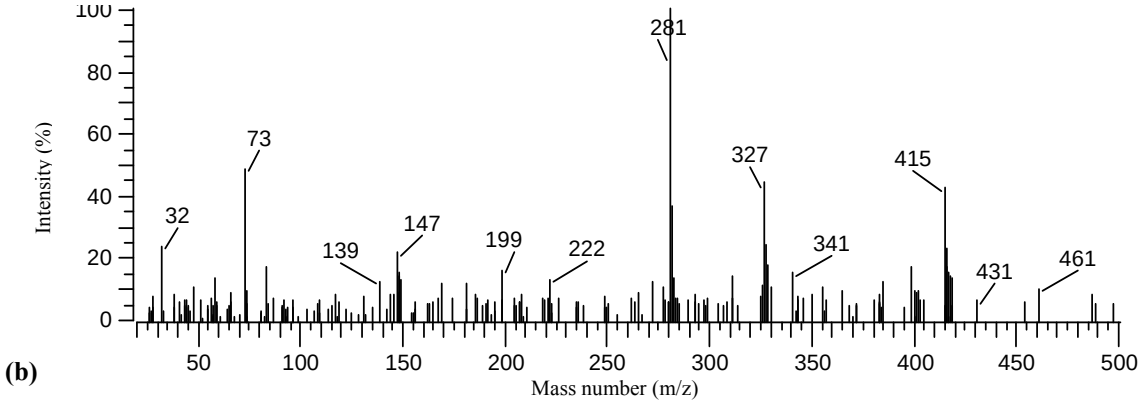


**(b)**

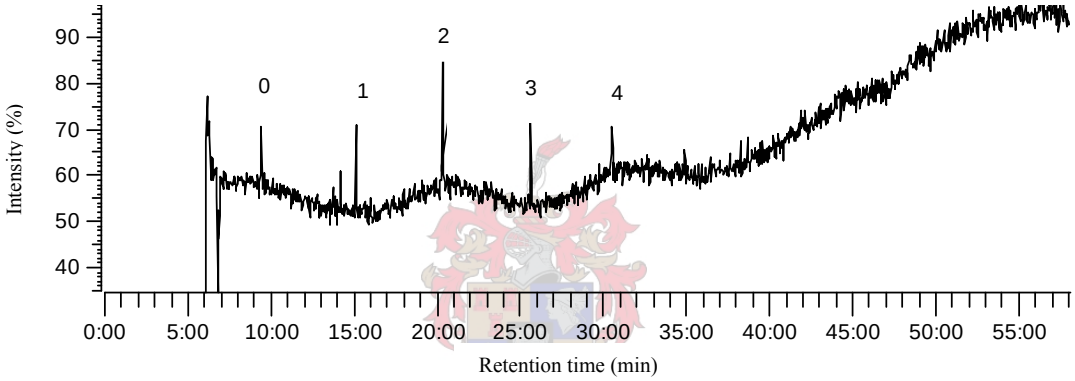


**(c)**

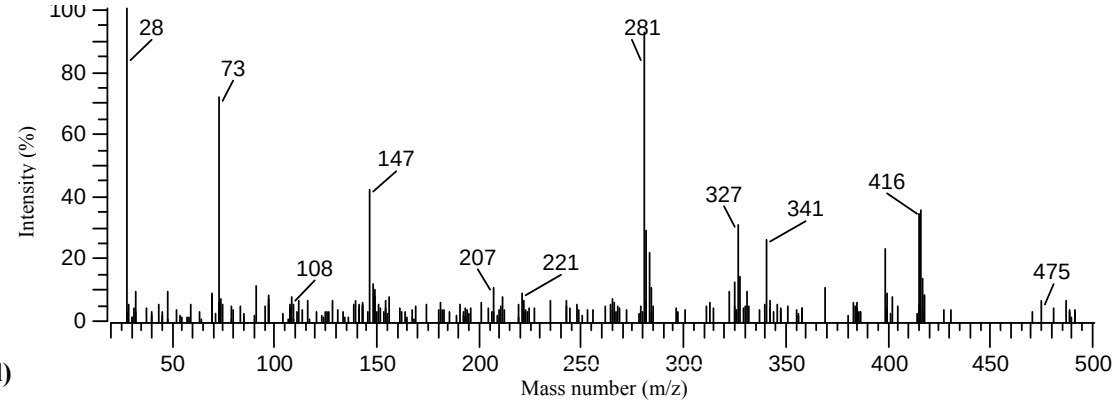


**(d)**

**Figure 5.27: GC/MS chromatograms of (a) virgin PDMS sample, (b) LMW species corresponding to virgin PDMS sample, (c) 24 h French corona treated PDMS sample and (d) LMW species corresponding to 24 h French corona treated PDMS sample.**

Table 5.12 shows the various LMW PDMS species detected and their relative intensity for the virgin compounds and after French corona treatment, as was explained above.

**Table 5.12: PDMS siloxane units observed in GC/MS chromatograms of the model compound sample before and after 24 h French corona ageing**

| Siloxane unit "n" | Virgin sample | | French corona aged sample | |
|---|---|---|---|---|
| | Mass number $(M-15)^+$ | Abundance (%) | Mass number $(M-15)^+$ | Abundance (%) |
| $D_3$ | - | - | 207 | 17 |
| $D_4$ | 281 | 30 | 281 | 20 |
| $D_5$ | 355 | 35 | 355 | 25 |
| $D_6$ | 429 | 25 | 429 | 25 |
| $D_7$ | 475 | 10 | 475 | 13 |

*$(M-15)^+$ is the mass number of the missing methyl group

These cyclic species are stable and have high diffusivity through PDMS samples due to their compact shape that allows them to migrate freely to the surface. (Once again, this finding supports the recovery process taking place via diffusion of the LMW cyclic silicones from the bulk to the surface). The majority of these LMW species are formed in-situ during the degradation process.

Further investigation of the degradation mechanism of PDMS materials was carried out on corona aged LMW PDMS sample model compound. The PDMS sample was French corona aged for 24 h. SEC analysis was used to monitor changes in the molecular mass of the model compound. Results are shown in Figures 5.28.

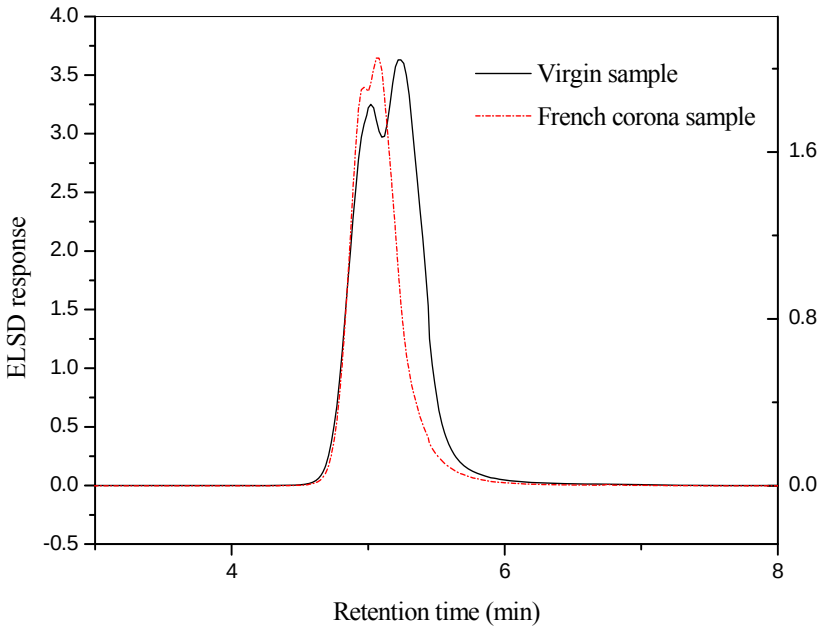


**Figure 5.28: SEC diagrams of LMW PDMS of virgin PDMS sample and 24 h French corona treated sample.**

The corona treated PDMS model compound showed a shift in the molecular mass to a shrter retention time. This might be attributed to the early stages of a "crosslinking" reaction taking place during corona ageing, leading to some higher molecular mass chains.

SEC-LC-transform FTIR analysis was carried out on the virgin sample and the French corona aged PDMS sample to investigate the possible changes in the chemical composition taking place in the PDMS structure as a result of corona ageing. The coupling of FTIR to SEC analysis allows for the investigation of how the various chemical groups are distributed in the molecular mass of the polymer chains. Figure 5.29 show the so-called waterfall plot generated using the LC transform technique. Each of the spectra in the figure corresponds to a specific retention time along the molecular mass distribution curve. Each of the FTIR spectra show the peaks that are characteristic of the PDMS polymer.

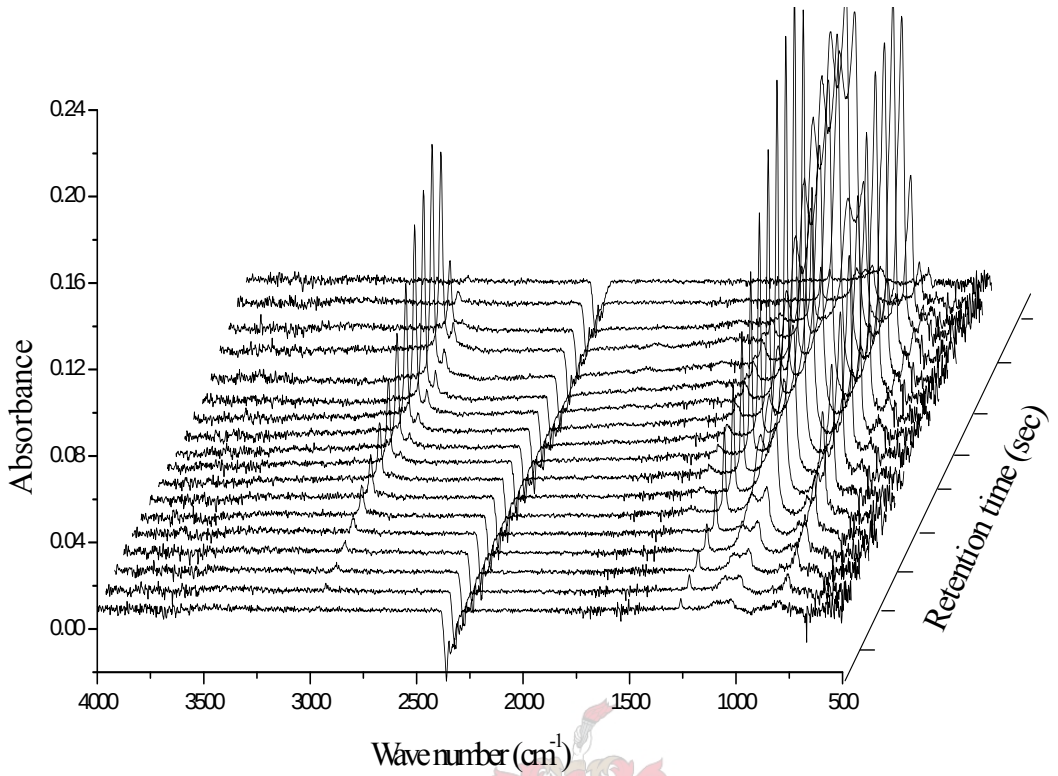


**Figure 5.29: Waterfall plot of PDMS model compound and its IR absorption bands.**

The relative changes in the peak intensities within each spectra can be analysed. This gives an indication of the relative variation in the different functional groups in the polymer chains. Figure 5.30 shows the relative Si-CH peaks (1260 $cm^{-1}$) and the Si-O-Si peaks (1018 $cm^{-1}$) ratios for the virgin and corona aged samples. The ratios of the $Si-CH_3$ peaks (867 $cm^{-1}$) relative to Si-O-Si peaks (1018 $cm^{-1}$) were investigated in the similar fashion and results are shown in Figure 5.31. The Gram-Schmidt profiles give the overall integrated peak intensities for each FTIR spectrum and correspond to the total amount of material present at each retention time, while the relative changes in the peak intensities indicate changes in the chemical composition of the material at each point.

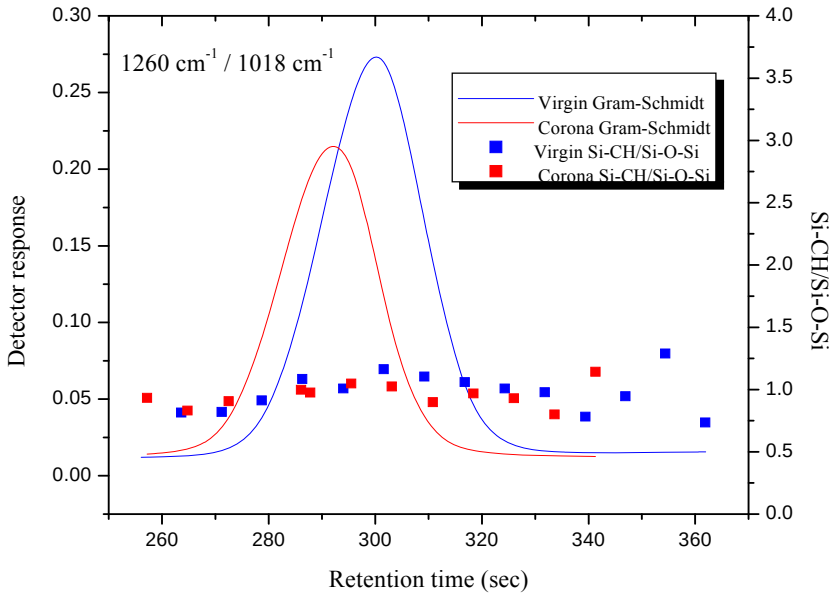


**Figure 5.30: The overlay Gram-Schmidt profiles of virgin and 24 h French corona treated PDMS model compound at 1260 cm$^{-1}$/1018 cm$^{-1}$.**

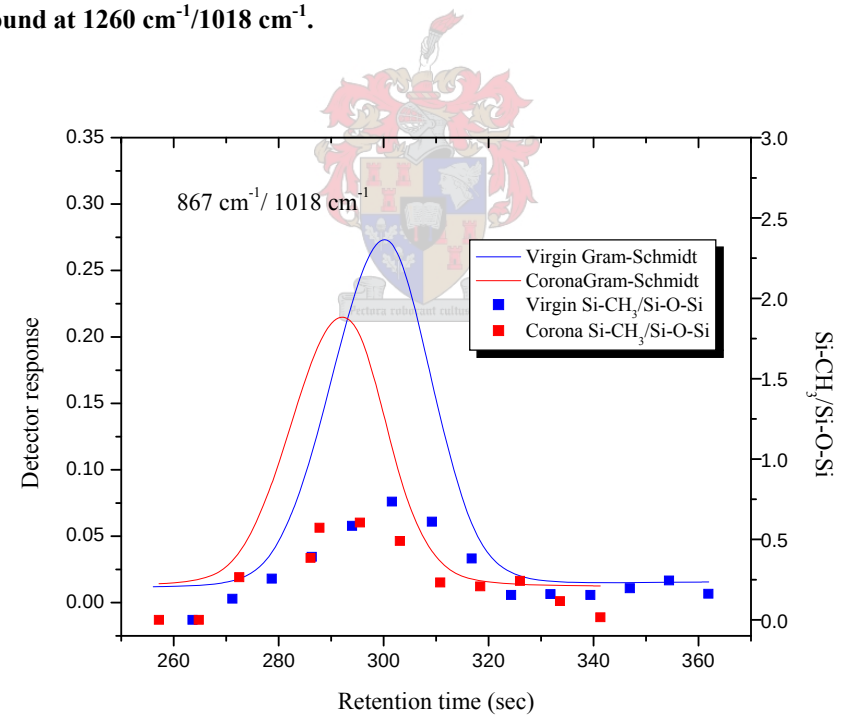


**Figure 5.31: The overlay Gram-Schmidt profiles of virgin and 24 h French corona treated PDMS model compound at 867 cm$^{-1}$/1018 cm$^{-1}$.**

Figure 5.30 shows the overlay of the Gram-Schmidt profiles for the virgin PDMS model compound and a sample after corona treatment, as well as the ratio of the 1260 cm$^{-1}$ (Si-CH) peak to the 1018 cm$^{-1}$ (Si-O-Si) peak at each of the measured retention times. For the

corona treated sample the ratio was lower than for the virgin sample, particularly in the lower molecular mass region (indicated by a longer retention time). A similar trend is observed in Figure 5.31 where the ratio of the 867 $cm^{-1}$ ($Si-CH_3$) peak plotted relative to the 1018 $cm^{-1}$ (Si-O-Si) peak is. This shows an increase in the Si-O-Si peak relative to the two peaks associated with the methyl groups along the polymer chain. The molecules in this region represent the remaining polymer molecule fragments that have undergone extensive degradation (loss of the methyl groups), but still remain soluble. The remaining fragments of these molecules are in the form of the low molecular weight oligomers (detected via GC analysis) and the $SiO_x$ layer, observed on the surface of the polymer after corona degradation. The decrease in the $Si-CH_3$ concentration indicates the loss of the methyl groups along the polymer chain during the corona treatment prior to the formation of the $SiO_x$ degradation layer. The shift in the overall Gram-Schmidt profile to shorter retention times (higher molecular masses) indicate that those molecules have undergone a crosslinking reaction during the corona exposure.

### 5.2.3 UV radiation

In-service, high voltage insulators are exposed to UV radiation from sunlight and UV produced during electrical discharge activity. It is believed that PDMS is highly resistance to UV-A (340 nm) and UV-B (313 nm) radiation due to the strong bonding between oxygen and silicone atoms. EPDM rubbers, however, do not show such good resistance towards UV radiation [16]. UV wavelengths between 313-340 nm are believed to be the main cause of material degradation by UV radiation. Shorter UV-B wavelengths may have an effect on PDMS housings after long term exposure. An investigation of the long term exposure of the materials considered in this study to UV-B radiation was carried out to determine wthether there were significant material changes over time.

A hydrophobicity recovery investigation was carried out on selected UV aged samples. SCA measurements are correlated to hydrophobicity of the insulator surface. Results of SCA measurements as a function of the recovery time after UV-B exposure are shown in Figures 5.32 (a)-(d) for UV exposure times of 1000 h, 2000 h, 3000 h and 8000 h. The SCA was monitored as a function of the time of exposure to determine whether the

compounds showed a hydrophobicity recovery similar to that observed after corona treatment.

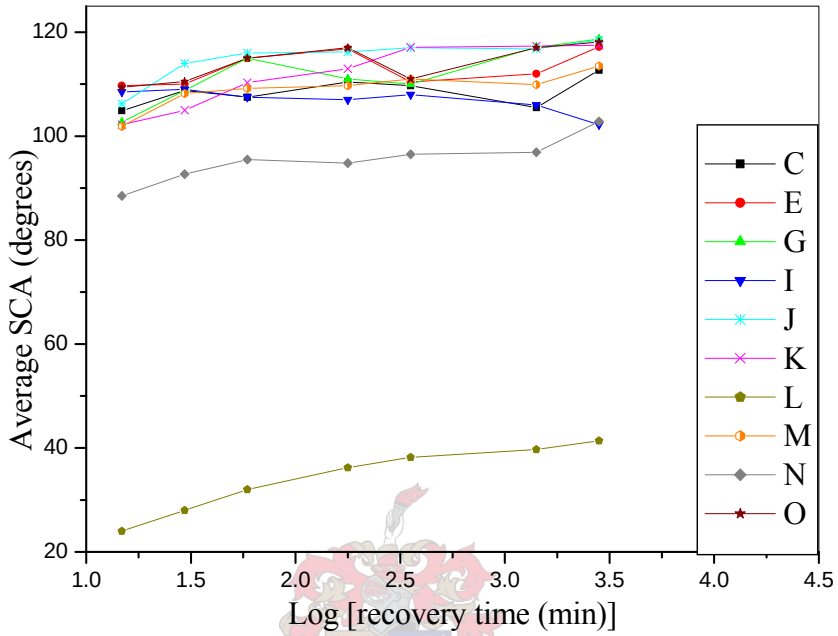


**(a)**

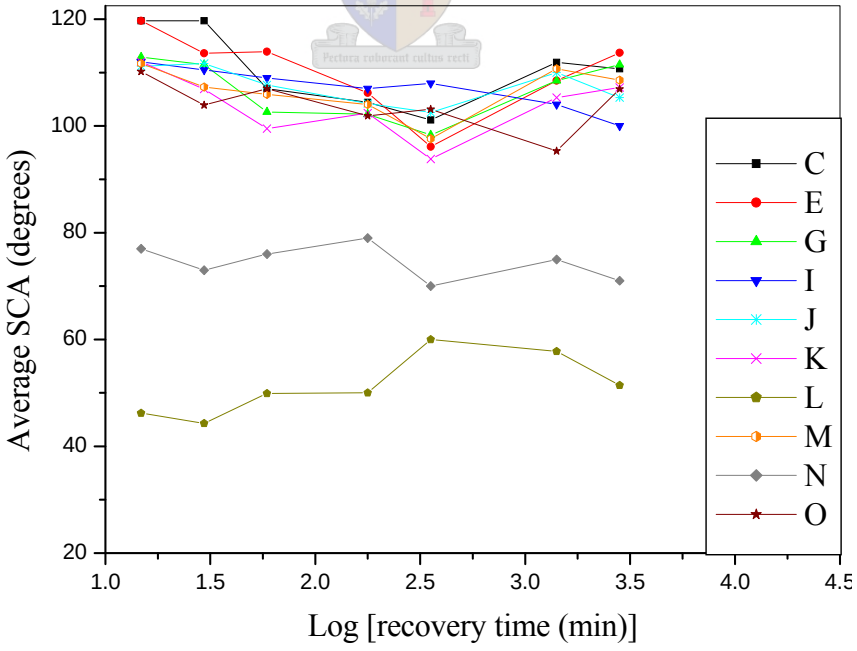


**(b)**

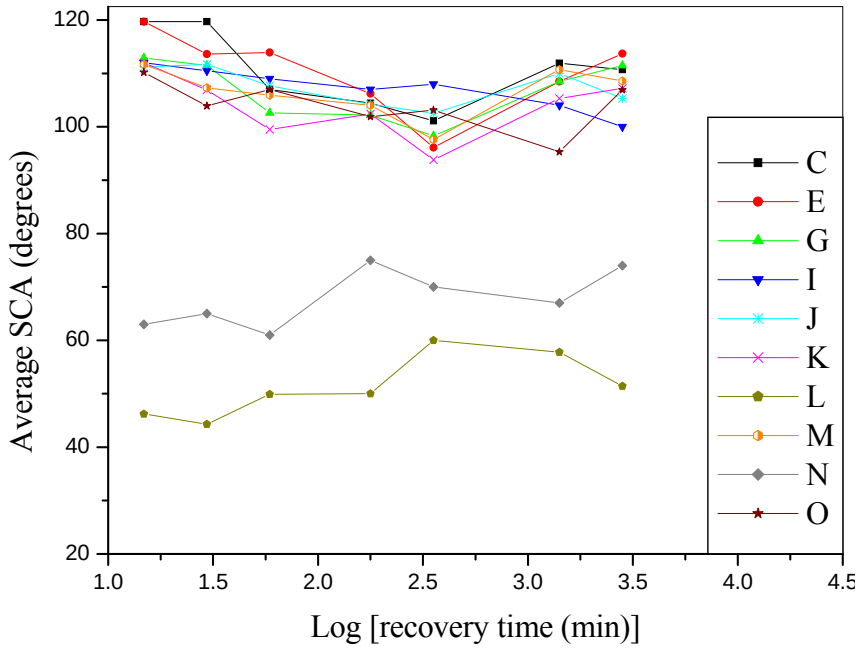


**(c)**

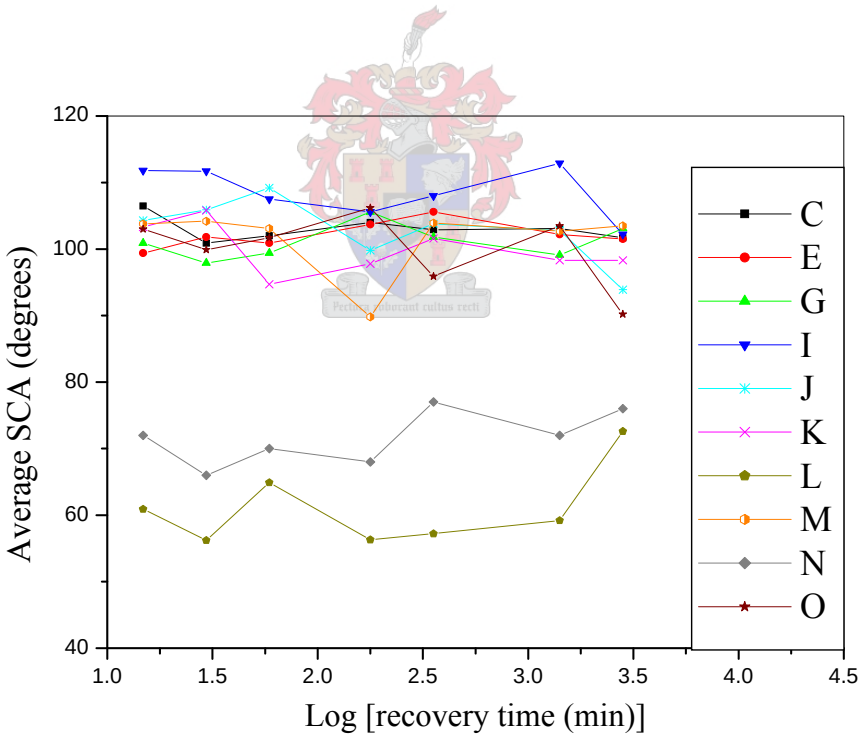


**(d)**

**Figure 5.32: Hydrophobicity recovery of the controlled formulations and the commercial samples after various UV exposure times: (a) 1000 h, (b) 2000 h, (c) 3000 h and (d) 8000 h.**

The PDMS samples C, E, G, I, J, K, M and O showed a very slight decrease 5º in their SCA values after 1000 h UV-B ageing (Figure 5.32 (a)). This means that they maintain a

good hydrophobic character after exposure. The EPDM samples N and L, on the other hand, had a more pronounced decrease in SCA values 55º relative to the virgin sample. This is especially true at the onset of SCA measurements when the sample surfaces were highly hydrophilic (corresponding to a relatively small contact angle). Commercial sample L had much lower SCA values than sample N and the PDMS samples. Contact angle values of commercial sample N were found to be lower than that of the PDMS samples C, E, G, I, as were the commercial samples J, K, M and O. There was a more pronounced reduction in the SCA values 10º after 3000 h UV-B ageing (Figure 5.32 (c)). The UV test was continued for 8000 h in order to investigate any further surface changes. Results are shown in Figure 5.32 (d).

Once again the PDMS samples showed sustained hydrophobic surface characteristics, with average static contact angles >90º. Nevertheless, in most samples the SCA values decreased by about 10º relative to the unexposed samples. This behaviour is attributed to the well-recognized PDMS resistance towards UV ageing. Yoshimura, Kumagai and Nishimura [17] studied the effect of UV irradiation on silicon rubber surfaces used for HV insulators and found a slight decrease in SCA values 10º after 6000 h UV ageing.

After 1000 h UV exposure commercial sample L showed a drastic loss of hydrophobicity; it had a very low average SCA value below 40°. The degradation of this sample was associated with a colour change and a change in the surface morphology (as discussed below).

There was a large difference in the SCA values measured for commercial samples N and L of the EPDM rubber type compared to the PDMS samples. EPDM is known for its intolerance to high doses of UV radiation: it degrades, forming highly conductive carbonated moieties on the surface. UV irradiated HV polyester insulators have shown similar results [18]. PDMS is highly resistant to UV-B ageing and therefore does not degrade to a significant extent upon UV-B radiation; therefore the PDMS samples used in this study show sustainable hydrophobic characteristics after UV ageing. For the shorter exposure times the PDMS samples do show a slight tendency to recover their hydrophobicity. At the longer exposure times of 3000 h and 8000 h the small decrease in

SCA shows no tendency to recover after exposure, showing that the changes on the surface are small and irreversible.

When UV aged commercial sample L was visualized under an optical microscope it showed the major degradation features associated with cracks on its surface. These can be clearly seen in Figure 5.33.

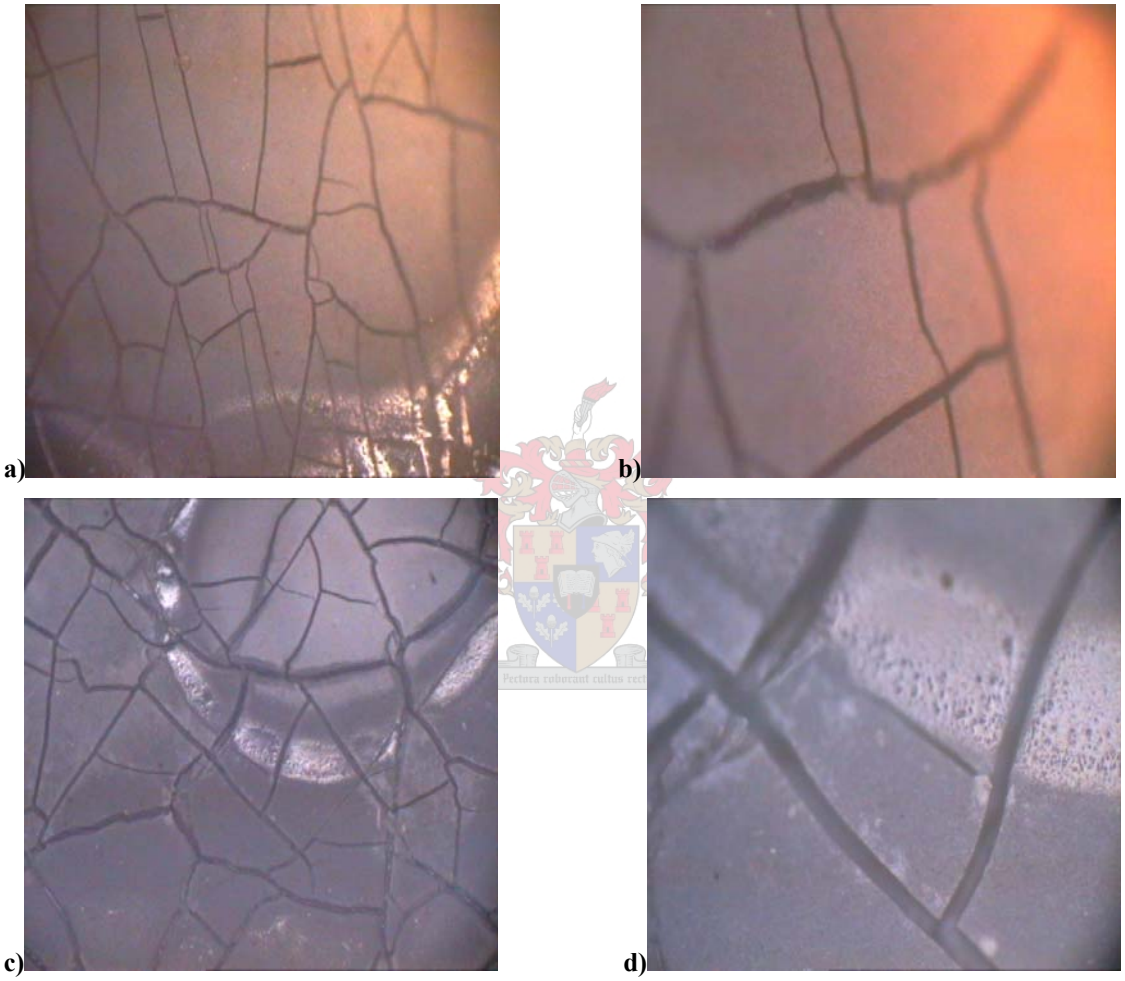


**Figure 5.33: Optical microscope images of sample L after (a, b) 1000 h and (c, d) 8000 h UV ageing.**

Besides the observed cracks, there appears to be loose particles on the surface. This is normally referred to as "chalking" of the polymer surface, as loose powdery particles of the filler ($Al_2O_3$) are exposed due to the effect of UV irradiation. Commercial sample N after 1000 h UV-B also exhibited signs of ageing associated with cracks on the insulator surface but theses appeared to a lesser degree in comparison with commercial sample L.

The optical microscope images of commercial sample N showed chalking of its surface and it had a whitish appearance due to the filler particles exposed and cracks, as shown in Figure 5.34.

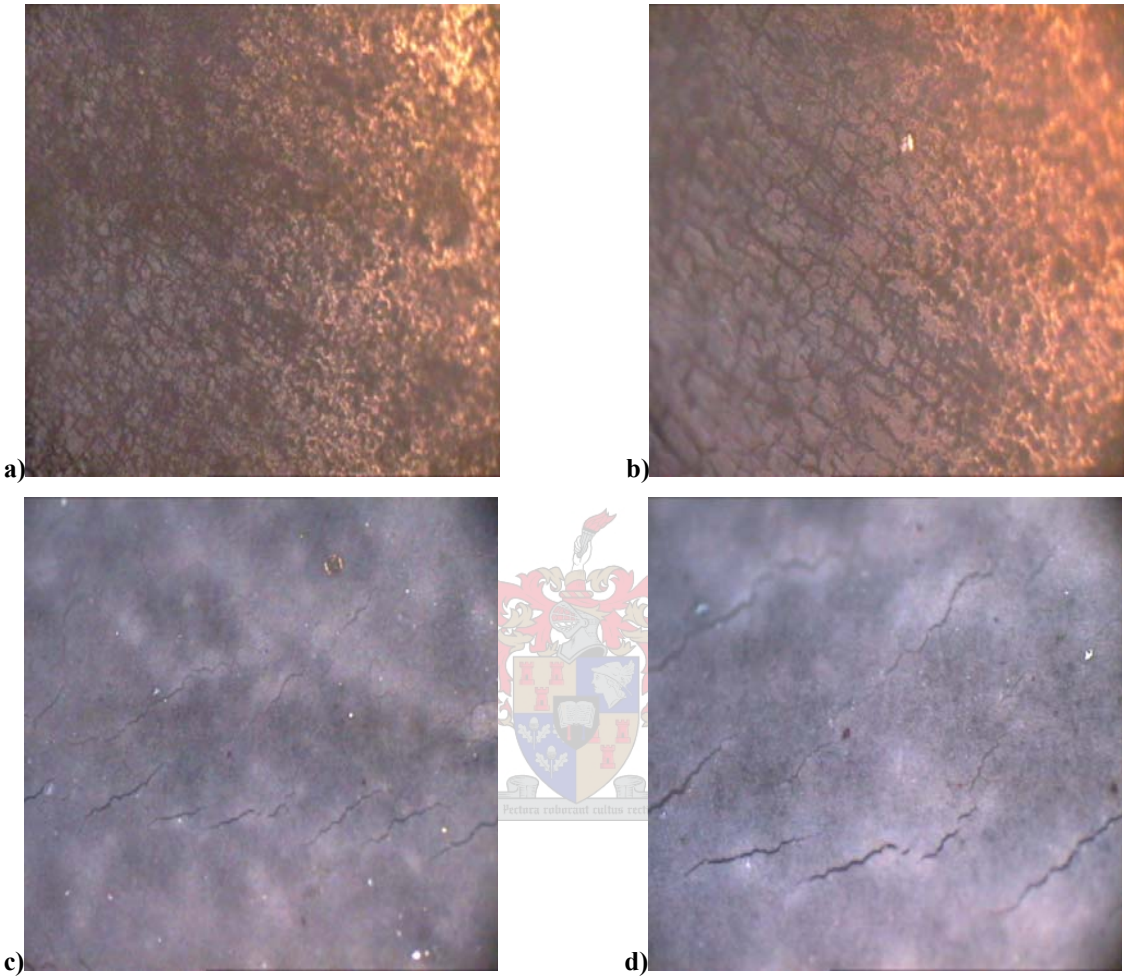


**Figure 5.34: Optical microscope images of sample N after (a, b) 1000 h and (c, d) 8000 h UV ageing.**

Upon prolonged UV ageing of 8000 h the cracks appeared more severe and deeper in both the EPDM samples. Commercial sample L seems to degrade much faster after the initial period of UV exposure (1000 h) and has much more deep and severe flaky cracks on its surface. These are associated with a faded surface colour and high wetting compared to commercial sample N. Contrary to this, all the PDMS samples, showed no signs of cracks but the surfaces appeared a little rough. The optical microscope images of all samples are included in Appendix C. The increased roughness of the surface of sample

L after increased exposure time is most likely responsible for the observed increase in the SCA values. The influence of surface roughness on the measured SCA values is discussed in Section 5.1.2.

The PDMS samples do not show significant cracks or erosion although a few loose filler particles are observed under SEM. Once again, the two EPDM samples L and N showed a high susceptibility towards UV degradation. This is confirmed by the presence of cracks and severe chalking on their surfaces. SEM imaging of commercial samples N and L shows deep cracks along the sample surfaces as well as a large number of filler particles exposed. Typical SEM results are shown in Figures 5.35 and all the SEM images are included in Appendix B.

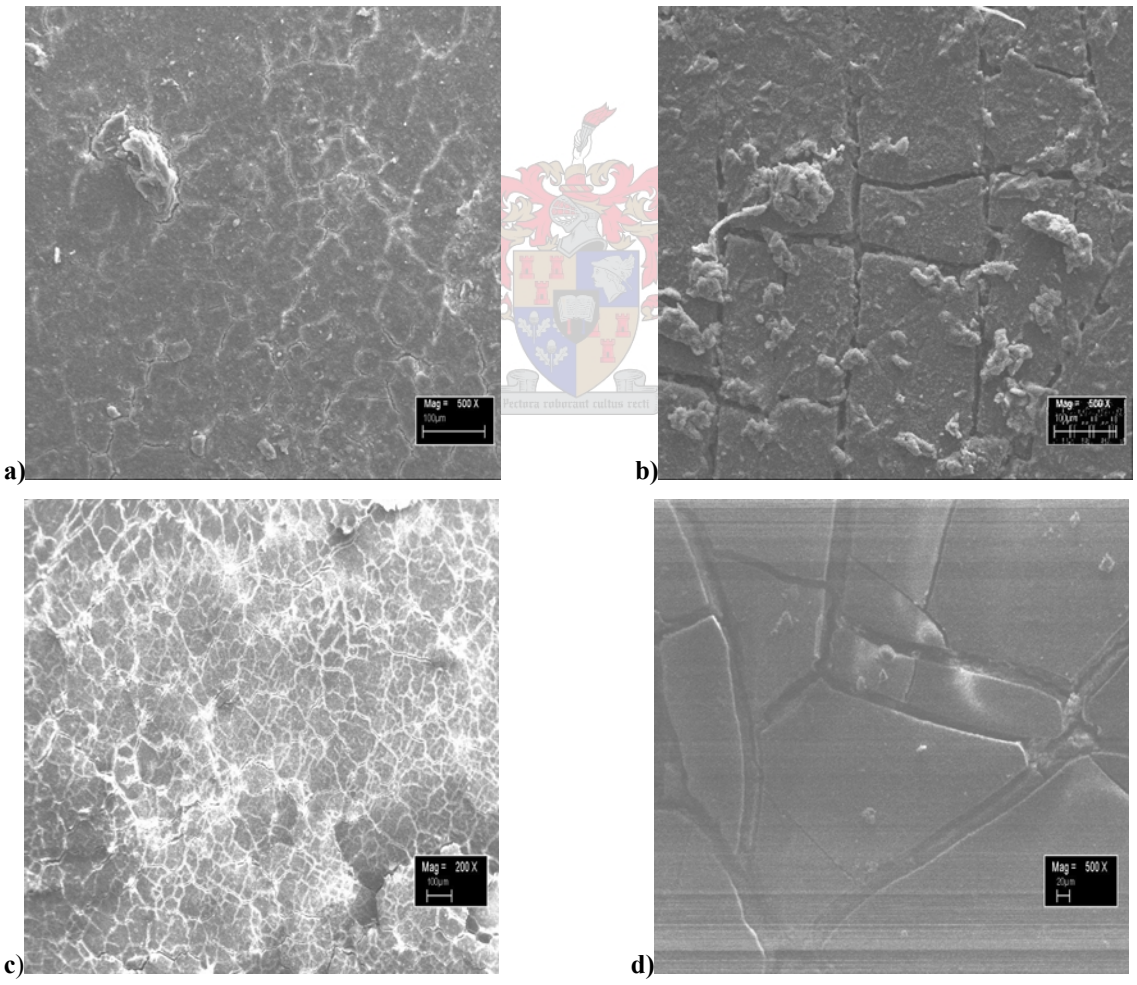


**Figure 5.35: SEM images of (a) sample N and (b) sample L after 3000 h UV ageing, (c) sample N and (d) sample L after 8000 h UV ageing.**

As is the case of the OM images, SEM images showed that the surface cracks were much deeper in commercial sample L compared to sample N, indicating that the former was more severly damaged by UV-B irradiation, it started to degrade rapidly, resulting in the filler particles becoming exposed, which leads to chalking on the surface.

A study carried out in South Korea by Youn and Huch [19] on the surface degradation of HTV silicone rubber and EPDM used for outdoor insulators showed less surface damage on PDMS insulators than EPDM insulators (which suffered severe chalking and cracking). Silicone rubber undergoes mainly crosslinking reactions whereas EPDM surface damage occurs due to chain scission reactions followed by the generation of free radicals and groups containing oxygen.

EDS was used on the UV aged samples to determine the relative changes of the various elements ratios on the sample surface such as carbon, oxygen, aluminium, and silicone after ageing. The results of UV aged samples at different periods of exposure are shown in Table 5.13.

EDS results showed that there is a slight increase in the oxygen ratios (compared to the other elements) at the PDMS sample surfaces after 3000 h UV ageing relative to the untreated samples. However, a more pronounced increase in the oxygen ratios was observed in commercial samples N and L, where the oxygen percentage increased from 30% and 22% to 53% and 43% for samples L and N respectively after 3000 h. No significant changes were observed for the PDMS samples after shorter exposure times.

Prolonged UV ageing of the samples up to 8000 h was carried out to investigate possible further changes in the elemental composition of the surface after ageing. An overall progressive increase in the oxygen levels of the samples associated with a decrease in the carbon and silicone ratios was found.

Schnyder et al. [20] investigated the effect of UV irradiation on PDMS films using XPS and found that there is an increase in the oxygen and silicone contents associated with a decrease in the carbon levels upon prolonged UV exposure. Similar results were reported for another study carried out by Xu et al. [21] on UV aged EPDM insulators using XPS.

**Table 5.13: EDS results of 3000 h and 8000 h UV-B aged samples**

| Exposure time (h) | ID | C% | O% | Si% | Al% | Si/O | Si/C | C/O |
|---|---|---|---|---|---|---|---|---|
| 0 | C | 36.0 | 27.5 | 36.1 | - | 1.31 | 1.00 | 1.30 |
| | E | 36.5 | 24.7 | 38.9 | - | 1.57 | 1.06 | 1.47 |
| | G | 30.1 | 26.7 | 29.7 | 13.5 | 0.99 | 0.92 | 1.04 |
| | I | 34.6 | 37.4 | 23.6 | 4.4 | 0.63 | 0.68 | 0.92 |
| | J | 24.9 | 41.1 | 20.2 | 13.8 | 0.49 | 0.81 | 0.60 |
| | K | 23.8 | 43.2 | 20.1 | 12.9 | 0.46 | 0.84 | 0.55 |
| | L | 56.0 | 30.5 | - | 13.0 | - | - | 1.83 |
| | M | 25.2 | 45.5 | 16.4 | 12.6 | 0.36 | 0.65 | 0.55 |
| | N | 65.0 | 22.6 | - | 9.4 | - | - | 2.87 |
| | O | 24.2 | 38.8 | 25.0 | 12.0 | 0.64 | 1.03 | 0.62 |
| 3000 | C | 40.7 | 24.2 | 34.8 | - | 1.88 | 0.86 | 1.68 |
| | E | 45.8 | 28.2 | 26.0 | - | 0.92 | 0.57 | 1.62 |
| | G | 34.8 | 28.7 | 30.0 | 6.5 | 1.05 | 0.86 | 1.21 |
| | I | 37.0 | 26.0 | 29.0 | 8.0 | 1.11 | 0.78 | 1.42 |
| | J | 25.3 | 41.7 | 19.3 | 13.7 | 0.46 | 0.76 | 0.61 |
| | K | 26.4 | 44.6 | 17.5 | 10.9 | 0.39 | 0.66 | 0.59 |
| | L | 26.0 | 53.0 | - | 18.1 | - | - | 0.49 |
| | M | 20.4 | 43.2 | 16.4 | 14.2 | 0.38 | 0.80 | 0.47 |
| | N | 39.0 | 43.1 | - | 14.1 | - | - | 0.90 |
| | O | 24.9 | 40.6 | 21.7 | 12.7 | 0.53 | 0.87 | 0.61 |
| 8000 | C | 17.3 | 65.6 | 16.9 | - | 0.26 | 0.98 | 0.26 |
| | E | 16.9 | 65.3 | 17.7 | - | 0.27 | 1.05 | 0.26 |
| | G | 17.8 | 65.6 | 14.1 | 2.5 | 0.22 | 0.79 | 0.27 |
| | I | 20.0 | 62.0 | 13.0 | 5.0 | 0.21 | 0.65 | 0.32 |
| | J | 18.0 | 65.1 | 8.8 | 8.1 | 0.14 | 0.49 | 0.28 |
| | K | 17.9 | 65.2 | 10.1 | 6.5 | 0.16 | 0.56 | 0.28 |
| | L | 18.2 | 64.3 | - | 15.1 | - | - | 0.28 |
| | M | 18.6 | 65.6 | 8.0 | 7.8 | 0.12 | 0.43 | 0.28 |
| | N | 20.5 | 65.9 | - | 11.0 | - | - | 0.31 |
| | O | 18.4 | 65.6 | 9.6 | 6.4 | 0.15 | 0.52 | 0.28 |

### 5.2.4 Acid rain (hydrolysis ageing)

The surfaces of housing sheds may be chemically degraded by the introduction of highly polar conductive moieties present in acid rain, as a result of hydrolysis. This can result in an increase in the surface wettablity, with a subsequent surface conductivity increase and accompanying leakage current. Another type of failure possibly due to acid rain is brittle fracture, which takes place between the rubber shed and the fibre-reinforced plastic core, where moisture and nitric acid attack the interfaces and erode the material away, leading to serious damage [22]. Figures 5.36 (a) and (b) show the hydrophobicity recovery of all samples after 50 and 75 days acid rain ageing.

All the PDMS samples showed a relatively slight decrease in static contact angle values upon immersion in synthetic acid rain for 50 days. The EPDM commercial samples N and L showed the most dramatic decrease in the static contact angle values, as shown in Figure 5.36 (a).

After 75 days ageing the PDMS samples showed a slight decrease in static contact angle values compared with SCA values obtained after 50 days of acid rain ageing. Sample C exhibited the lowest SCA value among the PDMS samples of both the controlled formulation and commercial samples. The EPDM commercial samples still showed dramatic surface characteristic changes, as indicated by lower static contact angle values compared with PDMS samples. This illustrates the higher susceptibility of the EPDM rubber towards the oxidation caused by acid rain ageing. The SCA of the PDMS samples for both the 50 and 75 days showed very little increase, indicating that little to no recovery in the SCA occurs after removal from the acid rain solution. It is however noted that the EPDM samples show a significant increase in the SCA as a function of the recovery time after 50 day of exposure. It is also noted that there is a relatively large degree of scatter in the SCA measurement, which may be a results of changes in the surface morphology of the samples.

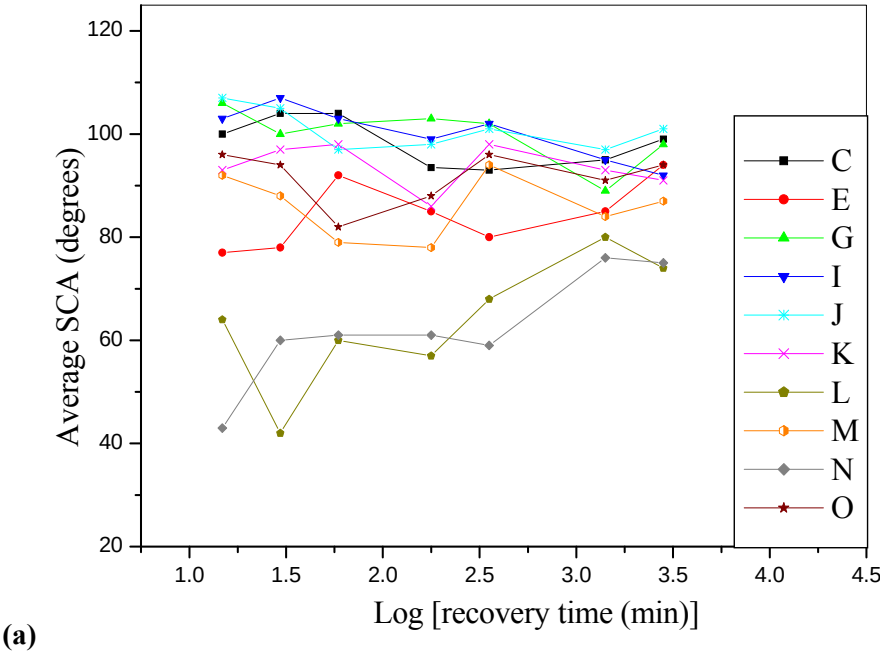


**(a)**

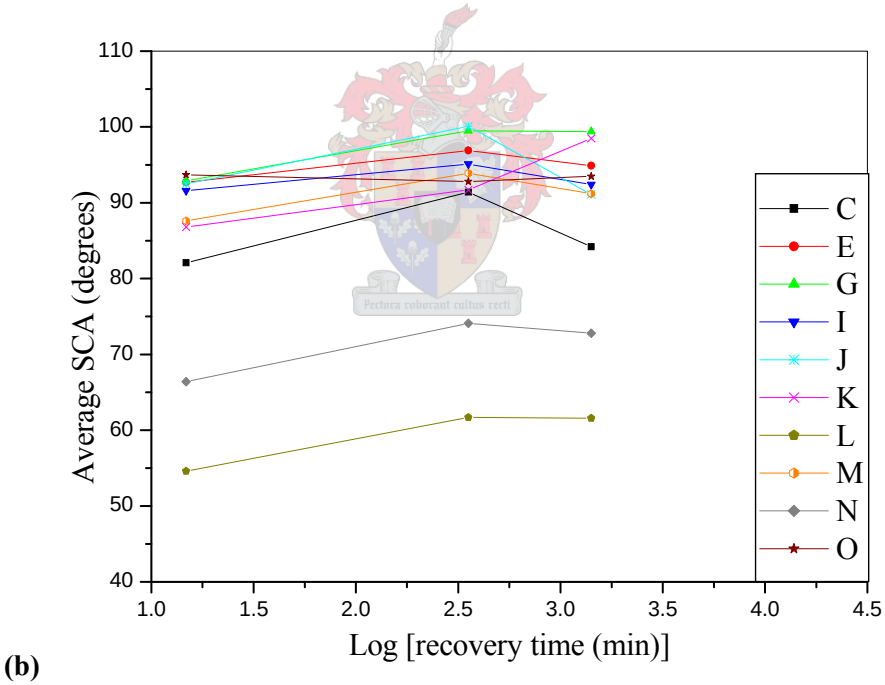


**(b)**

**Figure 5.36: Hydrophobicity recovery of acid rain aged PDMS samples after (a) 50 and (b) 75 days of exposure.**

As noted earlier, the PDMS sample C shows the most dramatic decrease in the SCA after 75 days. The decrease is associated with visible changes on the sample surface. After artificial acid rain ageing the eroded areas appear as deep holes on the surface. An optical

microscope image illustrating the effect of erosion on the surface is illustrated in Figure 5.37.

**Figure 5.37: Surface erosion in PDMS sample C caused by acid rain ageing, observed after 75 days.**

The investigation of acid rain ageing was continued for 125 and 200 days to determine any further surface changes. The hydrophobicity recovery for these longer exposure times is shown in Figures 5.38 (a) and (b) respectively.

Samples C, E, G and I showed very slight decreases in SCA values after prolonged immersion in artificial acid rain for 125 and 200 days, which correlates with the findings of a previous investigation after 75 days acid rain ageing. The lowest contact angles were obtained for sample C at the onset of the measurements. Similar results were obtained for the commercial PDMS samples J, O and M. Commercial EPDM samples N and L again exhibited the more pronounced decrease in SCA values. Some recovery of the SCA was observed for the samples exposed to the longer periods of acid rain.

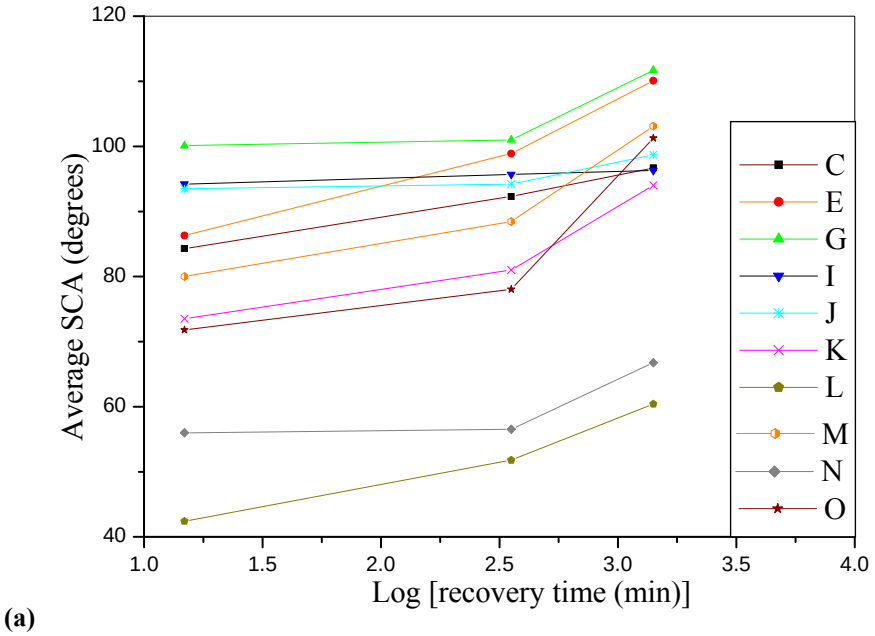


**(a)**

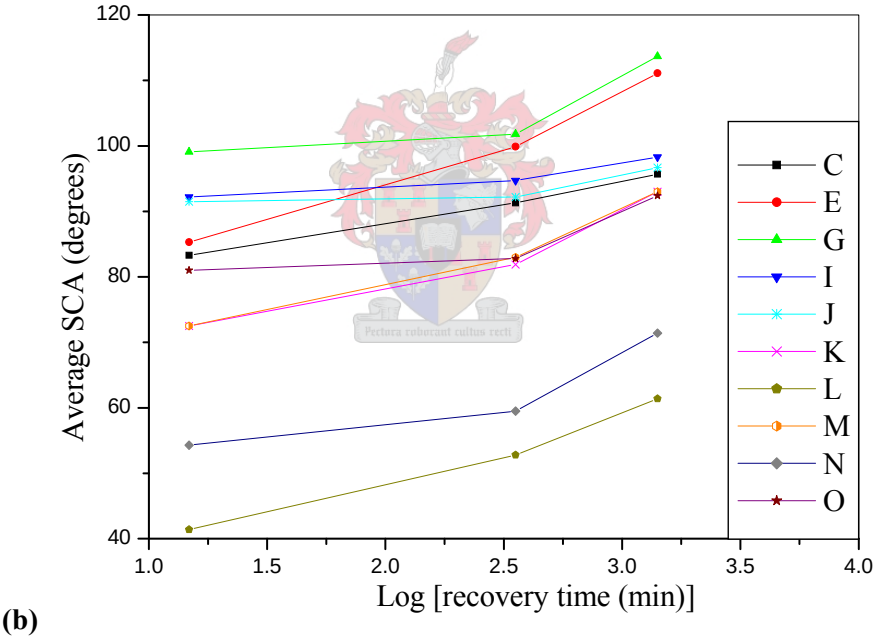


**(b)**

**Figure 5.38: Hydrophobicity recovery of samples after (a) 125 and (b) 200 days acid rain ageing.**

Static contact angle values of the acid rain aged samples after various periods are summarized in Table 5.14. The values indicated in the table are the values obtained immediately after removal of samples from the synthetic acid rain solution.

**Table 5.14: Average static contact angle values of the controlled formulation and the commercial samples after various periods (days) of acid rain ageing**

| ID | Average SCA (degrees) after number of days | | | | |
|---|---|---|---|---|---|
| | 0 | 50 | 75 | 125 | 200 |
| C | 107.0 | 98.3 | 91.9 | 91.1 | 91.9 |
| E | 111.0 | 94.7 | 94.0 | 98.4 | 99.6 |
| G | 115.0 | 99.9 | 97.2 | 104.0 | 106.0 |
| I | 108.0 | 100.0 | 93.0 | 95.4 | 99.9 |
| J | 109.0 | 101.0 | 94.5 | 95.5 | 95.1 |
| K | 106.0 | 93.5 | 92.3 | 82.8 | 85.4 |
| L | 90.0 | 71.1 | 63.4 | 51.5 | 50.0 |
| M | 107.0 | 91.9 | 90.9 | 85.2 | 76.3 |
| N | 84.0 | 62.7 | 59.3 | 61.4 | 62.1 |
| O | 101.0 | 94.7 | 93.3 | 92.1 | 96.9 |

There was generally a decrease in the SCA values with the number of days of acid rain exposure, relative to untreated samples. Sample I showed the lowest decrease in SCA 8º for the RTV samples, followed by samples G and E. The unfilled compound (sample C) showed that largest change. The variation in SCA values may be due to mechanical strength imparted by the effect of the filler incorporation within the PDMS matrix. It appears as if the fillers provide improved resistance to surface erosion. Fillers may act as barriers to the development of the deep holes, as observed in the surface of sample C, illustrated in Figure 5.37. Commercial samples J and K had lower SCA values, but sample O shows a much lower decrease of 14º, however, the samples still have hydrophobic surfaces. Commercial sample O exhibits the lowest decrease of the SCA value, which indicates a much higher stability against oxidation. Of the commercial PDMS based compounds sample M shows the largest SCA decrease, 30º. Once again, commercial samples L and N showed the greatest decrease in SCA values upon acid rain ageing; decreases were 40º and 22º, respectively after 200 days of acid rain ageing. The relatively good stability of PDMS samples towards oxidation is ascribed to the strong

siloxane bonds. Once again, the higher susceptibility of EPDM samples to oxidation and subsequent deterioration of the EPDM surface upon acid rain immersion was illustrated.

To further investigate the surface chemical changes taking place upon acid rain ageing, elemental analyses of the sample surfaces were determined. The results of this analysis are shown in Table 5.15. There was a progressive increase in the oxygen content and a decrease in the carbon content. A considerably more pronounced increase in the oxygen level was found in the commercial EPDM samples N and L relative to the PDMS samples.

Optical microscope and SEM images of acid rain aged samples showing the most pronounced surface changes are shown in Figures 5.39 and 5.40 respectively. Images of other samples are included in Appendices B and C.

The OM image of the surface of sample C in Figure 5.39 (b) showed holes, which occurred as a result of surface erosion caused by the acid rain. The SEM image in Figure 5.40 (b) showed similar feature. Aged commercial sample L and N had a rough surface relative to the untreated sample.

A study carried out by Wang, Chen and Yoshimura [22] to investigate the tracking of various polymeric insulators including porcelain, EPM/silicone alloy, silicon rubber and EPDM used in high voltage applications showed similar holes in the insulator surfaces. No failure was observed for porcelain and EPM surfaces.

Koo et al. [23] have also reported that the effects of relatively high acid rain concentrations on silicone rubber HV insulators, there is a decrease in the crosslink density and chain scission of the base polymer. The critical pH value for the onset of serious surface degradation is between pH 1.5 and 2.5. They also found that besides the removal of ATH filler from the insulator surface there is an increase in the surface roughness at low pH values.

**Table 5.15: EDS results of samples exposed to a synthetic acid rain after 75, 125 and 200 days**

| Exposure time (days) | ID | C% | O% | Si% | Al% | Si/O | Si/C | C/O |
|---|---|---|---|---|---|---|---|---|
| 75 | C | 40.0 | 29.2 | 30.8 | - | 1.05 | 0.77 | 1.37 |
| | E | 34.6 | 27.6 | 37.7 | - | 1.37 | 1.09 | 1.25 |
| | G | 42.6 | 23.1 | 28.8 | 5.5 | 1.25 | 0.68 | 1.84 |
| | I | 31.9 | 28.1 | 33.4 | 6.6 | 1.19 | 1.05 | 1.14 |
| | J | 33.1 | 34.1 | 19.2 | 13.6 | 0.56 | 0.58 | 0.97 |
| | K | 26.4 | 41.5 | 20.8 | 11.3 | 0.50 | 0.79 | 0.64 |
| | L | 52.5 | 30.1 | - | 15.2 | - | - | 1.74 |
| | M | 26.2 | 38.3 | 18.9 | 16.6 | 0.49 | 0.72 | 0.68 |
| | N | 58.8 | 22.9 | - | 14.4 | - | - | 2.57 |
| | O | 22.5 | 37.1 | 24.6 | 15.8 | 0.66 | 1.09 | 0.61 |
| 125 | C | 43.0 | 30.3 | 26.7 | - | 0.81 | 0.62 | 1.42 |
| | E | 36.3 | 29.7 | 34.0 | - | 1.14 | 0.93 | 1.22 |
| | G | 12.7 | 61.6 | 19.6 | 6.0 | 0.34 | 1.54 | 0.21 |
| | I | 13.9 | 62.5 | 17.8 | 5.7 | 0.29 | 1.28 | 0.22 |
| | J | 13.2 | 61.3 | 13.9 | 11.4 | 0.23 | 0.89 | 0.22 |
| | K | 15.5 | 63.2 | 13.3 | 7.0 | 0.21 | 0.86 | 0.25 |
| | L | 21.9 | 67.4 | - | 9.1 | - | - | 0.33 |
| | M | 12.3 | 60.4 | 13.0 | 14.1 | 0.22 | 1.05 | 0.20 |
| | N | 23.0 | 68.6 | - | 6.8 | - | - | 0.33 |
| | O | 13.5 | 61.5 | 14.3 | 10.0 | 0.23 | 1.05 | 0.22 |
| 200 | C | 23.0 | 58.3 | 18.7 | - | 0.32 | 0.81 | 0.39 |
| | E | 18.9 | 60.1 | 21.0 | - | 0.35 | 1.11 | 0.34 |
| | G | 10.8 | 66.2 | 19.0 | 4.0 | 0.29 | 1.76 | 0.16 |
| | I | 11.9 | 68.1 | 15.0 | 5.0 | 0.22 | 1.26 | 0.18 |
| | J | 10.2 | 70.8 | 12.0 | 7.0 | 0.17 | 1.18 | 0.14 |
| | K | 13.5 | 69.5 | 12.0 | 5.0 | 0.17 | 0.89 | 0.19 |
| | L | 18.5 | 72.5 | - | 8.7 | - | - | 0.26 |
| | M | 11.5 | 66.5 | 10.0 | 12.0 | 0.15 | 0.87 | 0.17 |
| | N | 22.0 | 71.0 | - | 6.1 | - | - | 0.31 |
| | O | 12.5 | 65.5 | 13.0 | 9.0 | 0.19 | 1.04 | 0.19 |

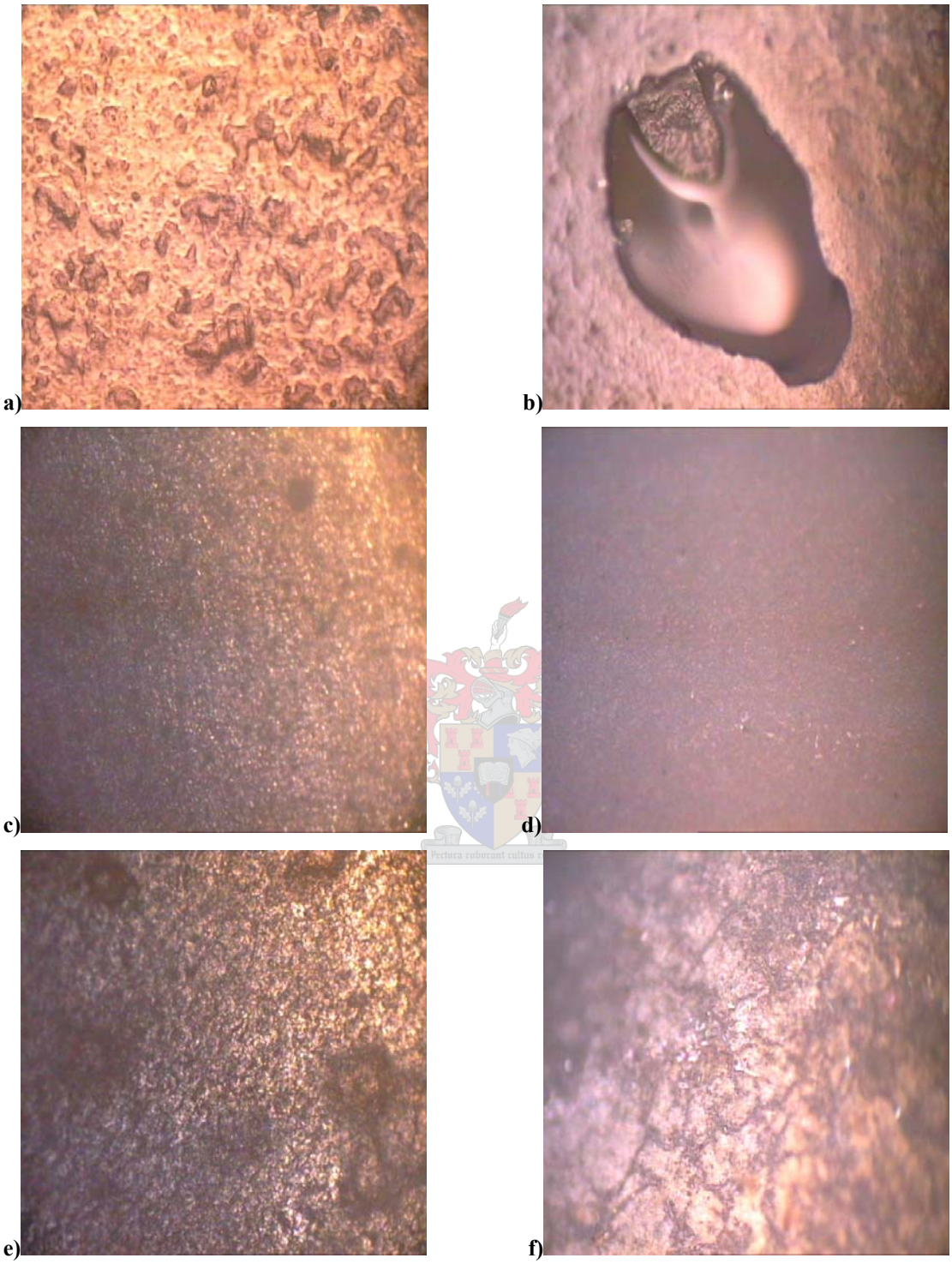


**Figure 5.39: OM images of samples: (a) virgin sample C, (b) acid rain aged sample C, (c) virgin sample L, (d) acid rain aged sample L, (e) virgin sample N and (f) acid rain aged sample N after 125 days acid rain.**

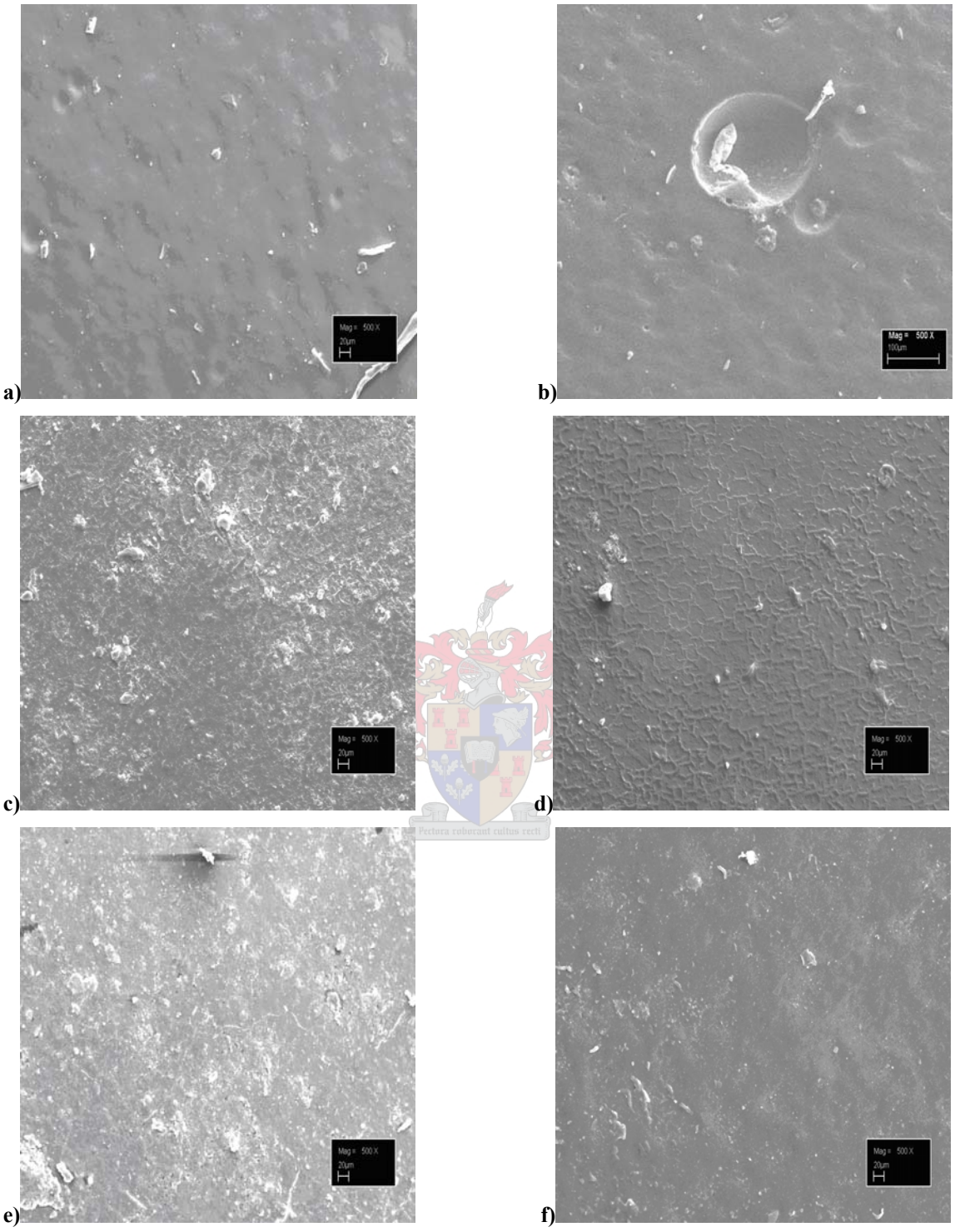


**Figure 5.40: SEM images of samples: (a) virgin sample C, (b) acid rain aged sample C, (c) virgin sample L, (d) acid rain aged sample L, (e) virgin sample N and (f) acid rain aged sample N after 125 days acid rain.**

### 5.3 Fourier-transform infrared spectroscopy

The chemical composition of the surface of samples was determined for the untreated samples as well as the needle corona, French corona, UV and acid rain aged counterparts. FTIR-PAS spectra of samples C, L and O after different forms of accelerated ageing are shown in Figures 5.41 (a), (b) and (c) respectively.

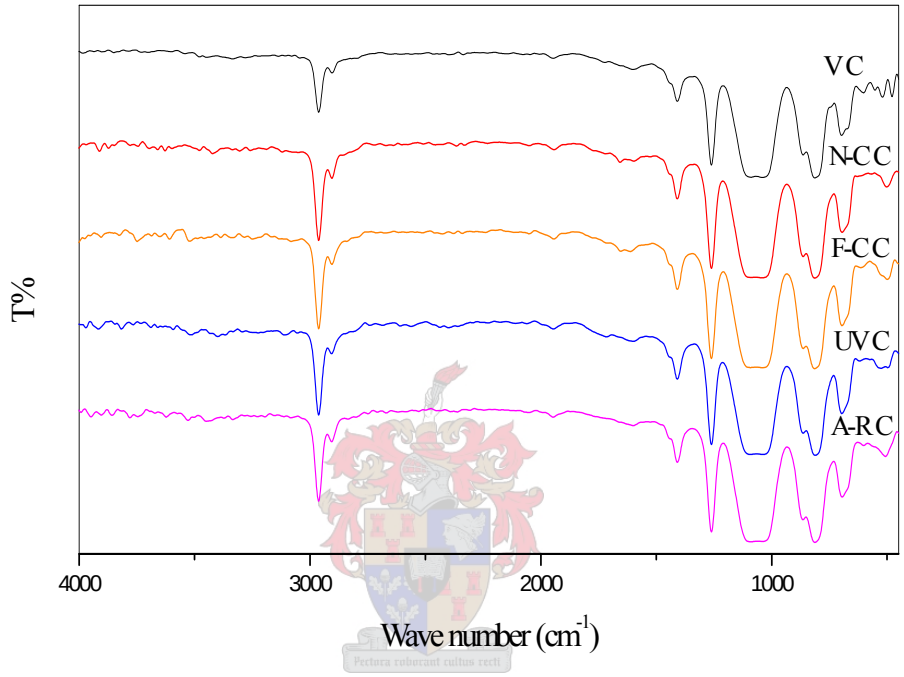


**(a)**

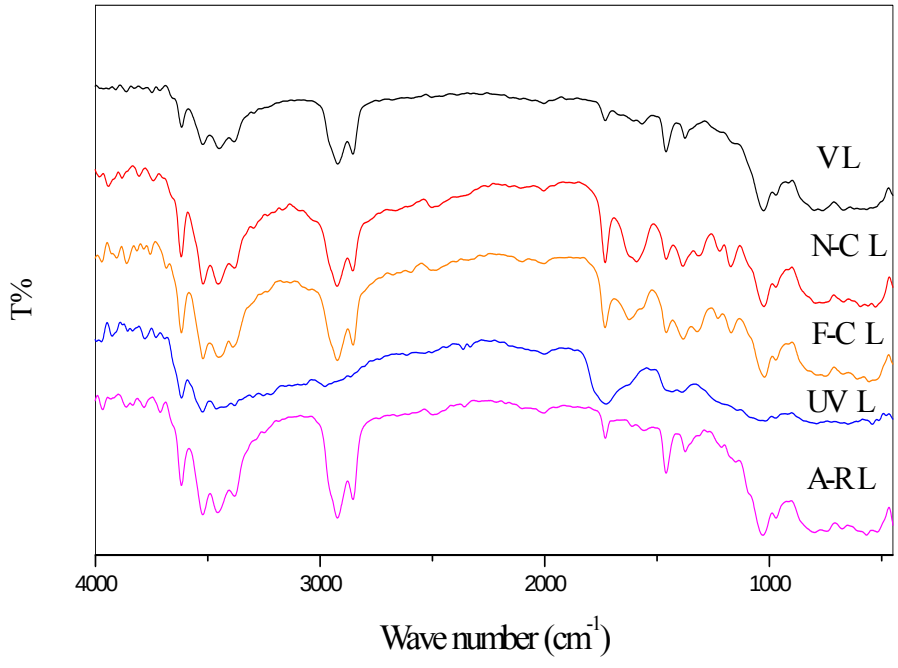


**(b)**

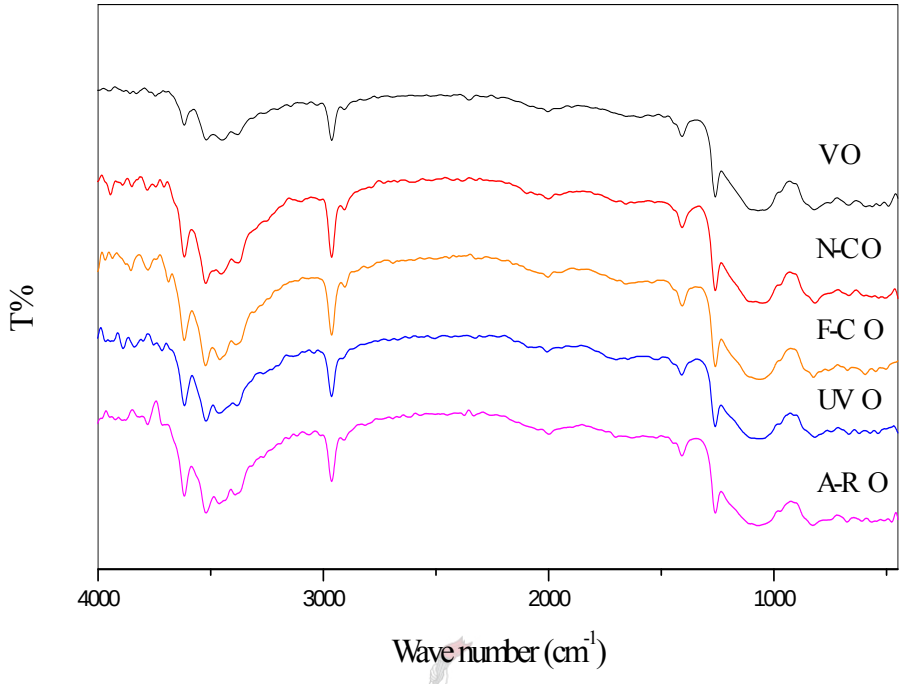


**(c)**

**Figure 5.41: FTIR spectra of virgin (V), needle corona (N-C), French corona (F-C), UV and acid rain (A-R) aged samples: (a) sample C, (b) sample L and (c) sample O.**

FTIR spectra show the various absorption bands characteristic of the PDMS sample surface. In the spectrum of the virgin PDMS sample C, absorption bands from the following groups appear: CH from methyl groups at 2962-2955 $cm^{-1}$, Si-$CH_3$ from the side chains at 1262 $cm^{-1}$, Si-O-Si bonds in the main chain at 1090-1000 $cm^{-1}$, and $Si(CH_3)_2$ groups at 870-750 $cm^{-1}$. In the spectra of the unaged commercial PDMS sample O and EPDM sample L, additional absorption bands appear, including those of the OH groups at 3350-3600 $cm^{-1}$, $CH_2$ groups at 2950-2855 $cm^{-1}$, water at 1300-1480 $cm^{-1}$ and C=O at 1730-1680 $cm^{-1}$.

Figures 5.41 (a), (b) and (c) clearly show that in the case of the PDMS based materials there are no dramatic changes in the FTIR-PAS spectra. On the other hand, the EPDM based samples showed dramatic changes, particulary in carbonyl region at 1700 $cm^{-1}$, where both corona treatments as well as UV ageing lead to a strong absorption peak. This confirms the results of the previous analysis which showed the EPDM based materials are more susceptible to degradation upon the exposure to the ageing regimes.

Figures 5.42 (a), (b) and (c) show the FTIR spectra of samples C, L and O after various periods of UV exposure. The decrease in the intensity of $CH_3$ absorption bands of UV aged samples is shown in Figure 5.43.

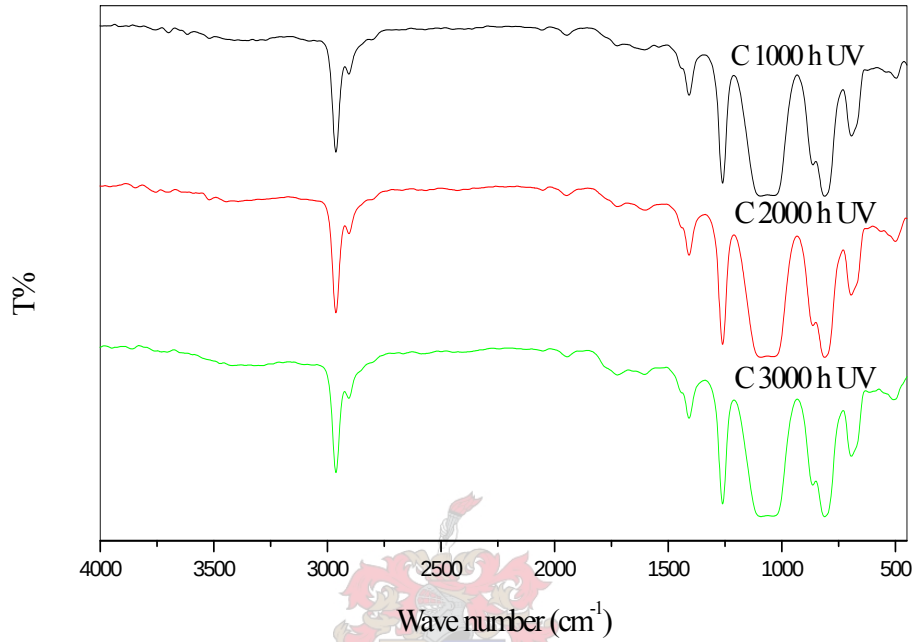


**(a)**

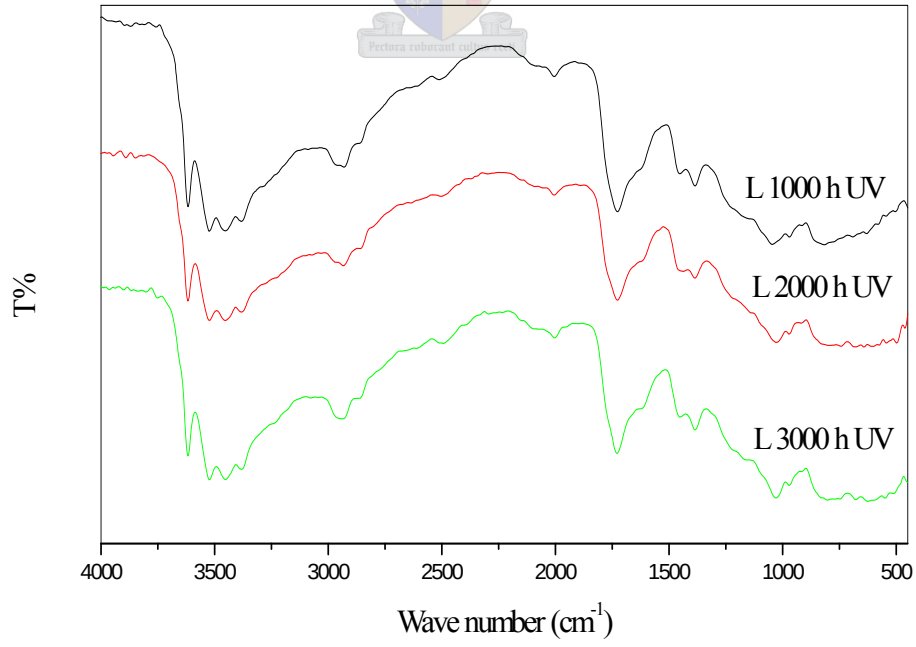


**(b)**

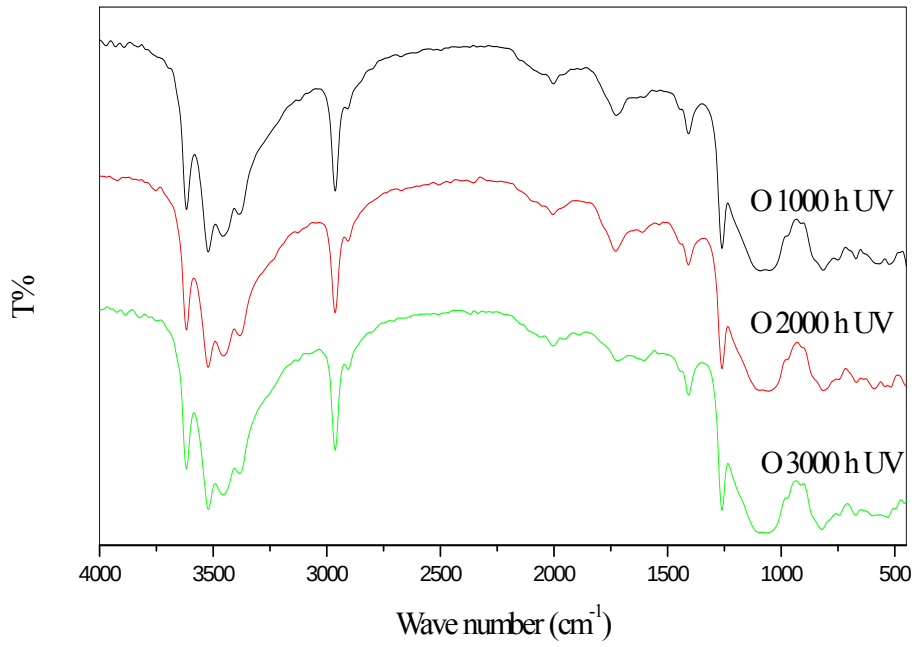


**(c)**

**Figure 5.42: FTIR spectra of UV aged samples: (a) sample C, (b) sample L and (c) sample O after different periods of exposure.**

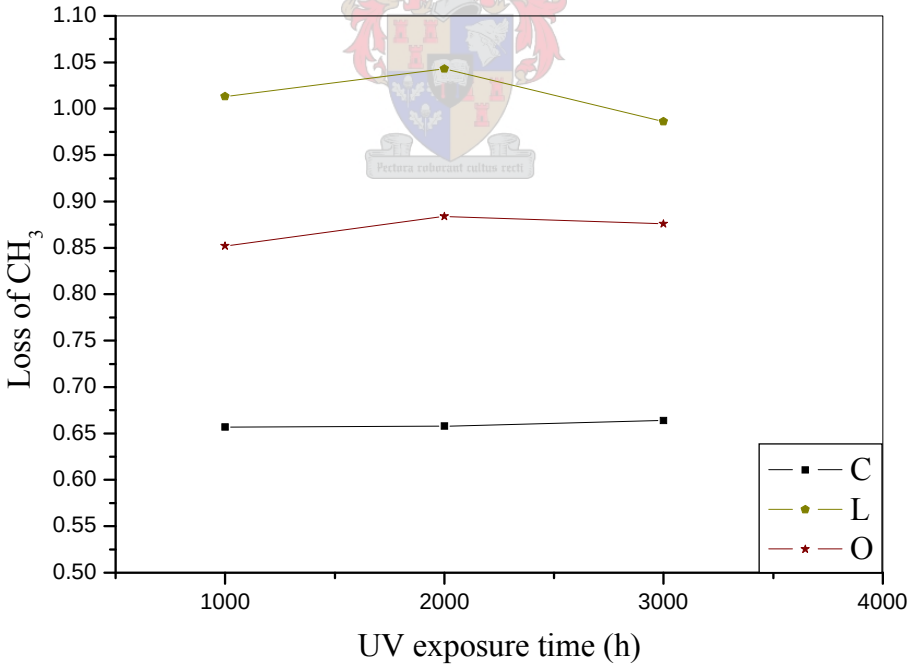


**Figure 5.43: Indication of loss of methyl groups in samples C, L and O as a function of UV exposure time (in terms of peak areas of aged samples to unaged samples).**

This loss of $CH_3$ is determined by measuring the peak intensity at 867 $cm^{-1}$ for aged samples at the different UV exposure times (1000 h, 2000 h, and 3000 h), relative to the peak intensity of the virgin samples. PDMS samples C and O show very little change in loss of methyl whereas the EPDM sample L shows a small decrease.

Once again, the most dramatic changes in the EPDM sample are seen in the carbonyl region of the spectra.

FTIR spectra of the samples C, L and O after acid rain (A-R) ageing for different periods of exposure are shown in Figures 5.44 (a), (b) and (c).

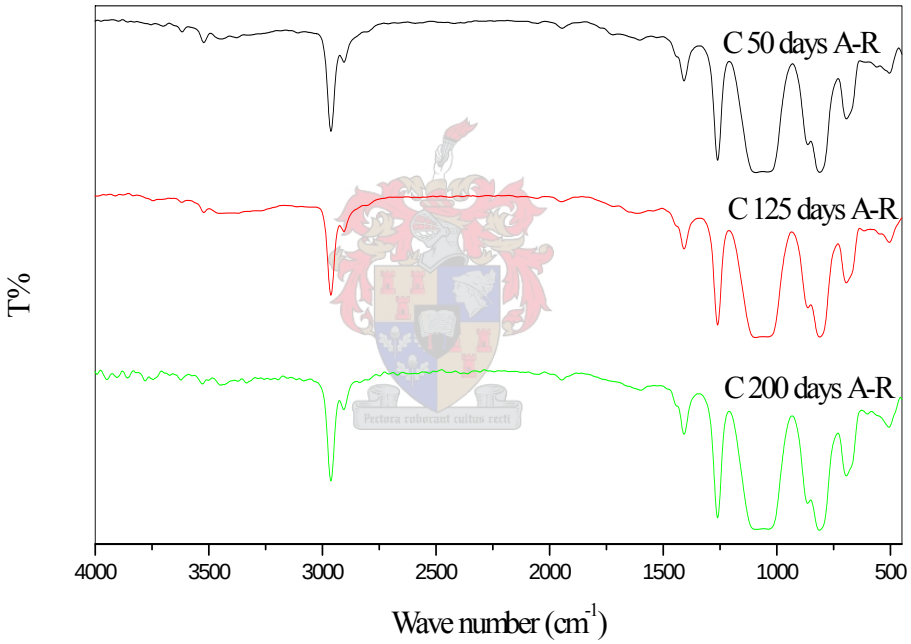


**(a)**

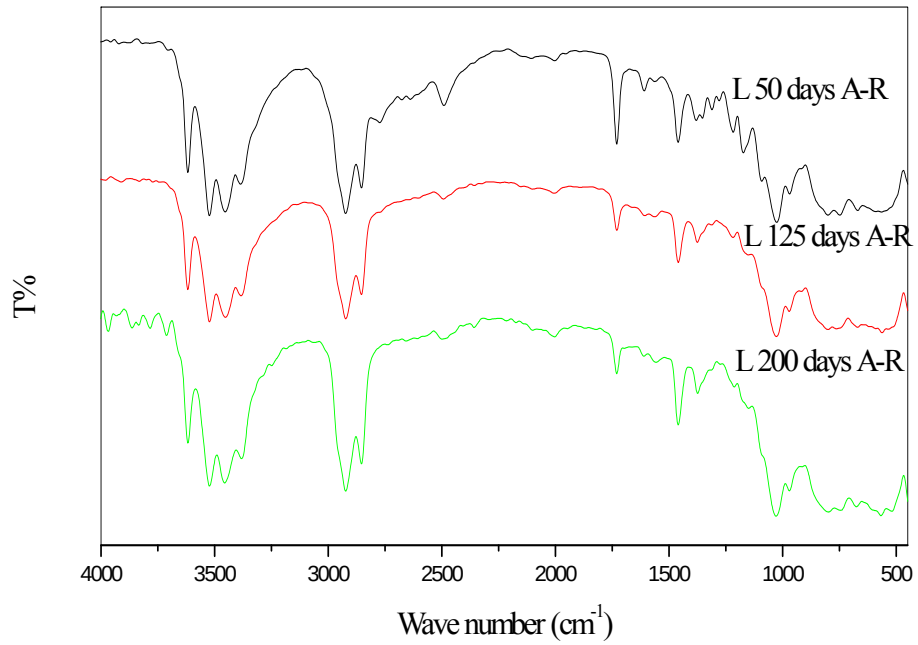


**(b)**

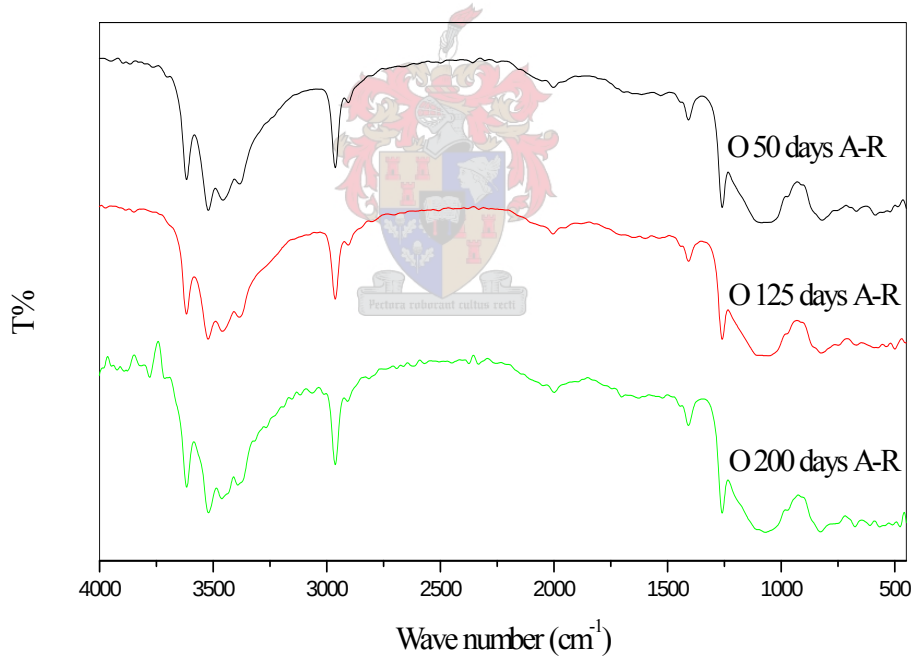


**(c)**

**Figure 5.44: FTIR spectra of acid rain (A-R) aged samples: (a) sample C, (b) sample L and (c) sample O.**

The decrease in the intensity of $CH_3$ absorption bands of the acid rain aged samples is shown in Figure 5.45.

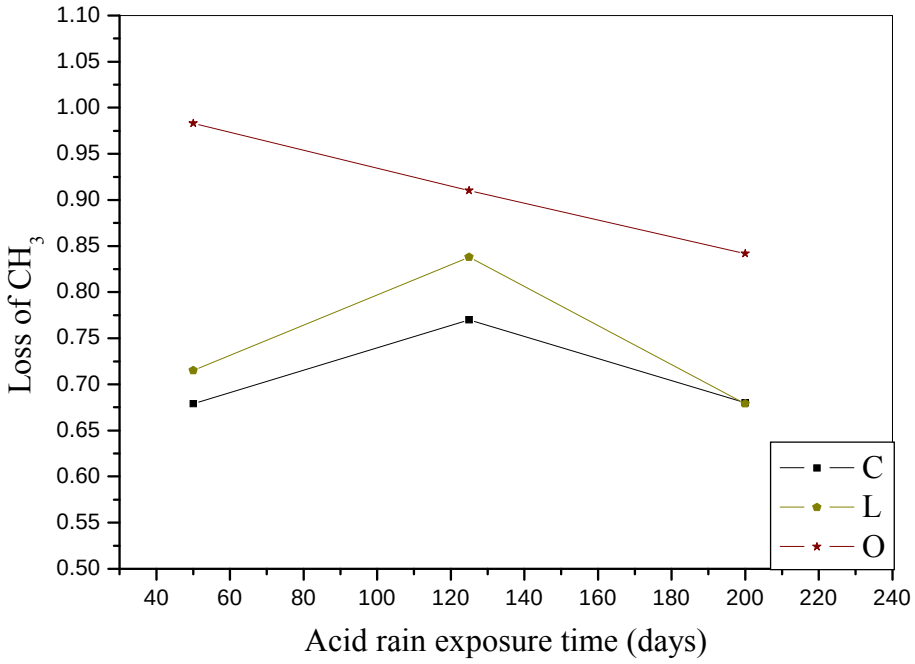


**Figure 5.45: Indication of loss of methyl in the samples C, L and O as a function of acid rain exposure time (in terms of peak areas of aged samples to unaged samples).**

UV aged sample L shows the highest loss of methyl groups, followed by sample O and then sample C. Sample C exhibits different trends; first the loss curve increases very slightly and then becomes almost steady. Acid rain aged samples, on the other hand, exhibit a more pronounced increase in the loss of methyl groups in the case of sample O, followed by samples L and C, as shown in Figure 5.45. When comparing the difference between UV ageing and acid rain ageing it is found that the loss of $CH_3$ for the acid rain aged samples is higher than that for the UV aged samples. For example, UV aged sample C has a methyl loss of 0.66 while the acid rain aged sample has a loss of 0.77, and the UV aged sample O has a loss of 0.87 whereas the acid rain aged one is 0.91. This finding indicates that the effect of acid rain is more severe than UV ageing on these samples.

One of the factors that must be kept in mind with the FTIR-PAS analysis of the sample surfaces is the depth of the sampling from the surface. In the case of FTIR-PAS, the sampling depth is between 3-34 μm from the surface [24]. In the case of very surface-specific chemical changes, such as those that occur after corona ageing, the dramatic chemical changes that occur on the surface are not as apparent. In the case of the corona

aged samples the positron beam analysis shows that the $SiO_x$ degradation layer formed on the surface is only 30-50 nm thick in the case of the needle corona and much less in the case of the French corona. This means that despite the dramatic changes in the surface composition the FTIR-PAS spectra do not show such as dramatic differences. Hillborg and Gedde [25] also found that despite the dramatic changes in the surface composition, FTIR spectra did not show as dramatic effect due to the large sampling depth.

## 5.4 Naturally field-aged samples

The SCA values of virgin and field-aged samples are shown in Table 5.16.

**Table 5.16: Average SCA values of virgin and field-aged samples**

| ID | Average static contact angle of virgin samples (degrees) | Average static contact angle of field-aged samples (degrees) |
|---|---|---|
| C | 107 | - |
| E | 111 | - |
| G | 115 | - |
| I | 108 | - |
| J | 109 | 129 |
| K | 106 | 133 |
| L | 90 | 73 |
| M | 107 | 130 |
| N | 84 | 72 |
| O | 101 | 115 |

The SCA values of the field-aged samples were higher than their virgin counterparts. The field-aged PDMS samples J, K, M and O had SCA values of 129˚, 133˚, 130˚ and 115,˚ respectively, which are higher than the SCA values of the virgin samples. On the other hand, both the field-aged EPDM samples L and N had lower SCA values (73˚ and 72˚) than the virgin samples. The higher SCA values of the field-aged PDMS samples are explained by the release of higher amounts of cyclic LMW oligomers after ageing. These

compounds diffuse to the surface as a result of a chain scission reaction occurring during ageing, which in turn leads to enhancing the hydrophobicity. In addition, the surfaces of the field-aged samples were relatively rougher, which contributed to the larger static contact angles measured.

The field-aged samples L and N that showed much lower static contact angles compared to the other samples indicate the development of hydrophilic character, associated with high surface wettability. Sorqvist and Vlastos [26] carried out an investigation of the hydrophobicity during field tests on energized EPDM insulators at 300 KV for 7 years, and recorded a similar low hydrophobicity.

A variation in the SCA measurements was also found for the field-aged PDMS commercial insulators. This corresponds to results obtained by Vlastos and Gubanski [27], and is attributed to surface irregularity and variation in surface roughness. During in-service life the surface of insulators becomes rougher due to corona discharge activity as well as dry-band arcing and pollution. As mentioned earlier, SCA values also are affected by PDMS surface roughness; as the surface roughness increases so the SCA values increase, exceeding >90º [28]. It is clear evident that the SCA measurements of the field-aged samples do not give an indication of the state or performance of the underlying material, they are more dependent on the nature and types of pollutants on the surface. The SCA does, however, provide an indication on the relative ability of the materials to transfer their hydrophobicity to the pollution layer.

OM and SEM images of commercial samples field-aged for one year are shown in Figures 5.46 and 5.47 respectively.

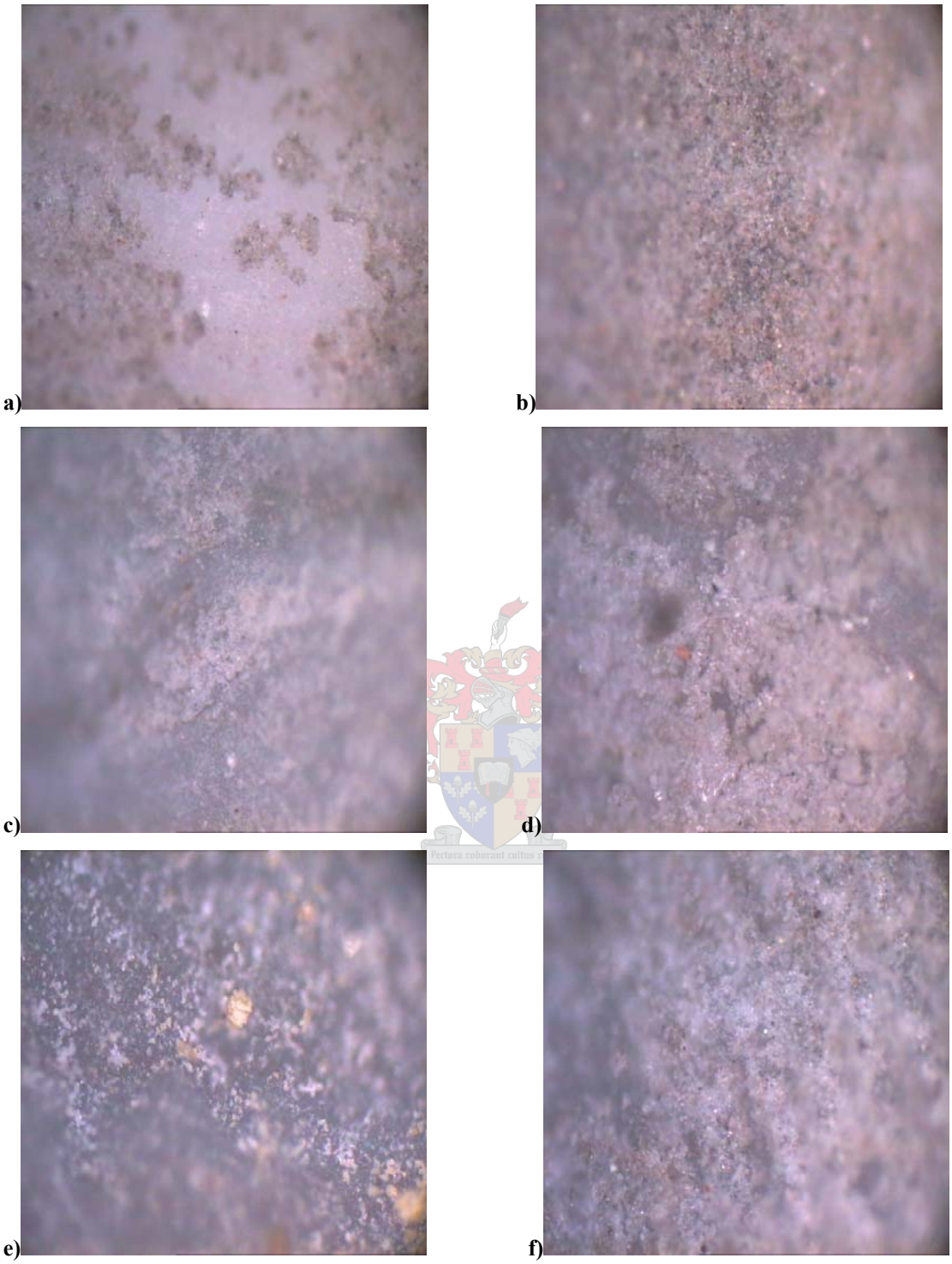


**Figure 5.46: Optical microscope images of commercial samples field-aged for one year: (a) sample J, (b) sample K, (c) sample L, (d) sample M, (e) sample N and (f) sample O.**

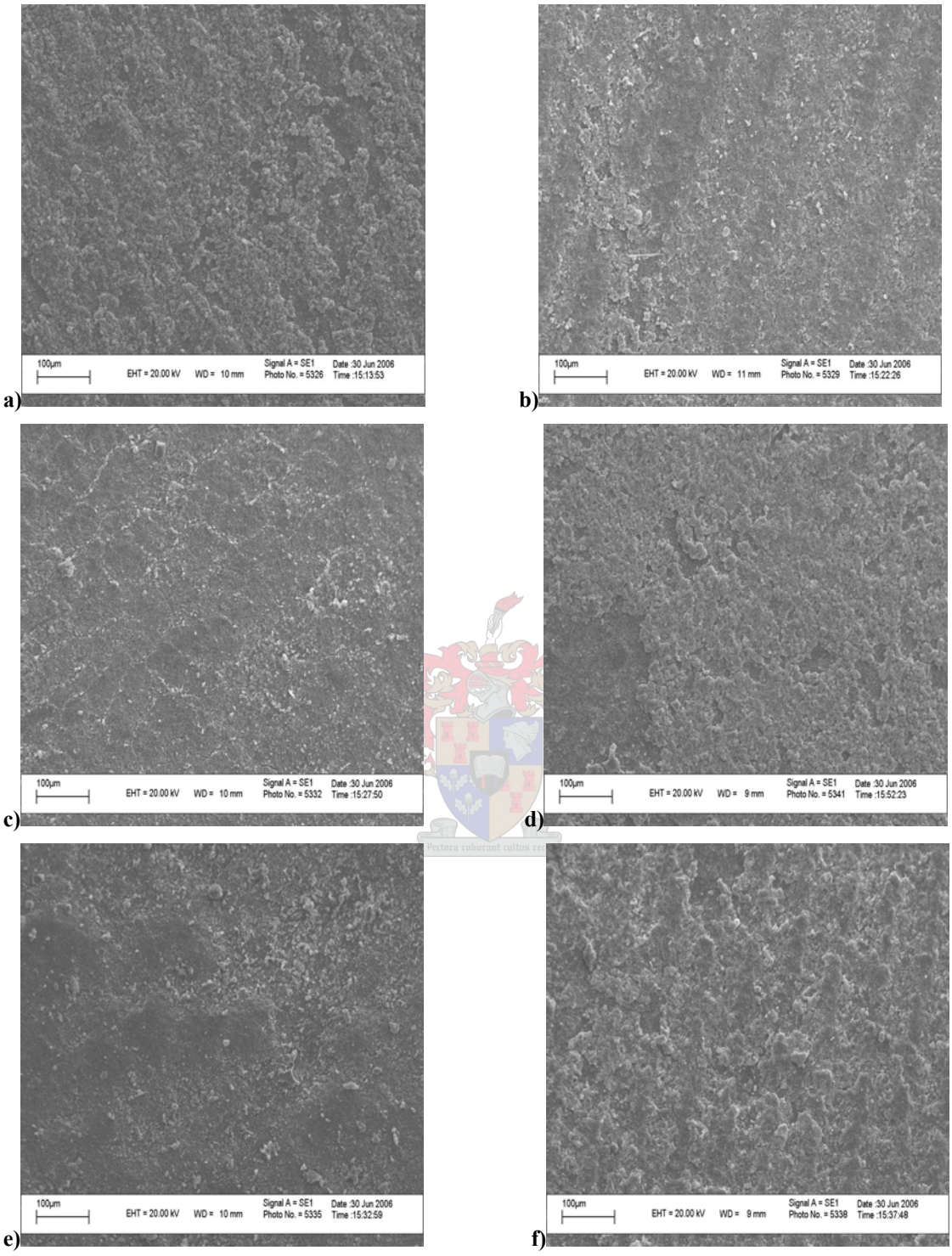


**Figure 5.47: SEM images of commercial samples field-aged for one year: (a) sample J, (b) sample K, (c) sample L, (d) sample M, (e) sample N and (f) sample O.**

The commercial samples used in this study, namely PDMS and EPDM rubber, and are characterized by three different distinctive colours, i.e. light grey for samples J and K, grey for samples L and M, dark grey for samples N and O.

The colour of the commercial samples after one-year operation in the field faded as a result of the UV exposure. The surface of some of the insulators showed various degrees of cracking and roughness depending on the type of insulating material.

The field-aged commercial samples J and K had very polluted surfaces, with few cracks but rough surfaces. Samples M and O had mildly-polluted surfaces, with many cracks and very rough surfaces. Sample N was a medium-polluted surface with many cracks and very rough surface. Sample L had the most pronounced cracks, distributed along its surface, accompanied with little pollution and a relatively very rough surface. Large numbers of loose filler particles were clearly recognized as whitish spots on the insulator surfaces, as shown in Figure 5.46. Similar features regarding cracks and roughness were observed using SEM visualization. Results are in Figure 5.47. Once again, the surfaces of field-aged samples J, K and M showed no cracks but the surface was rough, with an uneven appearance. More pronounced roughness and cracks were observed in samples L, N and O, as illustrated in Figures 5.47 (c), (e) and (f) respectively.

The roughness in the case of the EPDM is believed to be caused by erosion and cracking of the surface, associated with exposure of the filler. The SCA values of EPDM field-aged samples L and N decreased after in-service ageing due to the formation of aluminium oxide as a white layer on the surface. This is recognized as chalking, in which the surface conductivity and wetting increases. In the case of PDMS based housings J, K, M and O the pollutants that deposit on the surface become coated in a thin layer of LMW silicone oils, causing them to adhere to the surface, resulting in a chemically homogeneous surface.

**5.5 References**

1. J. Kindersberger, A. Schutz, H. C. Karner and R. v. d. Huir, CIGRE 33-303, 1-5, 1996.
2. S. H. Kim, E. A. Cherney and R. Hackam, IEEE Trans. Pow. Deliv., Vol. 5, 1491-1499, 1990.
3. H. Hillborg and U. W. Gedde, IEEE Trans. Diel. Elect. Insul., Vol. 6, 703-717, 1999.
4. J. K. Kim and I. H. Kim, J. Appl. Polym. Sci., Vol. 79, 2251-2257, 2001.
5. S. M. Gubanski and A. E. Vlastos, IEEE Trans. Diel. Elect. Insul., Vol. 5, 1527-1535, 1990.
6. M. Meincken, T. A. Berhane and P. E. Mallon, Polymer, Vol. 46, 203-208, 2005.
7. H. Hillborg, J. F. Anker, U. W. Gedde, D. D. Smith, H. K. Yasuda and K. Wikstrom, Polymer, Vol. 41, 6851-6863, 2000.
8. T. A. Berhane, Degradation and Recovery of Polydimethylsiloxane (PDMS) based Compounds used as High Voltage Insulators, MSc Thesis, Stellenbosch University, 2004.
9. P. E. Mallon, C. J. Greyling, W. L. Vosloo and Y. C. Jean, Rad. Phys. Chem., Vol. 68, 543-544, 2003.
10. P. E. Mallon, T. A. Berhane, C. J. Greyling, W. L. Vosloo, H. Chen and Y. C. Jean, Mat. Sci. Foru., Vol. 445-446, 322-324, 2004.
11. A. Toth, I. Bertoti, M. Blazso, G. Banhegyi, A. Bongar and X. Szaplonczay, J. Appl. Polym. Sci., Vol. 52, 1293-1925, 1994.
12. S. H. Kim, E. A. Cherney and R. Hackam, IEEE Trans. Diel. Elect. Insul., Vol. 6, 1065-1068, 1992.
13. W. Noll, Chemistry and Technology of Silicones, Academic Press, New York, 24, 1968.
14. H. Homma, T. Kuroyagi, K. Izumi, C. L. Mirley, J. Ronzello and S. A. Boggs, IEEE Trans. Diel. Elect. Insul., Vol. 15, 796-803, 2000.
15. H. Hillborg, S. Karlsson and U. W. Gedde, Polymer, Vol. 42, 8883-8889, 2001.
16. J. P. Reynders, I. R. Jandrell and S. M. Reynders, IEEE Trans. Diel. Elect. Insul., Vol. 6, 620-631, 1999.

17. N. Yoshimura, S. Kumagai and S. Nishimura, IEEE Trans. Diel. Elect. Insul., Vol. 5, 632-650, 1999.
18. M. Ugur, A. Kurtman and A. Merev, J. Elect. Engin., Vol. 3, 943-953, 2003.
19. B. Youn and C. Huh, IEEE Trans. Diel. Elect. Insul., Vol. 12, 1015-1024, 2005.
20. B. Schnyder, T. Lippert, R. Kotz, A. Wokam, V. Graubner and O. Nuyken, J. Surf. Sci., Vol. 532, 1067-1071, 2003.
21. Y. Xu, Y. He, F. Zeing and R. Zhang, IEEE Trans. Diel. Elect. Insul., Vol. 6, 60-66, 1999.
22. X. Wang, L. Chen and N. Yoshimura, J. Phys. D: App. Phys., Vol. 33, 1117-1127, 2000.
23. J. Y. Koo, I. T. Kim, J. T. Kim and W. K. Prak, Ann. Report of CEIDP, USA, 370- 373, 1997.
24. L. Gonon, J. Mallegol, S. Commereuc and V. Verny, Vib. Spec., Vol. 26, 43-49, 2001.
25. H. Hillborg and U. W. Gedde, Polymer., Vol. 39, 1991-1998.
26. T. Sorqvist and A. E. Vlastos, IEEE Trans. Pow. Deliv., Vol. 12, 1041-1048, 1997.
27. A. E. Vlastos and S. M. Gubanski, IEEE Trans. Pow. Deliv., Vol. 6, 890-898, 1992.
28. F. Exl and J. Kindersberger, Proceedings of the 14th International Symposium on High Voltage Engineering, Beijing, China, 2005.

# Chapter 6

## Conclusions

Several different PDMS and EPDM formulations were selected and studied for their performance and behaviour under various accelerated ageing conditions that simulate the conditions under which high voltage insulators are required to function. This was done in order to better understand the modes of degradation of the respective materials.

The commercial and controlled formulation samples were characterised in terms of their composition by FTIR-PAS, TGA and SCA measurements. In the case of the commercial PDMS samples a direct correlation was found between the distance between the fabrication lines on the surface and the SCA value measured. The PDMS based samples all show a higher measured SCA value than the EPDM samples, showing a more hydrophobic surface.

A new "in-situ" thermal analysis technique was developed to examine the relative thermal stability of the PDMS based materials. This technique allows for a relatively quick evaluation of the relative thermal stability of the various materials. It was also shown there is a limited capacity of the ATH filler to provide some degree of protection of the polymer surface by dehydration of the filler.

Two types of corona ageing techniques (needle and French corona) were evaluated as potential ageing techniques for the samples. As expected, all the PDMS based samples showed an initial drastic decrease in the surface SCA directly after corona treatment. This was followed by a progressive recovery (increase) in the SCA as a function of the time after corona treatment. The hydrophobicity recovery data was fitted with an exponential recovery function, which allowed for an estimation of the relative recovery rates of the different samples. By assuming a first-order type recovery rate, the half-life of the recovery process was also estimated from the SCA recovery data. Results showed that the type of insulator material and the composition have a significant effect on the rate of the recovery. Optical microscopy and SEM showed evidence of a $SiO_x$ layer which was later also observed in the slow positron beam results. It was found that the morphology

changes of the surface are more apparent after the removal of the LMW components from the surface prior to SEM analysis.

Furthermore, there was a significant difference between the two different types of corona treatments. The needle corona ageing had a much more severe effect on the samples relative to the French corona ageing. There was a smaller decrease in the SCA values after French corona treatment compared to needle corona ageing. The French corona aged samples also had a slower recovery rate than the needle aged samples, due to the milder effect of the French corona. This was attributed to the formation of a smaller amount of low molecular wieght PDMS species, which are considered to be responsible for the hydrophobicity recovery rate.

Slow positron beam techniques were used to estimate the relative intensities of the two corona treatment techniques. It was found that 100 h of the French corona treatment was approximately equal to 30 min of the needle corona treatment. This determination was based on the time it takes to detect the $SiO_x$ degradation layer on a surface of relatively the same thickness.

A model compound study of a low molar mass PDMS based material was used to further investigate the chemical effect of corona treatment on PDMS based materials. SEC-LC transform-FTIR showed evidence of an increase in the molar mass as a result of crosslinking of molecules, which is the first step in the degradation of the PDMS materials. GC-MS showed an increase in the low molecular mass PDMS species primarily the $D_3$ to $D_7$ cyclic components, after corona treatment as a result of the PDMS molecules that have completely degraded. Evidence was also found for the formation of a $SiO_x$ "skin layer" on the surface of the model compound after treatment.

Controlled formulation samples and commercial samples were exposed for various periods up to 8000 h of UV-B radiation. As expected, the PDMS based compounds showed very good resistance to the UV-B radiation, even after 8000 h. Only small decreases in the SCA values were observed even after the long exposure time. The EPDM based samples on the other hand showed relatively poorer UV-B resistance. The SCA values for these samples showed a dramatic decrease even after a very short UV-B exposure time. The decrease in the SCA value for these samples is also associated with

the severely damaged and cracked surface as observed in the optical and SEM images. "Chalking" is also observed in these samples. FTIR results confirm the greater degree of surface changes in the EPDM samples.

Hydrolysis ageing (acid rain) was performed on the samples for up to 200 days. Once again the EPDM based samples showed greater changes than the PDMS based materials. In the case of the PDMS materials the un-filled controlled formulation RTV PDMS sample showed the greatest effects of hydrolysis ageing with pitted-eroded areas appearing on the surface. All the samples showed a decrease in the measured SCA value on prolonged exposure to the synthetic acid rain solution. The decrease in the SCA values are far less than observed in the corona treatment of the samples. The samples showed some indication of SCA recovery after the acid rain treatment. This is most probably due to LMW species diffusing back to the surface after removal from the acid rain solution. EDS results show an increase in the oxygen content on the surface after the acid rain treatment. The results of this study indicate that 125 days of hydrolysis ageing is sufficient to distinguish the differences in the materials performance.

FTIR-PAS results show that in the case of the PDMS based materials, the sampling depth of the techniques results in only small changes in the spectra, despite the dramatic changes obsereved by other technique such as SCA measurment. This is because most of the change in the materials is confined to the first few nano-meters on the surface of the materials. In the case of the EPDM samples the changes are more apparent in the spectra due to the much larger degree of surface changes and the greater depth of the changes.

# Appendices

## Appendix A: SCA measurements of selected RTV PDMS samples after various laboratory accelerated ageing treatments.

**Sample C: 30 min needle corona aged**

| Recovery time | X1 | X2 | Y1 | Y2 | ΔX | ΔY | Theta (degrees) | Average |
|---|---|---|---|---|---|---|---|---|
| 0 min | | | | | | | Flat | - |
| 15 min | 121 | 558 | 247 | 341 | 437 | 94 | 46.6 | 36 |
| | 83.0 | 561 | 295 | 381 | 478 | 86 | 39.6 | |
| | 14.0 | 518 | 292 | 374 | 504 | 82 | 36.0 | |
| | 74.0 | 565 | 315 | 380 | 491 | 65 | 29.7 | |
| | 87.0 | 558 | 287 | 398 | 472 | 76 | 35.7 | |
| 30 min | 37.0 | 635 | 171 | 399 | 598 | 228 | 74.6 | 66 |
| | 90.0 | 553 | 199 | 407 | 463 | 208 | 83.8 | |
| | 66.0 | 577 | 203 | 408 | 511 | 205 | 77.5 | |
| | 60.0 | 533 | 178 | 386 | 473 | 208 | 76.5 | |
| | 28.0 | 601 | 204 | 405 | 573 | 201 | 70.1 | |
| | 60.0 | 584 | 201 | 401 | 524 | 200 | 74.7 | |
| | 26.0 | 636 | 337 | 360 | 630 | 53.0 | 12.9 | |
| | 39.0 | 659 | 301 | 375 | 650 | 194 | 55.7 | |
| | 30.0 | 540 | 341 | 364 | 532 | 60 | 38.7 | |
| | 40.0 | 660 | 302 | 376 | 651 | 195 | 56.0 | |
| 1 h | 39.0 | 525 | 187 | 408 | 486 | 217 | 83.5 | 80 |
| | 35.0 | 542 | 160 | 377 | 507 | 217 | 81.1 | |
| | 38.0 | 514 | 111 | 345 | 476 | 234 | 89.0 | |
| | 56.0 | 556 | 174 | 392 | 500 | 218 | 82.1 | |
| | 13.0 | 604 | 137 | 346 | 591 | 209 | 70.5 | |
| | 14.0 | 580 | 225 | 440 | 566 | 215 | 74.4 | |
| | 90.0 | 541 | 170 | 384 | 532 | 214 | 77.6 | |
| | 42.0 | 542 | 181 | 407 | 500 | 226 | 40.2 | |
| | 16.0 | 597 | 172 | 368 | 581 | 196 | 68.0 | |
| 3 h | 52.0 | 541 | 160 | 382 | 489 | 222 | 84.5 | 85 |
| | 99.0 | 538 | 142 | 351 | 439 | 209 | 87.2 | |
| | 59.0 | 548 | 137 | 377 | 489 | 240 | 88.9 | |
| | 38.0 | 597 | 155 | 363 | 559 | 208 | 73.3 | |
| | 161 | 618 | 201 | 444 | 457 | 243 | 93.5 | |
| | 42.0 | 542 | 181 | 407 | 500 | 226 | 90.3 | |
| | 136 | 570 | 136 | 366 | 434 | 230 | 93.3 | |
| | 60.0 | 486 | 99.0 | 339 | 426 | 240 | 96.8 | |

| | | | | | | | | |
|---|---|---|---|---|---|---|---|---|
| | 25.0 | 517 | 126 | 352 | 492 | 226 | 85.1 | |
| | 99.0 | 538 | 142 | 351 | 439 | 209 | 87.2 | |
| 6h | 65.0 | 502 | 132 | 339 | 437 | 207 | 86.9 | 92 |
| | 136 | 570 | 136 | 366 | 434 | 230 | 93.3 | |
| | 48.0 | 506 | 178 | 413 | 458 | 235 | 91.5 | |
| | 136 | 588 | 171 | 405 | 452 | 234 | 91.9 | |
| | 131 | 561 | 128 | 347 | 430 | 219 | 91.0 | |
| | 181 | 578 | 133 | 354 | 397 | 221 | 96.1 | |
| | 101 | 562 | 133 | 366 | 461 | 233 | 90.6 | |
| | 159 | 585 | 175 | 390 | 426 | 215 | 90.5 | |
| | 60.0 | 486 | 99.0 | 339 | 426 | 240 | 96.8 | |
| | 102 | 542 | 123 | 346 | 440 | 223 | 90.8 | |
| 24h | 62.0 | 513 | 171 | 419 | 451 | 248 | 95.4 | 94 |
| | 122 | 534 | 167 | 409 | 412 | 242 | 99.2 | |
| | 131 | 535 | 122 | 365 | 404 | 245 | 101 | |
| | 132 | 536 | 122 | 365 | 404 | 243 | 100 | |
| | 64.0 | 502 | 175 | 411 | 438 | 236 | 94.3 | |
| | 57.0 | 616 | 167 | 378 | 559 | 211 | 74.1 | |
| | 79.0 | 506 | 109 | 351 | 427 | 242 | 97.2 | |
| | 87.0 | 533 | 125 | 398 | 446 | 223 | 90.0 | |
| | 88.0 | 517 | 112 | 353 | 429 | 241 | 96.6 | |
| | 86.0 | 503 | 133 | 359 | 417 | 226 | 93.3 | |
| 48 h | 88.0 | 540 | 178 | 412 | 452 | 234 | 91.9 | 96 |
| | 74.0 | 485 | 191 | 441 | 411 | 250 | 101 | |
| | 116 | 520 | 148 | 396 | 404 | 248 | 102 | |
| | 135 | 562 | 184 | 434 | 427 | 248 | 98.6 | |
| | 39.0 | 486 | 122 | 363 | 447 | 241 | 94.3 | |
| | 99.0 | 527 | 109 | 345 | 428 | 236 | 95.6 | |
| | 29.0 | 505 | 146 | 368 | 476 | 235 | 89.3 | |
| | 85.0 | 500 | 133 | 361 | 415 | 228 | 95.4 | |
| | 51.0 | 541 | 112 | 385 | 490 | 273 | 96.2 | |
| | 94.0 | 522 | 116 | 362 | 428 | 246 | 97.2 | |
| Virgin | 249 | 536 | 262 | 443 | 287 | 181 | 103 | 107 |
| | 133 | 391 | 280 | 460 | 258 | 180 | 109 | |
| | 215 | 465 | 191 | 380 | 250 | 189 | 113 | |
| | 175 | 434 | 196 | 357 | 259 | 161 | 102 | |
| | 164 | 445 | 197 | 377 | 281 | 180 | 104 | |
| | 214 | 488 | 166 | 350 | 274 | 184 | 107 | |
| | 132 | 397 | 225 | 407 | 265 | 182 | 108 | |
| | 216 | 435 | 142 | 301 | 219 | 159 | 110 | |
| | 281 | 507 | 127 | 282 | 226 | 155 | 107 | |
| | 184 | 461 | 125 | 319 | 277 | 194 | 108 | |
| | 249 | 536 | 262 | 443 | 287 | 181 | 103 | |

**Sample J: 30 min needle corona aged**

| Recovery time | X1 | X2 | Y1 | Y2 | ΔX | ΔY | Theta (degrees) | Average |
|---|---|---|---|---|---|---|---|---|
| 0 min | | | | | | | Flat | - |
| 15 min | 42.0 | 557 | 287 | 376 | 515 | 89.0 | 38.1 | 39 |
| | 21.0 | 598 | 310 | 403 | 577 | 93.0 | 35.7 | |
| | 47.0 | 571 | 308 | 398 | 524 | 90.0 | 37.9 | |
| | 39.0 | 552 | 331 | 431 | 513 | 100 | 42.6 | |
| | 122 | 516 | 388 | 460 | 394 | 72.0 | 40.0 | |
| 30 min | 17.0 | 590 | 283 | 411 | 573 | 128 | 48.1 | 47 |
| | 15.0 | 590 | 207 | 329 | 575 | 122 | 45.9 | |
| | 25.0 | 636 | 309 | 438 | 631 | 149 | 45.8 | |
| | 16.0 | 642 | 286 | 394 | 636 | 118 | 38.0 | |
| | 28.0 | 589 | 210 | 374 | 591 | 164 | 45.9 | |
| | 22.0 | 612 | 291 | 434 | 600 | 154 | 51.7 | |
| | 24.0 | 578 | 292 | 439 | 554 | 147 | 45.9 | |
| | 89.0 | 604 | 345 | 477 | 515 | 132 | 54.3 | |
| | 33.0 | 538 | 306 | 442 | 505 | 136 | 56.6 | |
| | 20.0 | 639 | 229 | 353 | 629 | 134 | 43.6 | |
| 1 h | 101 | 542 | 284 | 465 | 441 | 181 | 78.8 | 65 |
| | 40.0 | 556 | 236 | 391 | 516 | 155 | 61.9 | |
| | 24.0 | 567 | 293 | 432 | 543 | 139 | 54.2 | |
| | 58.0 | 571 | 202 | 377 | 513 | 175 | 68.6 | |
| | 60.0 | 524 | 206 | 395 | 464 | 189 | 78.3 | |
| | 17.0 | 560 | 208 | 335 | 543 | 127 | 50.1 | |
| | 57.0 | 494 | 188 | 352 | 437 | 164 | 73.8 | |
| | 36.0 | 514 | 193 | 359 | 478 | 166 | 69.6 | |
| | 120 | 626 | 211 | 367 | 506 | 156 | 63.3 | |
| | 26.0 | 596 | 247 | 398 | 570 | 151 | 55.8 | |
| 3 h | 39.0 | 492 | 260 | 455 | 453 | 195 | 81.5 | 76 |
| | 124 | 590 | 223 | 426 | 466 | 203 | 82.1 | |
| | 102 | 555 | 200 | 392 | 453 | 192 | 80.6 | |
| | 43.0 | 514 | 192 | 376 | 471 | 184 | 76.0 | |
| | 40.0 | 486 | 173 | 393 | 446 | 220 | 89.2 | |
| | 80.0 | 494 | 188 | 380 | 414 | 192 | 85.6 | |
| | 79.0 | 537 | 197 | 394 | 458 | 197 | 81.4 | |
| | 83.0 | 501 | 182 | 342 | 418 | 160 | 74.8 | |
| | 45.0 | 572 | 300 | 444 | 577 | 144 | 57.3 | |
| | 23.0 | 586 | 238 | 389 | 563 | 151 | 56.4 | |
| | 67.0 | 443 | 177 | 318 | 376 | 141 | 73.7 | |
| | 63.0 | 358 | 130 | 281 | 298 | 151 | 90.7 | |
| | 66.0 | 438 | 189 | 334 | 372 | 145 | 75.8 | |
| | 197 | 518 | 277 | 426 | 321 | 149 | 85.7 | |

| | | | | | | | | |
|---|---|---|---|---|---|---|---|---|
| 6 h | 243 | 534 | 305 | 430 | 291 | 175 | 101 | 86 |
| | 172 | 435 | 232 | 369 | 263 | 137 | 92.3 | |
| | 206 | 490 | 239 | 368 | 284 | 129 | 84.5 | |
| | 240 | 511 | 245 | 380 | 271 | 135 | 89.8 | |
| | 209 | 494 | 204 | 331 | 285 | 127 | 83.4 | |
| 24 h | 79.0 | 549 | 145 | 428 | 470 | 283 | 101 | 92 |
| | 26.0 | 605 | 197 | 481 | 579 | 284 | 88.9 | |
| | 21.0 | 540 | 166 | 440 | 519 | 274 | 93.1 | |
| | 38.0 | 548 | 168 | 443 | 510 | 275 | 94.3 | |
| | 27.0 | 534 | 186 | 466 | 507 | 280 | 95.6 | |
| | 33.0 | 567 | 140 | 435 | 534 | 295 | 95.7 | |
| | 11.0 | 623 | 124 | 374 | 612 | 250 | 78.5 | |
| | 45.0 | 541 | 170 | 442 | 496 | 272 | 95.3 | |
| | 42.0 | 558 | 177 | 463 | 516 | 286 | 95.9 | |
| | 14.0 | 617 | 155 | 420 | 603 | 265 | 82.6 | |
| 48 h | 45.0 | 596 | 189 | 487 | 551 | 298 | 94.5 | 94 |
| | 2.00 | 623 | 63.0 | 350 | 621 | 287 | 85.5 | |
| | 13.0 | 549 | 206 | 484 | 536 | 278 | 92.0 | |
| | 36.0 | 594 | 167 | 443 | 558 | 276 | 89.3 | |
| | 30.0 | 550 | 147 | 461 | 520 | 314 | 101 | |
| | 20.0 | 557 | 185 | 505 | 537 | 320 | 100 | |
| | 37.0 | 604 | 192 | 497 | 567 | 305 | 94.2 | |
| | 10.0 | 596 | 196 | 491 | 586 | 295 | 90.4 | |
| | 2.00 | 633 | 306 | 475 | 631 | 169 | 96.0 | |
| | 3.00 | 635 | 204 | 423 | 632 | 219 | 85.4 | |
| Virgin | 133 | 494 | 306 | 510 | 361 | 204 | 96.9 | 109 |
| | 148 | 432 | 241 | 464 | 284 | 223 | 115 | |
| | 130 | 430 | 211 | 407 | 300 | 196 | 105 | |
| | 212 | 531 | 167 | 362 | 319 | 195 | 101 | |
| | 37.0 | 368 | 287 | 489 | 331 | 202 | 101 | |
| | 195 | 464 | 235 | 453 | 269 | 218 | 117 | |
| | 217 | 495 | 182 | 403 | 278 | 221 | 116 | |
| | 29.0 | 302 | 130 | 347 | 273 | 217 | 116 | |
| | 143 | 488 | 157 | 303 | 345 | 146 | 98.8 | |
| | 130 | 430 | 211 | 407 | 300 | 196 | 105 | |

**Sample C: 500 h UV-B aged**

| Recovery time | X1 | X2 | Y1 | Y2 | ΔX | ΔY | Theta (degrees) | Average |
|---|---|---|---|---|---|---|---|---|
| 0 min | | | | | | | Not flat | - |
| 15 min | 310 | 493 | 241 | 392 | 183 | 151 | 118 | 107 |
| | 304 | 478 | 238 | 387 | 174 | 149 | 119 | |
| | 320 | 491 | 248 | 400 | 171 | 152 | 121 | |

| | | | | | | | | |
|---|---|---|---|---|---|---|---|---|
| | 367 | 565 | 278 | 414 | 198 | 136 | 108 | |
| | 325 | 519 | 266 | 404 | 194 | 138 | 110 | |
| 30 min | 337 | 522 | 301 | 453 | 489 | 152 | 63.7 | 109 |
| | 335 | 540 | 237 | 385 | 205 | 148 | 111 | |
| | 213 | 403 | 225 | 367 | 190 | 142 | 112 | |
| | 302 | 470 | 232 | 382 | 168 | 150 | 121 | |
| | 338 | 509 | 245 | 398 | 171 | 153 | 122 | |
| | 319 | 513 | 275 | 408 | 194 | 133 | 107 | |
| | 342 | 535 | 267 | 418 | 193 | 151 | 115 | |
| | 347 | 543 | 276 | 425 | 496 | 149 | 62 | |
| | 362 | 533 | 251 | 405 | 171 | 154 | 122 | |
| | 367 | 565 | 278 | 414 | 198 | 136 | 108 | |
| 1 h | 187 | 529 | 212 | 433 | 342 | 221 | 103 | 110 |
| | 273 | 603 | 206 | 461 | 330 | 255 | 114 | |
| | 267 | 580 | 223 | 431 | 313 | 208 | 106 | |
| | 212 | 493 | 213 | 436 | 281 | 223 | 116 | |
| | 257 | 562 | 222 | 442 | 305 | 220 | 111 | |
| | 202 | 487 | 176 | 383 | 285 | 207 | 110 | |
| | 325 | 519 | 266 | 404 | 194 | 138 | 110 | |
| | 213 | 403 | 225 | 367 | 190 | 142 | 112 | |
| | 335 | 540 | 237 | 385 | 205 | 148 | 111 | |
| | 319 | 513 | 275 | 408 | 194 | 133 | 107 | |
| 3 h | 126 | 431 | 127 | 356 | 305 | 229 | 113 | 109 |
| | 111 | 439 | 105 | 328 | 328 | 223 | 107 | |
| | 84.0 | 421 | 127 | 361 | 337 | 234 | 108 | |
| | 207 | 563 | 161 | 395 | 356 | 234 | 106 | |
| | 367 | 565 | 278 | 414 | 198 | 136 | 108 | |
| | 325 | 519 | 266 | 404 | 194 | 138 | 109 | |
| | 267 | 580 | 223 | 431 | 313 | 208 | 106 | |
| | 257 | 562 | 222 | 442 | 305 | 220 | 111 | |
| | 342 | 535 | 267 | 418 | 193 | 151 | 115 | |
| | 187 | 529 | 212 | 433 | 342 | 221 | 103 | |
| 6 h | 230 | 466 | 175 | 337 | 236 | 162 | 108 | 108 |
| | 242 | 482 | 178 | 329 | 240 | 161 | 107 | |
| | 253 | 501 | 193 | 361 | 248 | 168 | 107 | |
| | 255 | 506 | 209 | 373 | 251 | 164 | 105 | |
| | 231 | 482 | 218 | 387 | 251 | 169 | 107 | |
| | 181 | 440 | 232 | 410 | 259 | 178 | 108 | |
| | 247 | 489 | 236 | 431 | 242 | 195 | 116 | |
| | 319 | 513 | 275 | 408 | 194 | 133 | 108 | |
| | 367 | 565 | 278 | 414 | 198 | 136 | 108 | |
| | 111 | 439 | 105 | 328 | 328 | 223 | 107 | |
| | 323 | 558 | 235 | 385 | 235 | 150 | 104 | |
| | 280 | 504 | 225 | 401 | 224 | 176 | 115 | |
| | 344 | 568 | 232 | 403 | 224 | 171 | 113 | |

| | | | | | | | | |
|---|---|---|---|---|---|---|---|---|
| 24 h | 225 | 444 | 239 | 392 | 219 | 153 | 109 | 111 |
| | 270 | 490 | 231 | 395 | 220 | 164 | 112 | |
| | 224 | 443 | 198 | 370 | 219 | 172 | 115 | |
| | 126 | 431 | 127 | 356 | 305 | 229 | 113 | |
| | 202 | 487 | 176 | 383 | 285 | 207 | 111 | |
| | 335 | 540 | 237 | 385 | 205 | 148 | 111 | |
| | 213 | 403 | 225 | 367 | 190 | 142 | 112 | |
| 48 h | 306 | 516 | 226 | 396 | 210 | 170 | 117 | 118 |
| | 327 | 543 | 229 | 395 | 216 | 166 | 114 | |
| | 333 | 547 | 234 | 413 | 214 | 179 | 118 | |
| | 328 | 529 | 235 | 411 | 201 | 176 | 121 | |
| | 173 | 377 | 242 | 423 | 204 | 181 | 121 | |
| | 304 | 478 | 238 | 387 | 174 | 149 | 119 | |
| | 320 | 491 | 248 | 400 | 171 | 152 | 121 | |
| | 212 | 493 | 213 | 436 | 281 | 223 | 116 | |
| | 342 | 535 | 267 | 418 | 193 | 151 | 115 | |
| | 362 | 533 | 251 | 405 | 171 | 154 | 122 | |

**Sample J: 500 h UV-B aged**

| Recovery time | X1 | X2 | Y1 | Y2 | ΔX | ΔY | Theta (degrees) | Average |
|---|---|---|---|---|---|---|---|---|
| 0 min | | | | | | | Not flat | - |
| 15 min | 95.0 | 458 | 174 | 429 | 363 | 255 | 109 | 116 |
| | 179 | 479 | 183 | 431 | 300 | 248 | 117 | |
| | 232 | 514 | 186 | 424 | 282 | 238 | 119 | |
| | 184 | 467 | 218 | 450 | 283 | 232 | 117 | |
| | 259 | 523 | 253 | 479 | 264 | 226 | 119 | |
| 30 min | 228 | 394 | 290 | 425 | 166 | 135 | 117 | 114 |
| | 286 | 460 | 290 | 425 | 174 | 135 | 114 | |
| | 380 | 552 | 289 | 430 | 172 | 141 | 117 | |
| | 293 | 470 | 305 | 436 | 177 | 131 | 1122 | |
| | 376 | 565 | 312 | 445 | 189 | 133 | 109 | |
| | 371 | 542 | 221 | 354 | 171 | 133 | 115 | |
| | 322 | 567 | 181 | 377 | 245 | 196 | 116 | |
| | 163 | 400 | 197 | 391 | 237 | 194 | 117 | |
| | 198 | 445 | 219 | 417 | 247 | 198 | 116 | |
| | 218 | 481 | 247 | 424 | 263 | 177 | 108 | |
| 1 h | 285 | 544 | 208 | 398 | 259 | 190 | 111 | 106 |
| | 179 | 436 | 243 | 420 | 257 | 177 | 108 | |
| | 239 | 501 | 232 | 409 | 262 | 177 | 107 | |
| | 229 | 474 | 221 | 402 | 245 | 181 | 111 | |
| | 218 | 481 | 247 | 424 | 263 | 177 | 107 | |
| | 289 | 508 | 257 | 392 | 219 | 135 | 102 | |
| | 282 | 498 | 272 | 411 | 216 | 139 | 104 | |

| | | | | | | | | |
|---|---|---|---|---|---|---|---|---|
| | 317 | 553 | 295 | 434 | 236 | 139 | 99.3 | |
| | 338 | 548 | 300 | 445 | 210 | 145 | 108 | |
| | 337 | 541 | 314 | 458 | 204 | 144 | 109 | |
| 3 h | 162 | 523 | 249 | 440 | 361 | 191 | 93.2 | 106 |
| | 136 | 417 | 206 | 410 | 281 | 204 | 110.9 | |
| | 180 | 508 | 234 | 426 | 328 | 192 | 98.9 | |
| | 145 | 426 | 212 | 416 | 281 | 204 | 111 | |
| | 134 | 410 | 196 | 406 | 276 | 210 | 113 | |
| | 230 | 407 | 297 | 444 | 177 | 147 | 118 | |
| | 274 | 445 | 288 | 445 | 171 | 157 | 123 | |
| | 336 | 523 | 281 | 431 | 187 | 150 | 116 | |
| | 355 | 547 | 277 | 424 | 192 | 147 | 114 | |
| | 385 | 579 | 163 | 302 | 194 | 139 | 110 | |
| 6 h | 219 | 434 | 289 | 455 | 215 | 166 | 114 | 110 |
| | 194 | 412 | 275 | 428 | 218 | 153 | 109 | |
| | 306 | 535 | 245 | 398 | 229 | 153 | 106 | |
| | 318 | 535 | 237 | 395 | 217 | 158 | 111 | |
| | 319 | 549 | 235 | 397 | 230 | 162 | 109 | |
| | 226 | 410 | 250 | 405 | 184 | 155 | 119 | |
| | 372 | 559 | 240 | 395 | 187 | 155 | 118 | |
| | 283 | 450 | 237 | 396 | 167 | 159 | 125 | |
| | 360 | 528 | 199 | 355 | 168 | 156 | 123 | |
| | 328 | 534 | 242 | 386 | 206 | 144 | 109 | |
| 24 h | 155 | 406 | 231 | 446 | 251 | 215 | 120 | 120 |
| | 331 | 567 | 228 | 426 | 236 | 198 | 118 | |
| | 319 | 546 | 175 | 377 | 227 | 202 | 121 | |
| | 272 | 499 | 203 | 402 | 227 | 199 | 121 | |
| | 231 | 459 | 163 | 366 | 228 | 203 | 121 | |
| | 211 | 388 | 284 | 442 | 177 | 158 | 122 | |
| | 344 | 547 | 291 | 450 | 203 | 159 | 115 | |
| | 363 | 568 | 251 | 401 | 205 | 150 | 111 | |
| | 398 | 607 | 253 | 401 | 209 | 148 | 110 | |
| | 322 | 523 | 205 | 354 | 191 | 149 | 115 | |
| 48 h | 263 | 549 | 212 | 430 | 286 | 218 | 114 | 116 |
| | 197 | 470 | 234 | 436 | 273 | 202 | 112 | |
| | 264 | 516 | 194 | 405 | 252 | 211 | 118 | |
| | 321 | 557 | 211 | 406 | 236 | 195 | 118 | |
| | 269 | 493 | 224 | 407 | 224 | 183 | 117 | |
| | 276 | 512 | 169 | 342 | 236 | 173 | 111 | |
| | 275 | 455 | 232 | 364 | 180 | 132 | 111 | |
| | 314 | 485 | 260 | 399 | 171 | 139 | 117 | |
| | 342 | 523 | 236 | 373 | 181 | 137 | 113 | |
| | 373 | 544 | 161 | 302 | 171 | 141 | 118 | |

**Sample C: 50 day acid rain aged**

| Recovery time | X1 | X2 | Y1 | Y2 | ΔX | ΔY | Theta (degrees) | Average |
|---|---|---|---|---|---|---|---|---|
| 0 min | | | | | | | Not flat | - |
| 15 min | 72.0 | 516 | 157 | 356 | 444 | 199 | 83.7 | 82 |
| | 19.0 | 456 | 158 | 355 | 437 | 197 | 84.0 | |
| | 65.0 | 508 | 112 | 304 | 443 | 192 | 81.8 | |
| | 60.0 | 523 | 106 | 301 | 463 | 195 | 80.2 | |
| | 58.0 | 613 | 107 | 344 | 555 | 237 | 80.9 | |
| 30 min | 69.0 | 519 | 107 | 391 | 450 | 284 | 104 | 104 |
| | 70.0 | 529 | 114 | 408 | 459 | 294 | 104 | |
| | 86.0 | 546 | 110 | 398 | 460 | 288 | 103 | |
| | 96.0 | 533 | 110 | 408 | 437 | 298 | 108 | |
| | 70.0 | 536 | 122 | 405 | 466 | 283 | 101 | |
| | 91.0 | 531 | 119 | 419 | 440 | 300 | 108 | |
| | 72.0 | 516 | 157 | 356 | 444 | 199 | 83.7 | |
| | 19.0 | 456 | 158 | 355 | 437 | 197 | 192 | |
| | 65.0 | 508 | 112 | 304 | 443 | 192 | 81.8 | |
| | 60.0 | 523 | 106 | 301 | 463 | 195 | 80.9 | |
| 1 h | 119 | 517 | 104 | 377 | 398 | 273 | 108 | 104 |
| | 105 | 533 | 136 | 386 | 428 | 250 | 98.9 | |
| | 122 | 531 | 137 | 402 | 409 | 265 | 105 | |
| | 66.0 | 468 | 147 | 415 | 402 | 268 | 106 | |
| | 46.0 | 468 | 147 | 415 | 402 | 268 | 102 | |
| | 27.0 | 608 | 175 | 428 | 581 | 253 | 82.1 | |
| | 61.0 | 598 | 132 | 430 | 537 | 298 | 95.9 | |
| | 41.0 | 570 | 137 | 433 | 529 | 296 | 96.4 | |
| | 25.0 | 555 | 151 | 372 | 530 | 221 | 79.7 | |
| | 48.0 | 570 | 178 | 395 | 522 | 217 | 79.5 | |
| 3 h | 164 | 526 | 149 | 354 | 362 | 205 | 97.1 | 93 |
| | 93.0 | 455 | 152 | 351 | 362 | 199 | 97.1 | |
| | 74.0 | 456 | 158 | 357 | 382 | 199 | 92.4 | |
| | 52.0 | 439 | 168 | 365 | 387 | 197 | 91.4 | |
| | 111 | 489 | 176 | 370 | 378 | 194 | 91.5 | |
| | 52.0 | 462 | 159 | 385 | 410 | 226 | 95.6 | |
| | 54.0 | 472 | 167 | 392 | 418 | 225 | 94.2 | |
| | 113 | 516 | 173 | 389 | 403 | 216 | 93.9 | |
| | 57.0 | 537 | 146 | 385 | 480 | 239 | 89.8 | |
| | 36.0 | 579 | 148 | 400 | 543 | 252 | 85.7 | |
| 6 h | 218 | 539 | 256 | 409 | 321 | 153 | 87.3 | 92 |
| | 129 | 414 | 233 | 394 | 285 | 161 | 96.9 | |
| | 129 | 415 | 229 | 395 | 286 | 166 | 98.5 | |
| | 132 | 478 | 245 | 409 | 346 | 164 | 86.9 | |
| | 90.0 | 399 | 238 | 238 | 400 | 309 | 162 | |
| | 116 | 485 | 169 | 357 | 369 | 188 | 91.1 | |

| | | | | | | | | |
|---|---|---|---|---|---|---|---|---|
| | 101 | 472 | 178 | 361 | 373 | 184 | 89.2 | |
| | 158 | 531 | 177 | 361 | 373 | 184 | 89.2 | |
| | 76.0 | 429 | 170 | 361 | 353 | 191 | 94.5 | |
| | 74.0 | 552 | 141 | 399 | 478 | 258 | 94.4 | |
| 24 h | 218 | 548 | 269 | 429 | 330 | 160 | 88.2 | 95 |
| | 174 | 475 | 266 | 422 | 301 | 156 | 92.0 | |
| | 189 | 478 | 255 | 424 | 289 | 169 | 98.9 | |
| | 281 | 561 | 244 | 425 | 280 | 181 | 105 | |
| | 156 | 449 | 200 | 355 | 293 | 155 | 93.2 | |
| | 51.0 | 534 | 253 | 463 | 483 | 210 | 82.0 | |
| | 32.0 | 492 | 218 | 447 | 460 | 229 | 89.8 | |
| | 90.0 | 534 | 215 | 431 | 444 | 216 | 88.4 | |
| | 75.0 | 527 | 240 | 435 | 448 | 195 | 82.0 | |
| | 79.0 | 557 | 281 | 471 | 478 | 190 | 76.9 | |
| 48 h | 103 | 548 | 96 | 346 | 445 | 250 | 96.7 | 98 |
| | 52.0 | 518 | 124 | 379 | 466 | 255 | 95.2 | |
| | 96.0 | 532 | 122 | 389 | 436 | 267 | 102 | |
| | 118 | 563 | 144 | 402 | 445 | 258 | 98.5 | |
| | 115 | 539 | 147 | 403 | 424 | 256 | 101 | |
| | 160 | 457 | 194 | 362 | 297 | 168 | 97.1 | |
| | 99.0 | 413 | 194 | 368 | 314 | 174 | 95.9 | |
| | 161 | 461 | 193 | 367 | 300 | 174 | 98.5 | |
| | 190 | 498 | 194 | 366 | 308 | 172 | 96.3 | |
| | 111 | 422 | 189 | 360 | 311 | 171 | 95.4 | |

**Sample J: 50 days acid rain aged**

| Recovery time | X1 | X2 | Y1 | Y2 | ΔX | ΔY | Theta (degrees) | Average |
|---|---|---|---|---|---|---|---|---|
| 0 min | | | | | | | Not flat | - |
| 15 min | 153 | 533 | 114 | 396 | 380 | 282 | 112 | 107 |
| | 71.0 | 446 | 120 | 402 | 375 | 282 | 113 | |
| | 146 | 518 | 110 | 389 | 372 | 279 | 112 | |
| | 163 | 571 | 130 | 400 | 408 | 270 | 106 | |
| | 36.0 | 504 | 163 | 407 | 468 | 244 | 92.4 | |
| 30 min | 170 | 562 | 159 | 415 | 392 | 256 | 105.1 | 105 |
| | 122 | 533 | 208 | 452 | 411 | 244 | 99.9 | |
| | 164 | 550 | 150 | 398 | 386 | 248 | 104 | |
| | 87.0 | 461 | 155 | 398 | 374 | 243 | 105 | |
| | 159 | 525 | 128 | 385 | 366 | 257 | 109 | |
| | 59.0 | 479 | 219 | 445 | 420 | 226 | 94.2 | |
| | 117 | 531 | 199 | 411 | 414 | 212 | 91.4 | |
| | 142 | 543 | 228 | 447 | 401 | 219 | 95.0 | |
| | 103 | 512 | 227 | 446 | 409 | 219 | 93.9 | |
| | 139 | 482 | 171 | 379 | 343 | 208 | 101 | |

| | | | | | | | | |
|---|---|---|---|---|---|---|---|---|
| 1 h | 140 | 515 | 162 | 404 | 375 | 242 | 104 | 97 |
| | 135 | 505 | 157 | 388 | 370 | 231 | 103 | |
| | 111 | 494 | 160 | 386 | 383 | 226 | 99.4 | |
| | 134 | 507 | 202 | 347 | 373 | 145 | 75.7 | |
| | 142 | 506 | 204 | 440 | 364 | 236 | 105 | |
| | 60.0 | 503 | 206 | 424 | 443 | 218 | 89.0 | |
| | 112 | 523 | 191 | 413 | 411 | 222 | 94.4 | |
| | 113 | 519 | 191 | 414 | 406 | 224 | 95.6 | |
| | 151 | 557 | 121 | 345 | 406 | 224 | 95.6 | |
| | 106 | 505 | 147 | 374 | 399 | 227 | 97.4 | |
| 3 h | 201 | 563 | 89 | 291 | 362 | 202 | 96.3 | 98 |
| | 216 | 570 | 107 | 319 | 354 | 212 | 100 | |
| | 160 | 521 | 132 | 347 | 361 | 215 | 99.9 | |
| | 218 | 584 | 155 | 358 | 366 | 203 | 95.9 | |
| | 72.0 | 440 | 188 | 402 | 368 | 214 | 98.6 | |
| | 139 | 482 | 171 | 379 | 343 | 208 | 101 | |
| | 75.0 | 426 | 194 | 383 | 351 | 189 | 100 | |
| | 140 | 483 | 196 | 397 | 343 | 201 | 99.1 | |
| | 123 | 480 | 131 | 346 | 357 | 215 | 97.8 | |
| | 145 | 487 | 141 | 353 | 342 | 212 | 102 | |
| 6 h | 149 | 442 | 208 | 384 | 293 | 176 | 101 | 99 |
| | 173 | 446 | 214 | 383 | 273 | 169 | 102 | |
| | 163 | 438 | 218 | 398 | 275 | 180 | 105 | |
| | 167 | 435 | 206 | 389 | 268 | 183 | 108 | |
| | 202 | 523 | 238 | 395 | 321 | 157 | 88.7 | |
| | 226 | 515 | 254 | 434 | 289 | 180 | 102 | |
| | 222 | 514 | 244 | 413 | 292 | 169 | 98.4 | |
| | 220 | 507 | 224 | 392 | 287 | 168 | 98.9 | |
| | 247 | 555 | 228 | 408 | 308 | 180 | 98.9 | |
| | 149 | 433 | 205 | 354 | 284 | 149 | 92.8 | |
| 24 h | 107 | 402 | 155 | 318 | 295 | 163 | 95.7 | 97 |
| | 149 | 437 | 184 | 350 | 288 | 166 | 98.1 | |
| | 175 | 469 | 209 | 364 | 294 | 155 | 93.0 | |
| | 97.0 | 379 | 224 | 391 | 282 | 167 | 99.7 | |
| | 91.0 | 535 | 180 | 421 | 444 | 241 | 94.7 | |
| | 42.0 | 479 | 99.0 | 337 | 437 | 238 | 94.9 | |
| | 71.0 | 517 | 172 | 423 | 446 | 251 | 96.8 | |
| | 64.0 | 537 | 161 | 400 | 473 | 239 | 90.6 | |
| | 27.0 | 561 | 73.0 | 291 | 534 | 218 | 78.5 | |
| | 178 | 439 | 300 | 429 | 261 | 129 | 89.3 | |
| 48 h | 59.0 | 486 | 89.0 | 348 | 427 | 259 | 101 | 101 |
| | 66.0 | 500 | 73.0 | 325 | 434 | 252 | 98.5 | |
| | 87.0 | 502 | 108 | 382 | 415 | 274 | 106 | |
| | 45.0 | 483 | 171 | 422 | 438 | 245 | 96.4 | |
| | 75.0 | 517 | 213 | 488 | 442 | 275 | 102 | |

| | | | | | | | | |
|---|---|---|---|---|---|---|---|---|
| | 157 | 450 | 284 | 430 | 293 | 146 | 89.8 | |
| | 153 | 432 | 264 | 413 | 279 | 149 | 93.8 | |
| | 159 | 452 | 254 | 427 | 293 | 173 | 99.5 | |
| | 146 | 469 | 215 | 406 | 323 | 191 | 99.6 | |
| | 188 | 520 | 196 | 384 | 332 | 188 | 97.1 | |

**Appendix B: SEM images of the controlled formulation and the commercial samples after various laboratory accelerated ageing treatments.**

Scanning electron microscope images of controlled formulation samples and commercial insulators, V (virgin), N-C (needle corona aged for 30 min), F-C (French corona aged for 12 h), UV (ultraviolet radiation aged for 3000 h), A-R (acid rain aged for 125 days) with various magnifications:

CV (200)

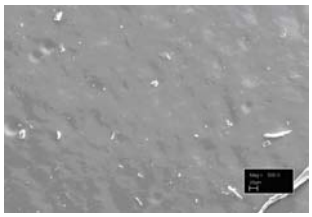

CV (500)

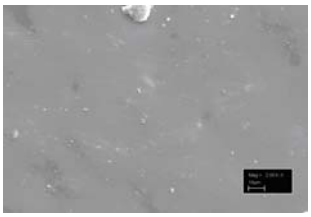

CV (2000)

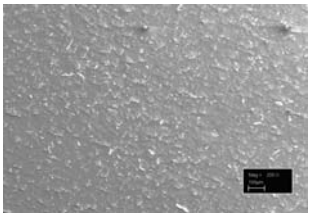

C N-C (200)

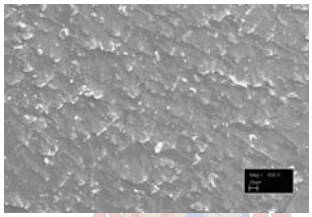

C N-C (500)

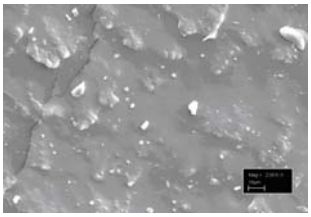

C N-C (2000)

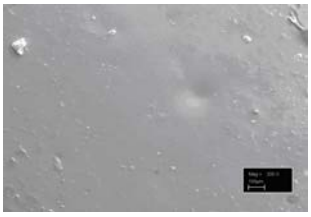

C F-C (200)

C F-C (500)

C F-C (2000)

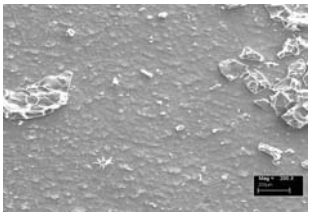

C UV (200)

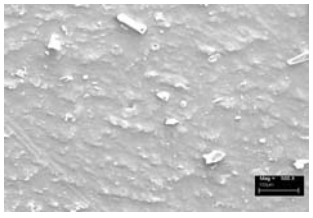

C UV (500)

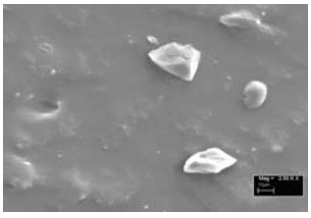

C UV (2000)

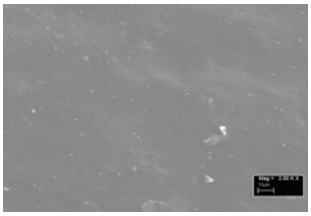

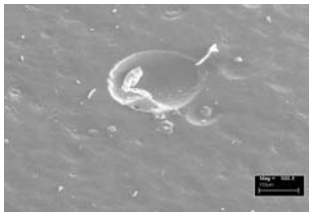

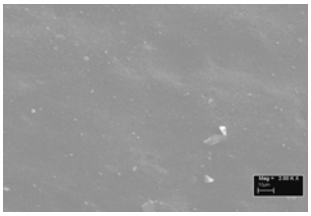

C A-R (200)

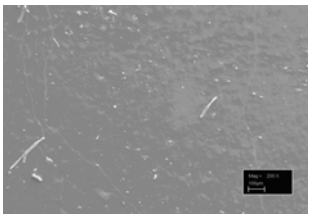

C A-R (500)

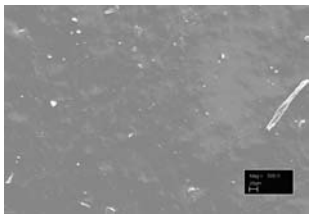

C A-R (2000)

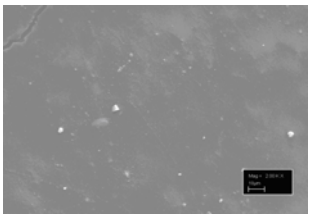

E V ( 200)

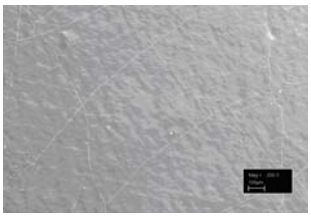

E V ( 500)

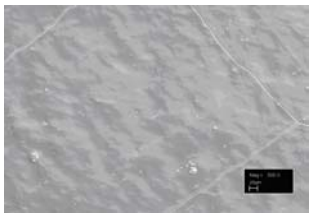

E V ( 2000)

E N-C (200)

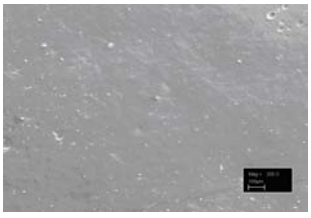

E N-C (500)

E N-C (2000)

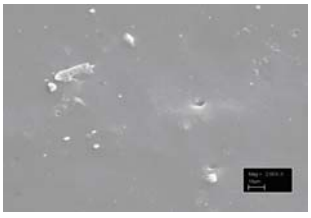

E F-C (200)



E F-C (500)



E F-C (2000)



E UV (200)

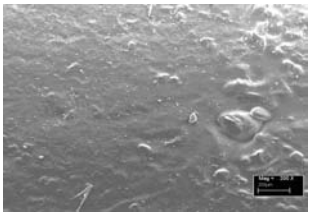

E UV (500)

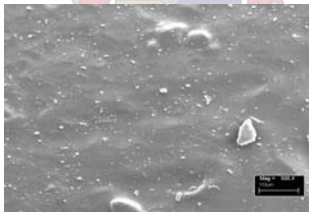

E UV (2000)

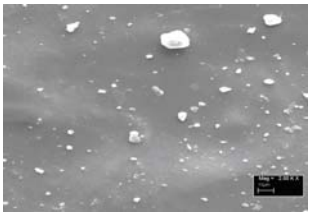

E A-R (200)

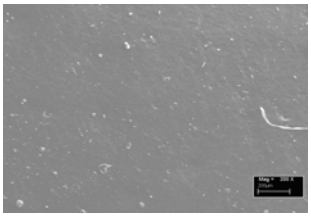

E A-R (500)

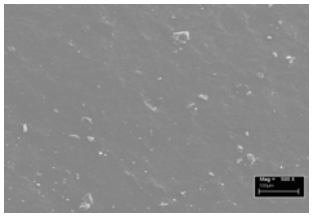

E A-R (2000)

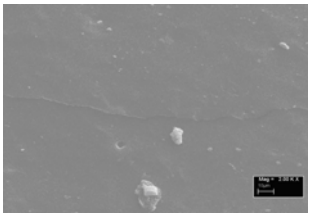

G V (200)

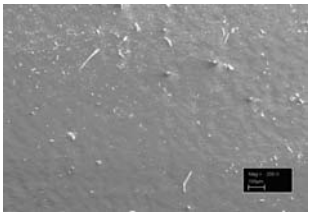

G V (500)

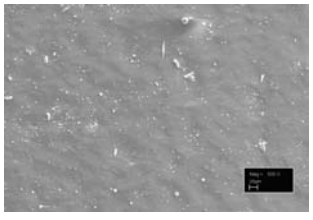

G V (2000)

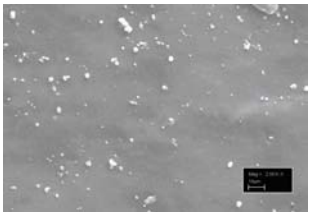

G N-C (200)

G N-C (500)

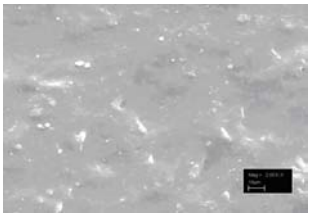

G N-C (2000)

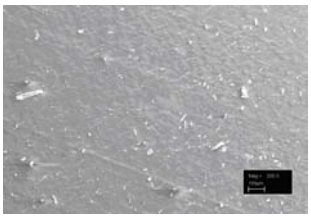

G F-C (200)

G F-C (500)

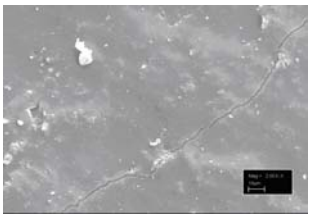

G F-C (2000)

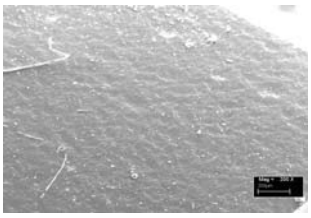

G UV (200)

G UV (500)

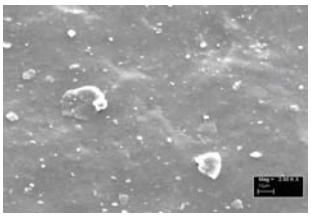

G UV (2000)

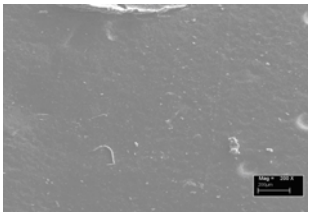

G A-R (200)

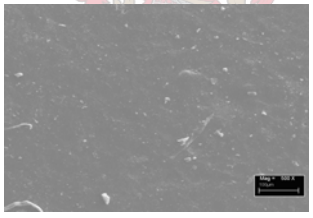

G A-R (500)

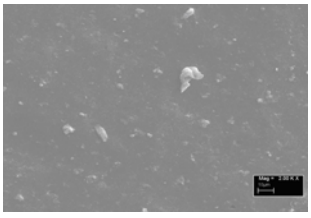

G A-R (2000)

I V (200)

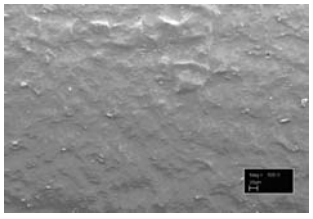

I V (500)

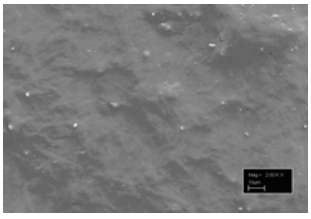

I V (2000)

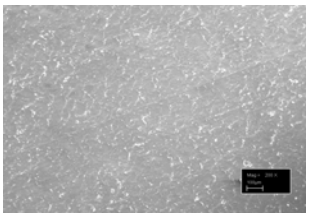

I N-C (200)

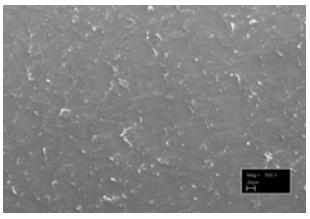

I N-C (500)

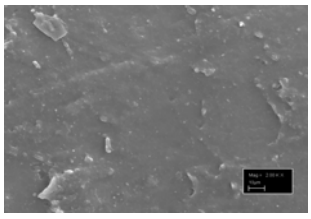

I N-C (2000)

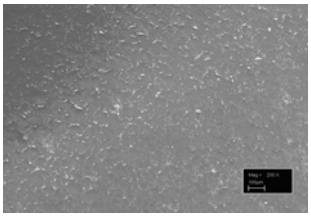

I F-C (200)

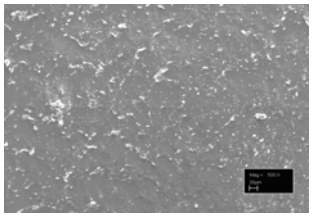

I F-C (500)

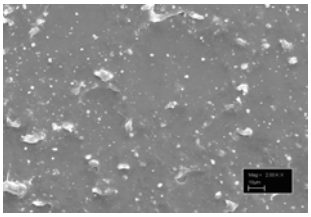

I F-C (2000)

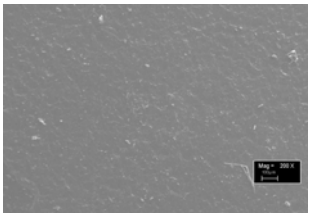

I UV (200)

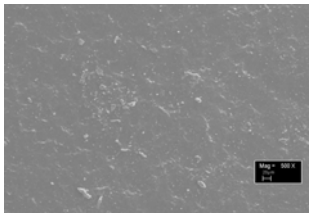

I UV (500)

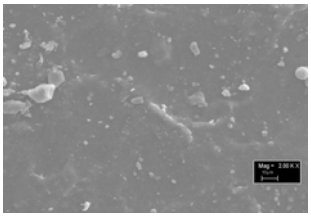

I UV (2000)

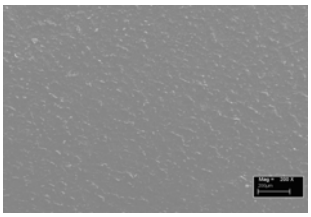

I A-R (200)

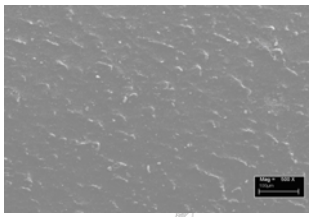

I A-R (500)

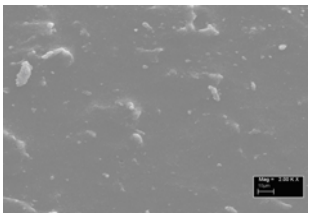

I A-R (2000)

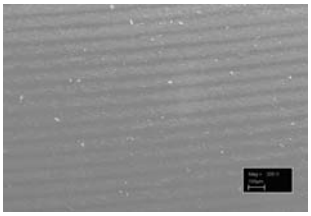

J V (200)

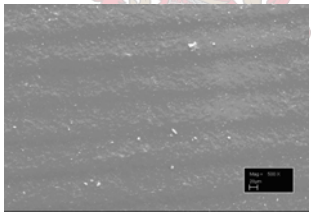

J V (500)

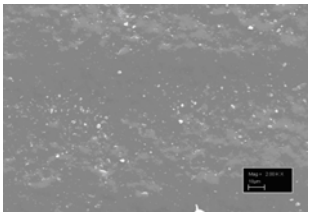

J V (2000)

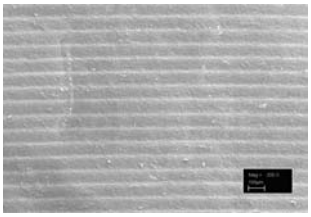

J N-C (200)

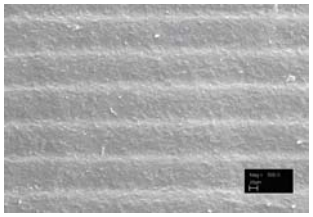

J N-C (500)

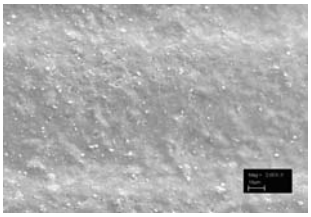

J N-C (2000)

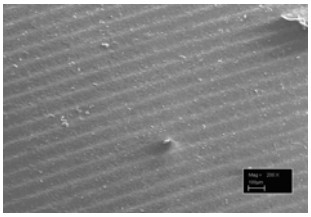

J F-C (200)

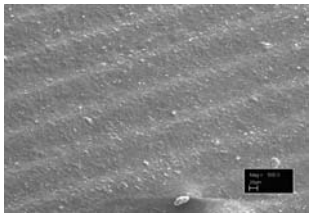

J F-C (500)

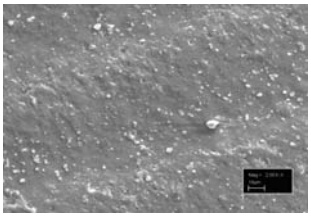

J F-C (2000)

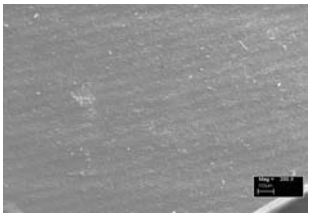

J UV (200)

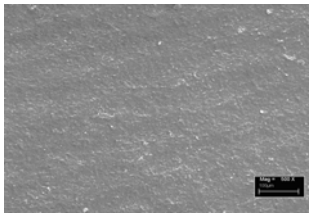

J UV (500)

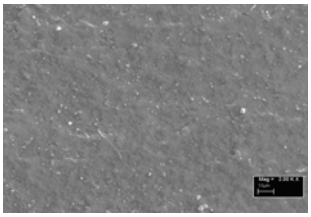

J UV (2000)

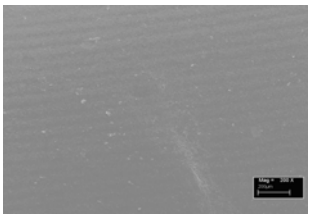

J A-R (200)

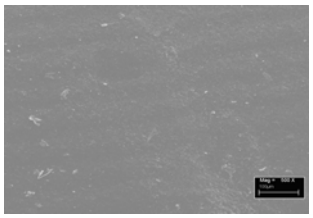

J A-R (500)

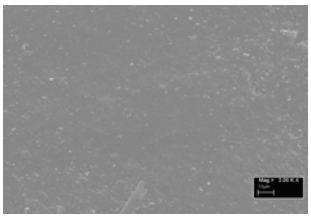

J A-R (2000)

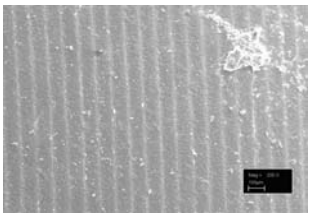

K V (200)

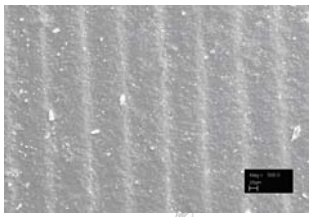

K V (500)

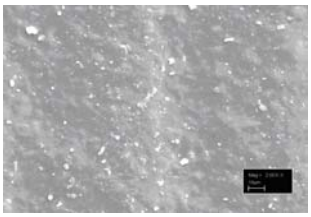

K V (2000)

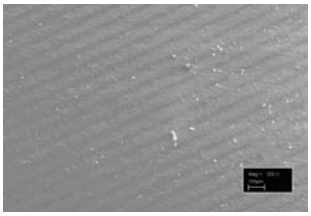

K N-C (200)

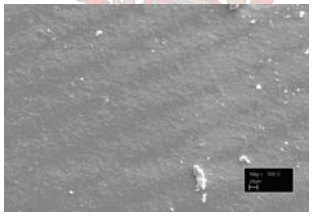

K N-C (500)

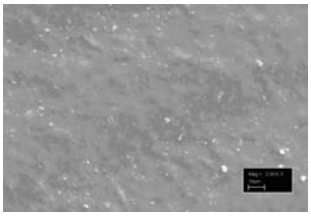

K N-C (2000)

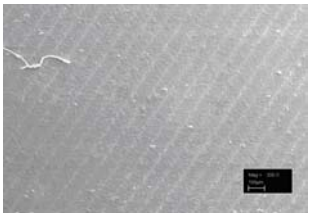

K F-C (200)

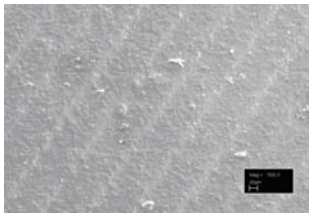

K F-C (500)

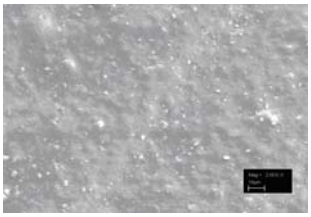

K F-C (2000) )

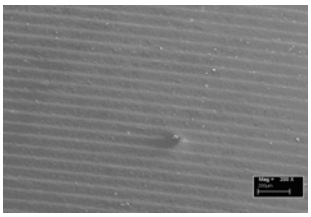

K UV (200)

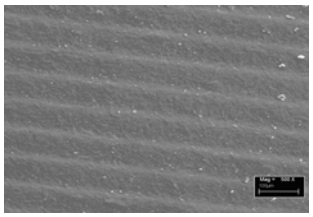

K UV (500)

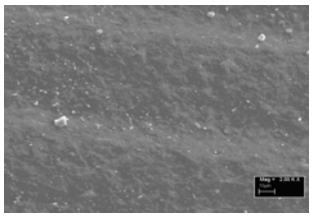

K UV (2000)

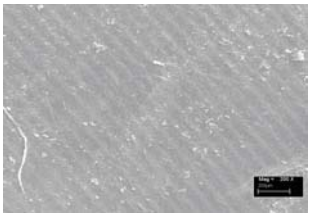

K A-R (200)

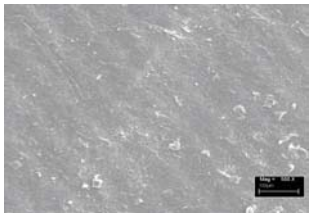

K A-R (500)

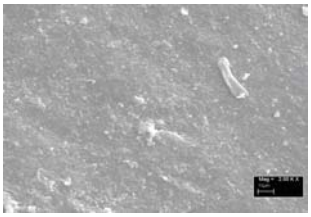

K A-R (2000)

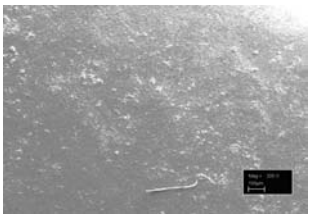

L V (200)

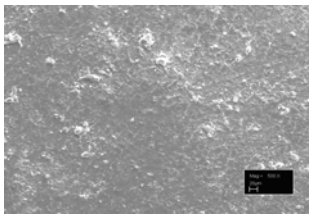

L V (500)

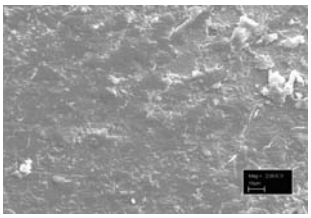

L V (2000)

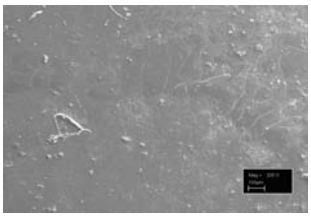

L N-C (200)

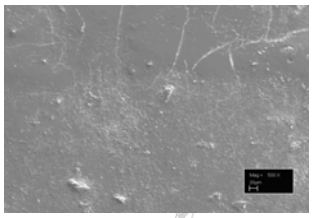

L N-C (500)

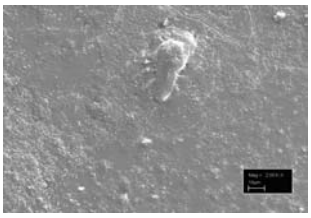

L N-C (2000)

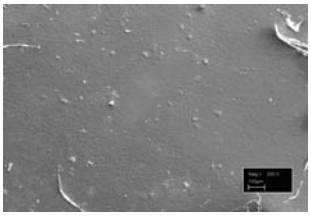

Cleaned J N-C (200)

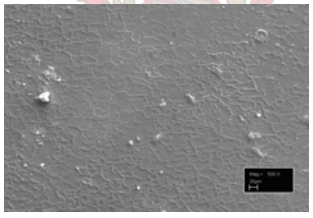

Cleaned J N-C (500)

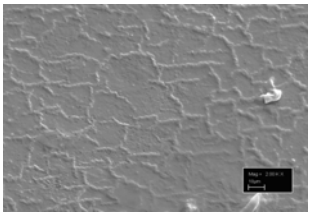

Cleaned J N-C (2000)

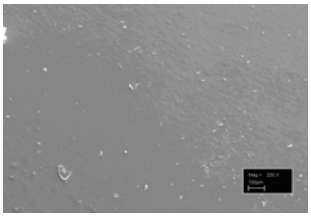

L F-C (200)

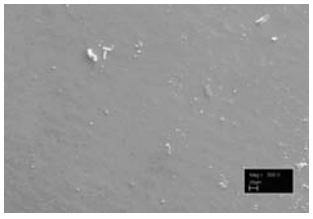

L F-C (500)

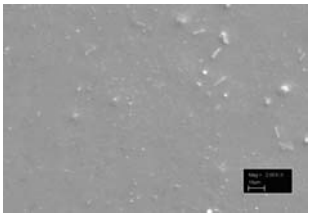

L F-C (2000)

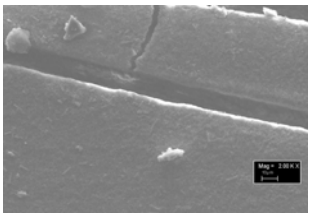

L UV (200)

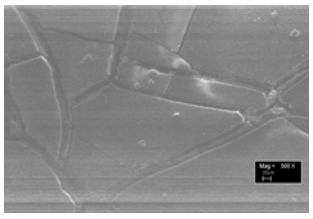

L UV (500)

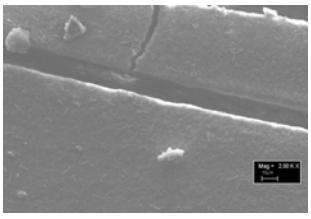

L UV (2000)

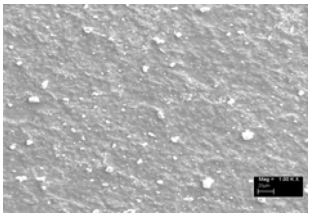

L A-R (200)

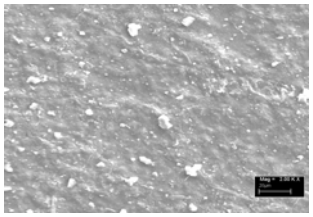

L A-R (500)

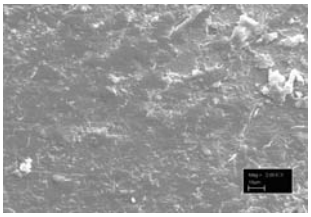

L A-R (2000)

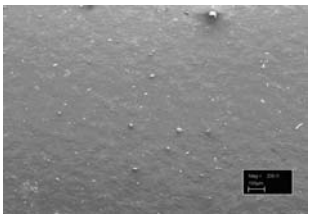

M V (200)

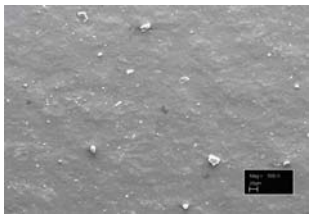

M V (500)

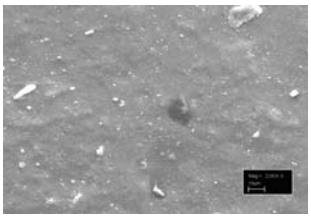

M V (2000)

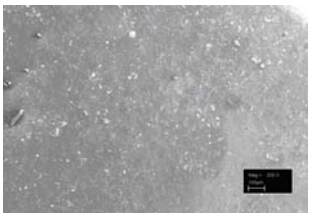

M N-C (200)

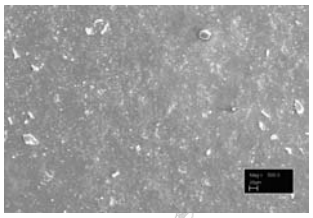

M N-C (500)

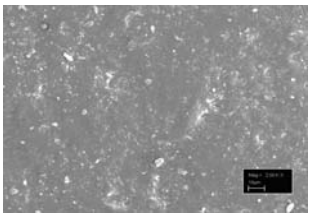

M N-C (2000)

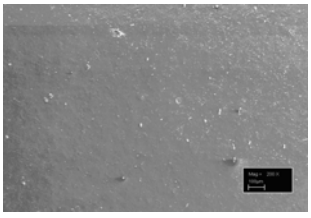

M F-C (200)

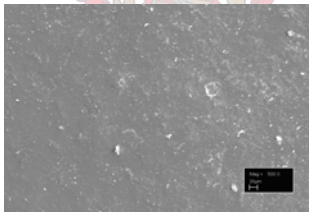

M F-C (500)

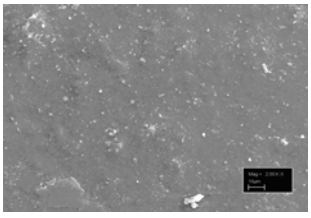

M F-C (2000)

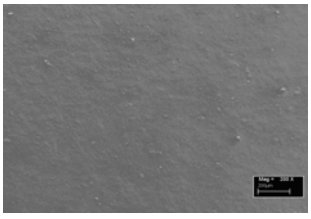

M UV (200)

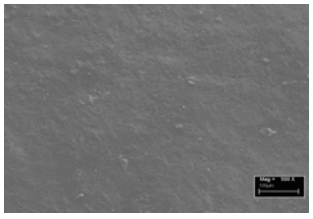

M UV (500)

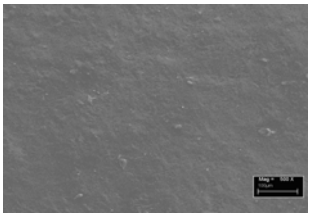

M UV (2000)

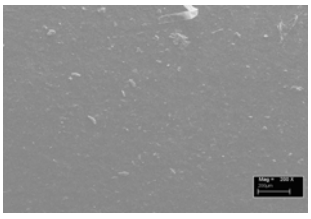

M A-R (200)

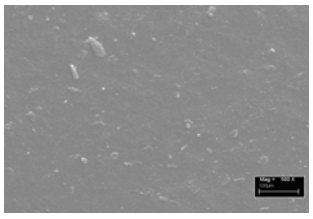

M A-R (500)

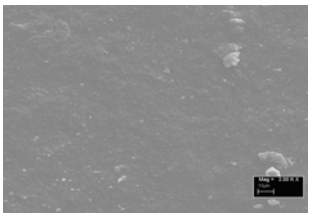

M A-R (2000)

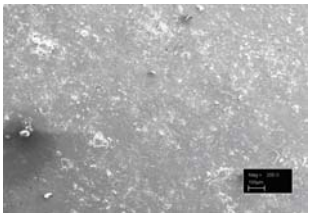

N V (200)

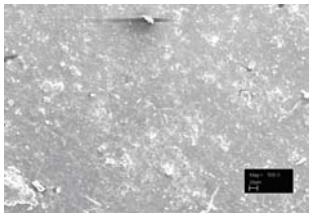

N V (500)

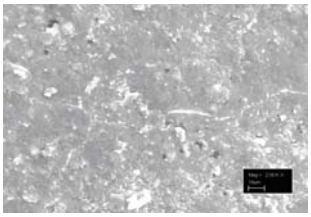

N V (2000)

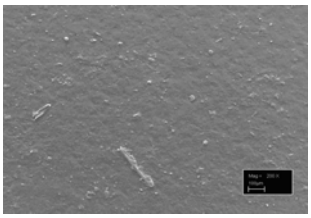

N N-C (200)

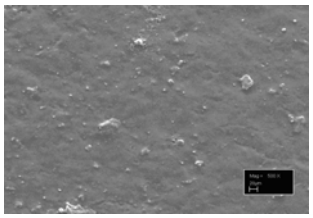

N N-C (500)

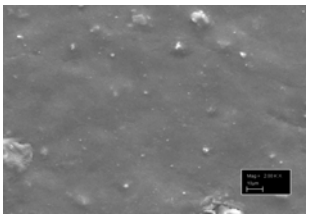

N N-C (2000)

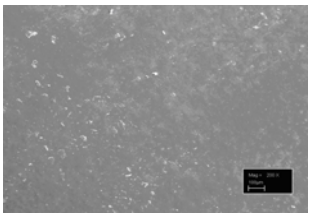

N F-C (200)

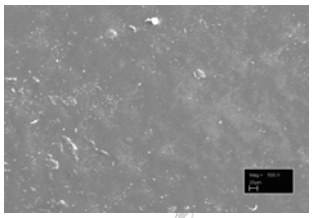

N F-C (500)

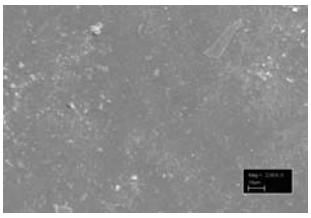

N F-C (2000)

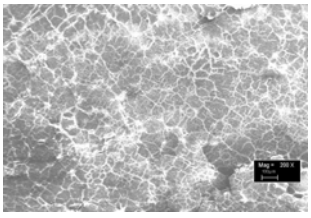

N UV (200)

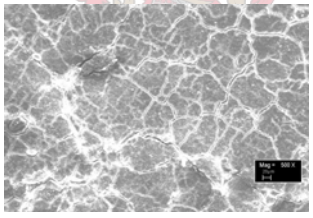

N UV (500)

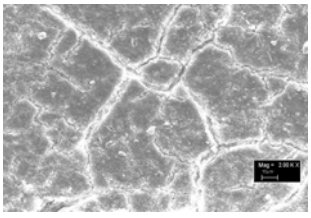

N UV (2000)

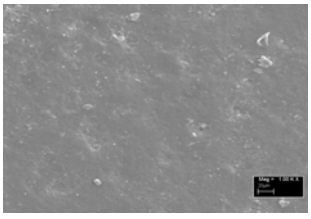

N A-R (200)

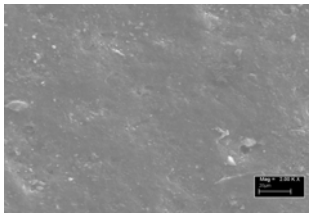

N A-R (500)

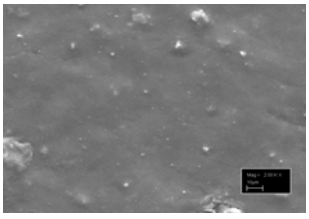

N A-R (2000)

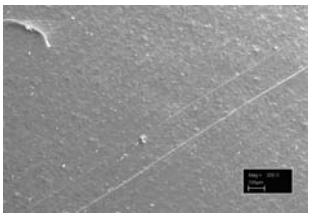

O V (200)

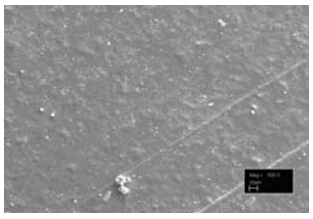

O V (500)

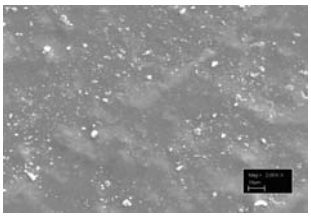

O V (2000)

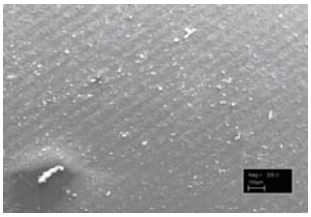

O N-C (200)

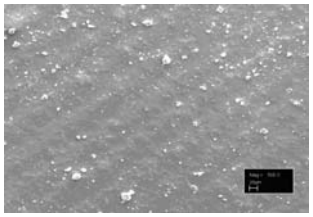

O N-C (500)

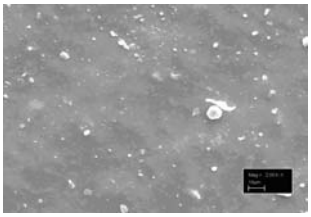

O N-C (2000)

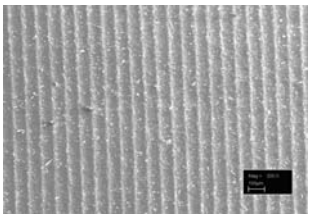

O F-C (200)

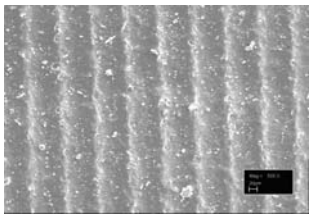

O F-C (500)

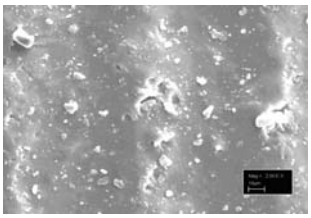

O F-C (2000)

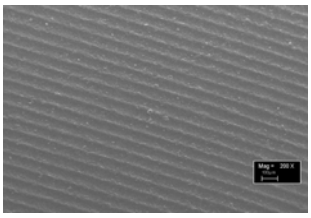

O UV (200)

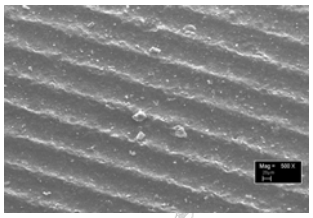

O UV (500)

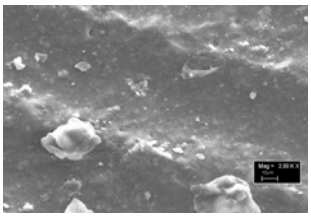

O UV (2000)

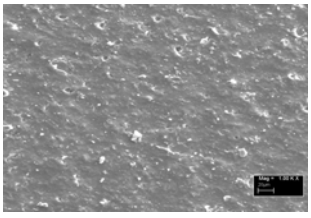

O A-R (200)

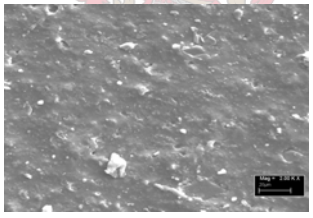

O A-R (500)

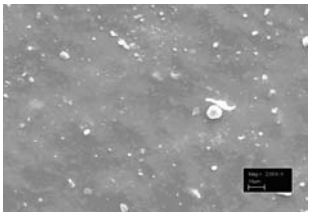

O A-R (2000)

**Appendix C: OP images of the controlled formulation and the commercial samples after various laboratory accelerated ageing treatments.**

Optical microscope images with two different magnifications of controlled formulations and commercial insulators after various types of laboratory accelerated ageing, V (virgin), N-C (needle corona aged for 30 min), F-C (French corona aged for 12 h), UV (ultraviolet radiation aged for 3000 h) and A-R (acid rain aged for 125 days).

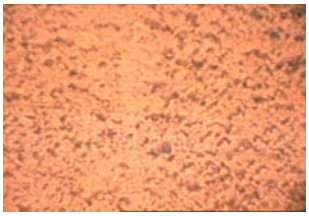

C V (200)

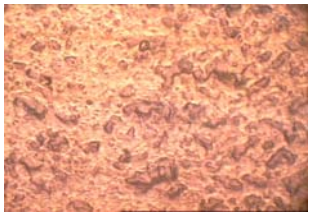

C V (500)

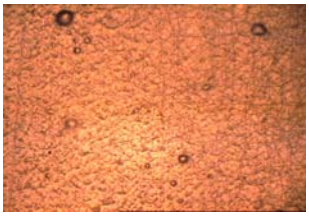

C N-C (200)

C N-C (500)

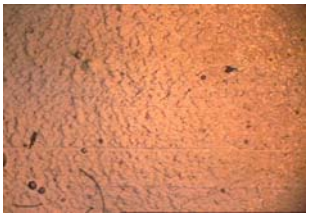

C UV (200)

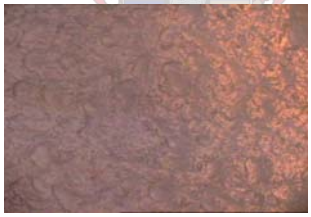

C UV (500)

C A-R (200)

C A-R (500)

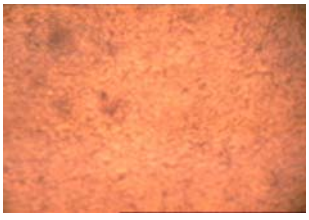

E V (200)

E V (500)

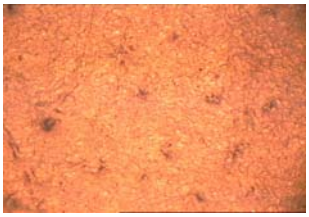

E N-C (200)

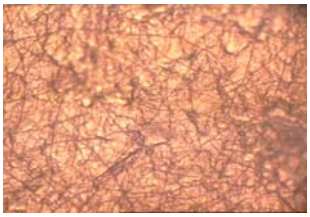

E N-C (500)

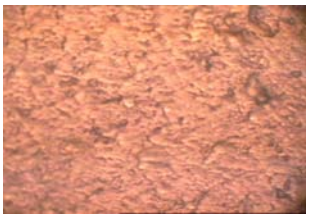

E F-C (200)

E F-C (500)

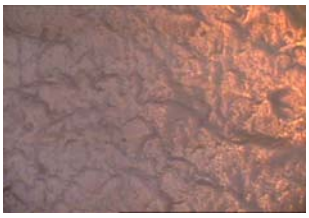

E UV-B (200)

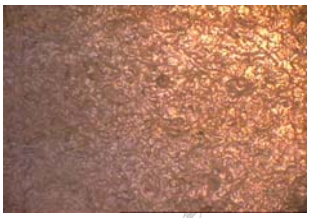

E UV-B (500)

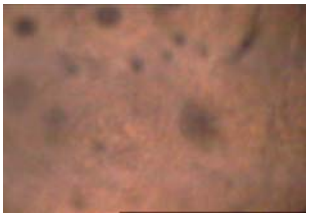

E A-R (200)

E A-R (500)

G V (200)

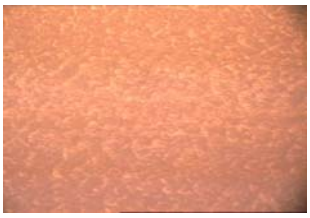

G V (500)

G N-C (200)

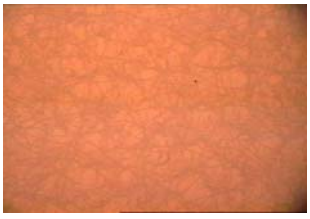

G N-C (500)

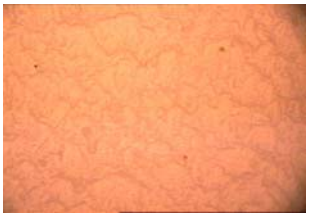

G F-C (200)

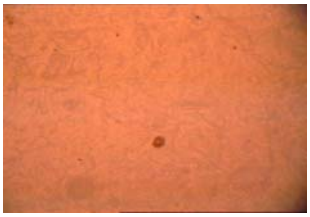

G F-C (500)

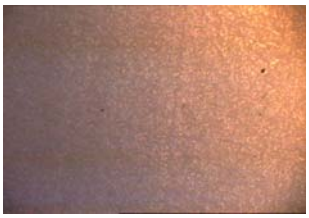

G UV-B (200)

G UV-B (500)

G A-R (200)

G A-R (500)

J V (200)

J V (500)

J N-C (200)

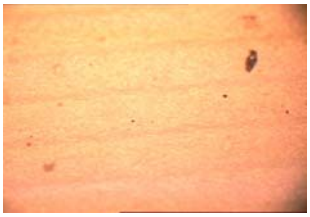

J N-C (500)

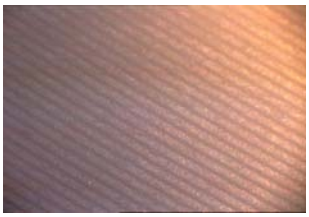

J F-C (200)

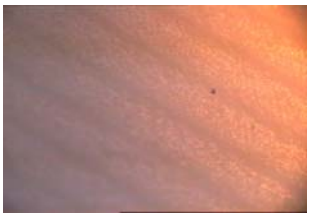

J F-C (500)

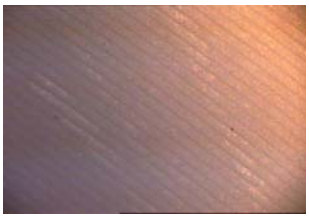

J UV (200)

J UV (500)

J A-R (200)

J A-R (500)

K V (200)

K V (500)

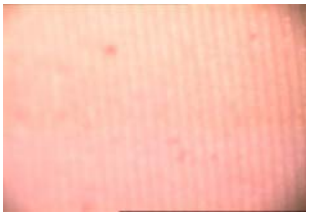

K N-C (200)

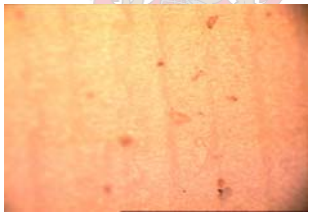

K N-C (500)

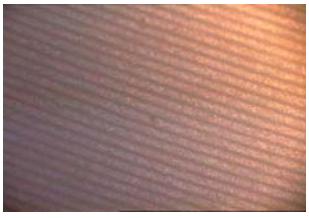

K F-C (200)

KF-C (500)

K UV-B (200)

K UV-B (500)

K A-R (200)

K A-R (500)

L V (200)

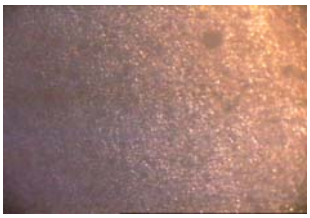

L V (500)

L N-C (200)

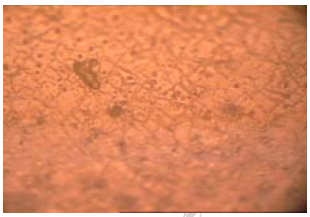

L N-C (500)

L F-C (200)

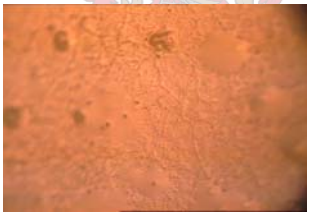

L F-C (500)

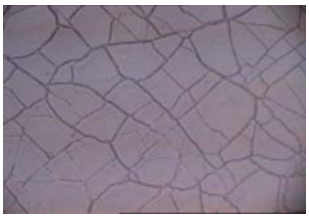

L UV (200)

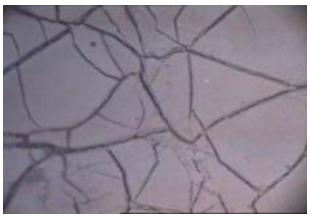

L UV (500)

L A-R (200)

L A-R (500)

M V (200)

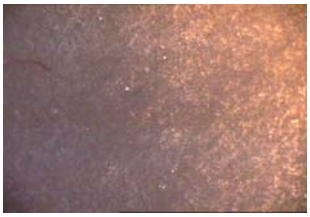

M V (500)

M N-C (200)

M N-C (500)

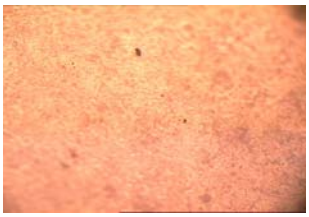

M F-C (200)

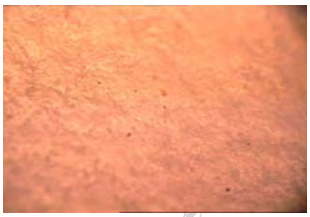

M F-C (500)

M UV (200)

M UV (500)

M A-R (200)

M A-R (500)

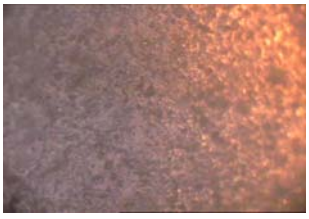

N V (200)

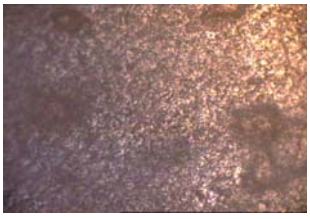

N V (500)

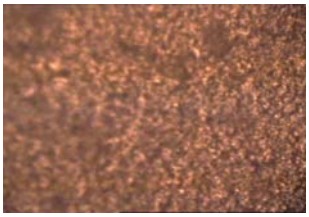

N N-C (200)

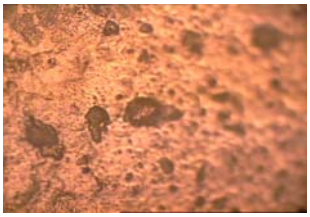

N N-C (500)

N F-C (200)

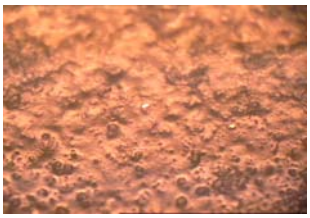

N F-C (500)

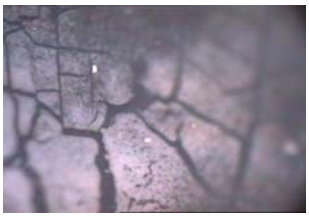

N UV-B (200)

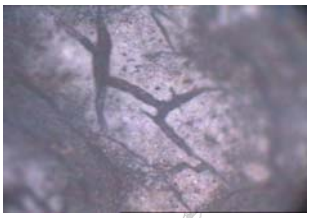

N UV-B (500)

N A-R (200)

N A-R (500)

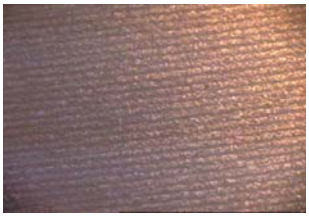

O V (200)

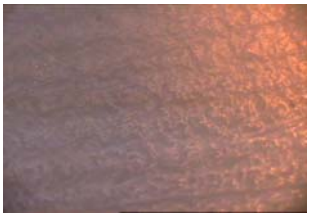

O V (500)

O N-C (200)

O N-C (500)

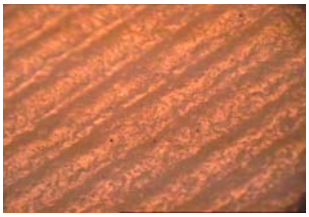

O F-C (200)

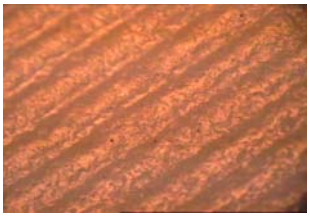

O F-C (500)

O UV-B (200)

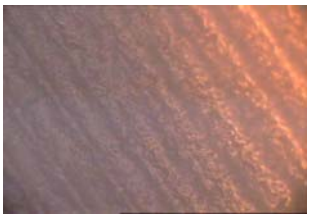

O UV-B (500)

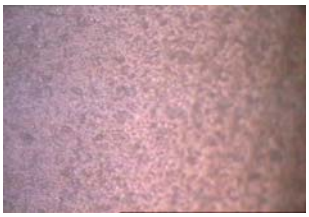

O A-R (200)

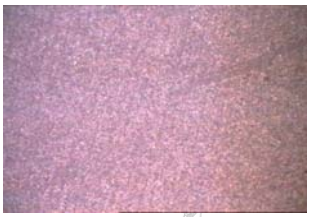

O A-R (500)

PDMS V (200)

PDMS V (500)

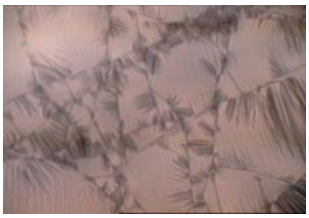

PDMS F-C (200)

PDMS F-C (500)